Winter 1-31-2024

Optimization of Vibro-Seismic Parameters for Enhanced Oil Recovery Application

Tarek Abdel Aal
tarek3932@aucegypt.edu

Graduate Studies

Optimization of Vibroseismic Parameters for Enhanced Oil Recovery Application

A THESIS SUBMITTED BY

Tarek Ahmed Abdel Fattah Abdel Aal

TO THE

Petroleum and Energy Engineering Department

SUPERVISED BY

Dr. Mostafa Oraby

10th January, 2024

in partial fulfillment of the requirements for the degree of

Degree of Master of Science in Petroleum and Energy Engineering

Declaration of Authorship

I, Tarek Ahmed Abdel Aal, declare that this thesis titled, "Optimization of Vibroseismic Parameters for Enhanced Oil Recovery Application" and the work presented in it are my own. I confirm that:

- This work was done wholly or mainly while in candidature for a research degree at this University.
- Where any part of this thesis has previously been submitted for a degree or any other qualification at this University or any other institution, this has been clearly stated.
- Where I have consulted the published work of others, this is always clearly attributed.
- Where I have quoted from the work of others, the source is always given. With the exception of such quotations, this thesis is entirely my own work.
- I have acknowledged all main sources of help.
- Where the thesis is based on work done by myself jointly with others, I have made clearexactly what was done by others and what I have contributed myself.

Signed:

Tarek Ahmed Abdel Aal

Date:

10/01/2024

The American University in Cairo
School of Sciences and Engineering

"Optimization of Vibro-Seismic Parameters for Enhanced Oil Recovery Application"

A Thesis Submitted by

Tarek Abdel Aal

To the

Petroleum Engineering Graduate Program

December 5th, 2023

In partial fulfillment of the requirements for the degree of

Master of Science in Petroleum Engineering

Has been approved by

Dr. Moustafa Oraby (Advisor)
Professor of Practice, Department of Petroleum and Energy Engineering
American University in Cairo

Dr. Ahmed El-Banbi (Internal Examiner)
Professor and Chair, Department of Petroleum and Energy Engineering
American University in Cairo

Dr. Ismail Shaaban Ismail Mahgoub (External Examiner)
Professor, Head of Petroleum Engineering Department
Future University in Egypt

Dr. Moustafa Oraby (Moderator)
Professor of Practice, Department of Petroleum and Energy Engineering
American University in Cairo

Graduate Program Director

_Dec. 5th, 2023__
Date

Dean

Jan 22 2024
Date

ABSTRACT

This thesis was conducted in the American University in Cairo by Tarek Ahmed Abdel Fattah Abdel Aal. The thesis is titled 'Optimization of Vibroseismic Parameters for Enhanced Oil Recovery Application.' The thesis discusses whether or not the combination of optimized physical vibration parameters with waterflooding would improve porosity, absolute permeability, relative permeability, and recovery when compared with just classical waterflooding. The optimized physical vibration parameters as well as methodology was used from a previous paper that was performed in conjunction with my thesis advisor on similar core samples. The experimentation was performed on five core samples with different porosities and absolute permeabilities. The original porosity, absolute permeability, relative permeability, and recovery which represents the classical waterflooding on its own were measured. These properties were then re-measured after the optimized physical vibration and waterflooding were performed. It was found that the coupling of optimized physical vibration parameters with waterflooding does improve all aspects of the core tested when compared with classical waterflooding.

Acknowledgements

I would like to thank everyone who have helped me on my journey to reach the end of this long road. I would like to extend thanks to my family as they are my main support system as well as my advisor, Dr. Mostafa Oraby, for constant guidance.

Contents

List of Figures

List of Tables

List of Abbreviations

EOR	Enhanced Oil Recovery
OOIP	Original Oil in Place
GOC	Gas-Oil-Contact
GOR	Gas-Oil-Ratio
OWC	Oil-Water-Contact
MMP	Minimum Miscibility Pressure
IFT	Interfacial Tension
WAG	Water Alternating Gas
SWAG	Simultaneous Water Alternating Gas
Hz	Hertz
KHz	Kilo Hertz
NaCl	Sodium Chloride
MPa	Mega Pascal
pu	Porosity Unit
md	Milli-Darcy
PV	Pore Volume
BOPD	Barrels Oil Per Day
PSI	Pounds per Square Inch

Chapter 1

Introduction

Throughout the life of a well, the production method changes with time as more hydrocarbons are being produced. Any well should pass through at least some if not all of the three stages of production. The three most common stages of recovery are: primary, secondary, and tertiary or enhanced oil recovery (EOR). Each of them has different aspects that are unique to each one. These recovery methods necessitate the employment of infrastructure and tools to access downhole and help in the production of hydrocarbons.

As production continues, the interaction of the fluids inside the rock with the rock itself also effects production. Many factors such as porosity; absolute permeability; and wettability affect how much of the hydrocarbon can be recovered before the well is abandoned. Many recovery methods and tools can be applied to prolong the time of abandonment and produce as much of the hydrocarbon as possible which will be mentioned and one method in specific has been taken as the main focus of research.

The primary goal of the study is to see what influence the combination of waterflooding and physical vibration has on rock characteristics, rock-fluid properties, and oil recovery. In terms of rock attributes, this study will look at the effect that physical vibration has on both porosity and absolute permeability. The rock-fluid properties are specified by the results of the relative permeability measurements. The oil recovery will be determined by waterflooding the core while undertaking relative permeability measurements. For each of the cores chosen for testing, all of these measures (porosity, absolute permeability, relative permeability, and oil recovery) will be repeated twice. Once before the physical vibration occurs with only waterflooding, and once after the physical vibration and waterflooding are combined.

1.1 Primary Recovery

The three typical stages of recovery are primary, secondary, and EOR. Primary recovery is when the “natural energy of the reservoir is used to transport hydrocarbons towards and out of the production wells” (Alagorni et al., 2015) There are four main drive mechanisms that are included in the primary recovery phase which are: solution gas drive, gas cap drive, water drive, and gravity drainage.

Solution gas drive is when the expansion of any gas that is dissolved in the oil and water is released and provides the energy for the oil and water to exit the pores as production continues on. When production is in the undersaturated section of the two-phase production curve (i.e., no gas production) then the expansion of the rock and fluids is what provides the drive energy. When in the saturated section of the two-phase production curve (i.e., gas production) then the release and expansion of the gas bubbles is what provides the energy for production. However, for this to occur the reservoir pressure needs to decrease below the bubble point pressure and this happens as

more oil and water has been produced. The typical recovery of this method is between twenty to thirty percent original oil in place (OOIP).

The gas cap drive occurs when there is a volume of gas above the oil being produced and the expansion of the gas cap pushes the oil out of the reservoir. Over time, the gas-oil-contact (GOC) will keep getting lower till it reaches the wellbore and then the amount of gas being produced by the oil will increase which is the gas-oil-ratio (GOR). The average recovery from this method is between twenty and forty percent of the OOIP.

The water drive production energy is provided by underground aquifers that have direct contact with the oil inside the reservoir and produce an oil-water-contact (OWC). As the oil production continues, the aquifer pushes further upwards and continues to drive the oil out of the pores. The usual recovery of this drive mechanism is from twenty to sixty percent of the OOIP depending on the size of the aquifer that is in contact with the oil. The main unique point for this drive mechanism is that the aquifer causes the production rate of the oil to become almost constant during production until the OWC reaches the well and the amount of produced water increases.

Gravity drainage drive mechanism is based upon the difference in density of the three phases: gas, oil, and water. These density differences cause a segregation differentiation to occur of the three phases which is the main drive mechanism in this case. This drive mechanism on its own is very weak and production is minimal and in nature usually occurs with any of the three previously described mechanisms.

Another primary recovery mechanism is through the use of artificial lift mechanisms. The two most famous artificial lift methods are the use of pumps to lift the oil out of the wellbore and towards the surface. The other is using gas lift which is when gas is injected inside the wellbore to lower the crude viscosity as well as increase the energy of the crude being produced.

1.2 Secondary Recovery

After the initial production drive mechanism energy begins to decrease with production continuation, the production of the oil also declines. This is when the second stage of recovery usually occurs and this entails the use of “external fluids” (Alagorni et al., 2015). The external fluids are water in a mechanism termed waterflooding or water injection or gas in a mechanism termed gas flooding or gas injection. The gas or water are injected from injection well(s) and the hydrocarbon oil is produced from production wells.

Water flooding is performed by injecting the water in several wells in a specific pattern around the production well in order to maintain the pressure inside the reservoir and produce the oil through the sweeping action of the water in much the same way as the water drive mechanism in the primary phase. The gas flooding has the same conceptual idea as the water flooding with some minor differences. The gas flooding is usually injected in the gas cap to maintain pressure of the gas cap and to drive the crude oil of the reservoir using the gas cap drive mechanism as previously mentioned in the primary production mechanism. The secondary production methods of water or gas flooding can add an incremental oil recovery between fifteen up to twenty percent of the OOIP.

1.3 Enhanced Oil Production (EOR)

The EOR methods come after both the primary and secondary methods no longer are capable of driving the oil out of the reservoir and to the surface. The main concept of EOR is to introduce external sources of fluids and energy to the reservoir production system in order to produce the oil and improve its recovery. The main purpose of the injected fluids is to: "boost the natural energy in the reservoir" and "second is to interact with the reservoir rock/oil system to create favorable conditions for residual oil recovery" (Alagorni et al., 2015). When speaking of favorable conditions, what is meant is through the "reduction of the interfacial tension (IFT) between the displacing fluid and the oil; increase the capillary number; reduce capillary forces; increase water drive viscosity; provide mobility control; create oil swelling; reduce oil viscosity; and alter the wettability of the reservoir rock" (Alagorni et al., 2015). Recovery enhancement of oil from EOR can reach between forty to sixty percent of the OOIP.

EOR methods are divided into two groups: thermal and non-thermal recovery techniques. The thermal techniques are steam injection, in-situ combustion and hot water flooding. The steam injection, as the name may suggest, is the injection of steam in the reservoir either in cycles or continuously. The difference between both techniques is that continuous injection requires injection and production wells in much the same way as water or gas flooding while cyclic injection of steam is done within the same production well. In-situ combustion is when oxygen rich gas is injected into the reservoir and then the gas is set on fire. This in turn creates a high temperature atmosphere inside the reservoir which leads to thinning of the oil and creating in-situ steam and hot water. All three of this combined drive the oil from the reservoir simultaneously in several fronts. With heavy oils, conventional water flooding is not a sufficient solution and therefore, hot water flooding is used instead. The hot water flooding is used to improve oil mobility and also enhance sweep efficiency.

For the non-thermal EOR mechanisms, there are two famous sub-groups of techniques commonly used which are chemical and gas injection. Chemical injection is when certain chemicals are added to water and injected inside the reservoir to modify flood efficiency which leads to higher oil recovery. The modification comes in three different ways which are: by increasing the viscosity of the injected water; lower the water relative permeability; and increasing the relative oil permeability.

The first type of chemical flooding is through the use of polymers which are aimed at enhancing both the vertical and horizontal sweep efficiency of the injected water. This is achieved by increasing the injected water's viscosity making it move at slower rate inside the reservoir and thus sweeping more oil and also lowering the injected water relative permeability which improves the mobility of the oil. Micellar when added to the injected water causes it to be miscible with the oil which when adding the polymer to it will improve the oil recovery and production. The main idea of the is to reduce the IFT between the oil and water along with the benefits of the polymer already discussed. Another method is to inject all three chemicals at the same time i.e., alkaline, polymer, and surfactant. The alkaline will minimize the adsorption by the reservoir rock; the surfactant will lower the IFT and create an emulsion; and the polymer will increase the viscosity improving the sweep efficiency.

Gas flooding is conventionally performed on its own or accompanied by water. The gas injection can be sub-classified into two groups: miscible and immiscible gas injection. Miscible gas injection is when the gas is injected above or at least at the minimum miscibility pressure (MMP) causing the injected gas to become miscible with the oil. This method improves oil recovery by increasing the oil displacement as there is no IFT. In addition, oil swelling as well as reduction of the viscosity of the oil. Immiscible gas injection is conducted at pressures under the MMP which is meant to maintain pressure of the reservoir. Water Alternating Gas (WAG) and Simultaneous Water Alternating Gas (SWAG) are both processes where both gas and water are injected inside the reservoir. This technique combines the advantages of both water and gas flooding which ultimately improves the oil recovery and production.

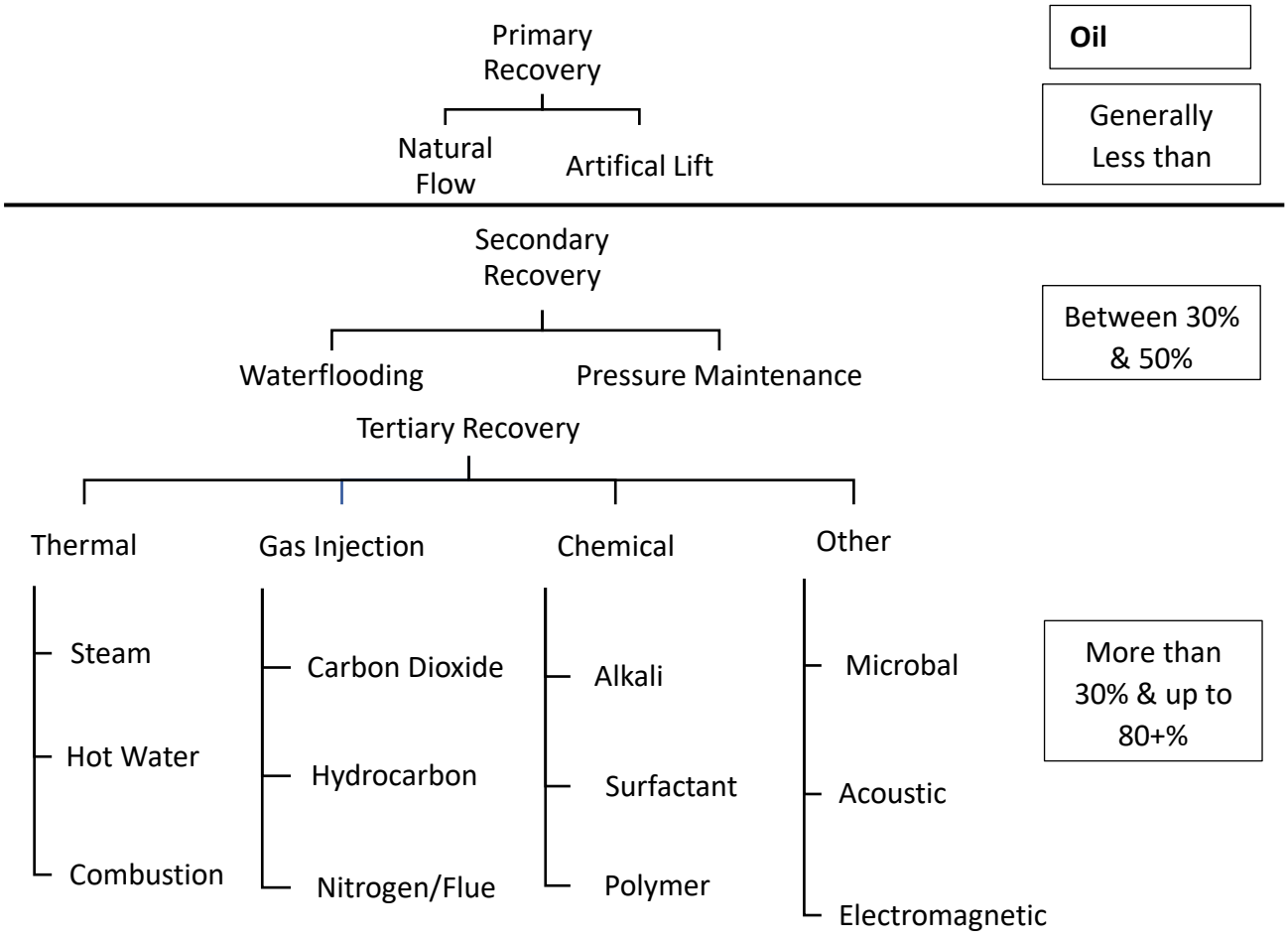

Fig 1: The Three Production Stages Categories and Sub-Categories

1.4 Rock and Fluid Properties Affecting Oil Production

The three conservation rules of "mass, energy, and momentum" regulate the quantity of flow as well as the relative displacement of oil from the reservoir (Yu-Shu Wu, 2015). To measure the quantity of flow inside reservoir rock, we must first understand and calculate many rock and fluid parameters, including absolute and relative permeability, fluid viscosity, interfacial tension

(IFT), wettability, and capillary pressure forces. Furthermore, as previously noted, it is critical to determine the reservoir's driving mechanism.

Reservoir rocks are porous medium meaning that the rock contains voids (pores) and rock-solid material (rock matrix). The pores are our main focus as they hold the reservoir fluids (gas, oil, and water) of which we are interested to produce (mainly the oil). These pores are connected to one another and how easily the fluids can pass through these connected cores is a measure of the permeability of the rock as per the equation developed by Darcy. Absolute permeability is the permeability of one single phase fluid; however, as the pores hold more than one fluid type at the same time (multi-phase) then the concept of relative permeability is vital. Relative permeability is the easiness to flow of one fluid phase relative to the other fluid phase or in other terms the "ratio of the effective permeability of the phase of interest to the absolute permeability" (Yu-Shu Wu, 2015). If the relative permeability of one fluid phase is higher than the other then the production and hence recovery of that specific phase is going to be much higher as the mobility of that phase is going to be higher. Relative permeability is dependent on saturation of the fluid along with the wettability of the fluid and pore size distribution.

Wettability comes into play when there are several immiscible fluids are found within the pores of the reservoir rock with one fluid (water or oil) wetting the solid rock matrix surface. From this, wettability can be defined as the "ability resulting from intermolecular interactions of a liquid to maintain contact with a solid surface when the two are brought together in the presence of other immiscible fluids" (Yu-Shu Wu, 2015). How much the fluid wets the surface is influenced by the cohesion and adhesion forces between the rock matrix and the fluid. These forces are governed by the rock mineral composition, the constitution of the fluid itself, and saturation of the fluid.

Capillary pressure comes into play when two or more immiscible fluids occupy the same space or in this case pore. The pressure of one fluid phase will be different than the other phase(s) located inside the pore. The less wetting phase or non-wetting phase (for gas phases specifically) the has a higher pressure than a more wetting one. Therefore, capillary pressure can be defined as the "difference across the interface between two immiscible fluids" (Yu-Shu Wu, 2015). The capillary force in porous medium such as reservoir rocks are affected by the wettability of the phase to the rock surface; the IFT; and the size of the pore itself. Interfacial tension is the tension found between any two liquids in this case the surface tension difference between water and oil as they are the main concern of this research. As wettability itself is controlled by the rock mineral and fluid properties then so does the capillary pressure. Capillary pressure is an important factor to consider as it determines the distribution of each fluid phase inside the pores of the reservoir rock and the amount of recoverable oil.

1.5 Enhancing Field Performance Methodologies

Normally, during the production life cycle, the hydrocarbons are produced through natural flow. As production resumes and the hydrocarbon volume decreases and so does the pressure difference thus lower the production rates. At this stage, secondary recovery mechanisms are used such as waterflooding and gas lift for pressure maintenance. Once all of the previously mentioned mechanisms become uneconomical, an external energy source is needed to produce the hydrocarbons which is entailed in enhanced oil recovery (EOR).

In order to choose the best enhanced oil recovery option for any field there are some parameters that must be looked into. One of the first parameters is the cost of acquiring and applying any technology. As the oil and gas industry is a business like all others, its main aim is profit; therefore, the capital and operational costs are very important to consider. Many projects are postponed or sometimes cancelled completely if it's not an economical option or if there are other more economical substitutes that would achieve the same outcome. Another parameter is the effectiveness that this technology has on the overall recovery of the crude oil. When choosing the best enhanced oil recovery option for any field, screening of the available options is performed and the most suitable option is selected. Furthermore, the risks that this enhanced oil recovery option poses on people and the environment is also carefully considered. All oil and gas companies perform risk analysis on the relative effect that each of the enhanced oil recovery option have on the personnel that will operate them as well as the impact it may have on the environment. If a certain enhanced oil recovery possibility possesses high risk to the personnel or to the environment then it could be disregarded as it is unsafe or acquires many risk mitigations.

Water flooding or water injection is a commonly used secondary recovery technique that increases the oil recovery. The water flooding enhanced oil recovery method, as the name suggests, uses formation rock compatible water to effectively sweep the oil inside the reservoir. It is widely used in the oil and gas industry as it is an exceedingly simple method that uses an inexpensive source of energy i.e., water. Moreover, the water that is injected into the formation is usually produced formation water and so its re-injection solves one of the main environmental problems most fields face which is safe disposal.

One of the main issues faced in water flooding is the poor sweep efficiency which arises from poor formation rock properties. Therefore, this research aims to combine water flooding coupled with the Vibroseismic technology to investigate the possibility of improving the overall produced oil through enhancing the porosity, absolute permeability and relative permeability of the cores.

1.6 The Vibroseismic Approach

The Vibroseismic is an old technology that commenced in the 1950s and since then has been researched with several applications being tested and employed. Vibroseismic technology is one that uses either an acoustic source from the surface or through the use of physical vibration downhole to vibrate the formation rock. The vibration of the formation rock alters and enhances the properties of the formation rock in both the rock properties such as porosity and permeability as well as the fluid-rock parameters. One of the applications of this technology is enhanced oil recovery as it improves the formation properties; therefore, it enhances the production of the oil inside the reservoir. These enhancements will not only improve the hydrocarbon recovered but will also improve injection efficiency.

The addition of the Vibroseismic method to an already established water-flooding system in a field should increase production by enhancing the injection, rock and fluid properties currently being undergone. This combination will make current mature fields more profitable and should maintain or increase production prolonging the lifetime of the field.

The Vibroseismic technology does not require excessive sums of capital or operational costs making it a cost-effective enhanced oil recovery method. In addition, it has little to no risk on personnel or the environment as it is a simple method that has no footprint on the environment. Moreover, a paper was published by myself and my professor and colleague regarding the optimization of frequency, amplitude and time factors in order to best improve the porosity and absolute permeability of cores. We were able to find the optimum 3 parameters to use in order best improve the porosity and absolute permeability which has provided great incentive to further the research in this coupling of waterflooding and optimized physical vibration.

Based on all of the above reasons, this provided me the motivation to choose this research topic as it holds many great opportunities for use in the field as well as it would also upgrade an already established enhanced oil recovery method.

1.7 Research Objectives

The first objective is obtaining the initial results of the cores in question by measuring the initial porosity and permeability of the cores as well as performing the classical waterflood experiment to get initial data to compare the effect of vibration. Afterwards, there is a need to optimize the frequency, amplitude and time factors to enhance the porosity, permeability, and fluid properties of the core samples. In order to confirm the results of the optimization a repeat of the waterflooding experiments after applying the optimized vibration parameters and measuring of the porosity and permeability to assess the results. All of these specific aims should then provide concrete evidence on whether or not the combination of Vibroseismic and waterflooding application should improve oil recovery or not.

1.8 Thesis Structure

The remaining thesis will be structured in such a way to present the research process step by step into why the research was conducted including the shortfalls of research performed by others. In addition, the thesis will also include how the research was conducted to make it as scientific and accurate as possible. Furthermore, the thesis will then present all of the results of the porosity, absolute permeability, relative permeability and oil recovery. Last but certainly not least, a thorough analysis will be conducted on the results obtained and how these results relate to both the hypothesis and to the previous work done (optimization paper of frequency, amplitude and time). The following is a list of all the chapters and what is expected of each chapter in terms of content.

1. Literature Review: Will provide the background information on the research performed by other authors that have completed work related to the same topic. It will also provide insight on the reasoning to choose this specific methodology and compare with results.
2. Research Gap and Hypothesis: Offers the missing part of literature that was found and what I expect the results to be according to the literature review.
3. Research Methodology: Outlines the methodology to reach test the hypothesis and how the experiments will be conducted to reach the required results
4. Results: Provide the initial and final results of all of the cores that have been measured for all of the properties that have been measured.

5. Discussion: Discuss the results from the previous section and relate to the literature review in chapter 2.
6. Conclusion and further work: Conclude the results of the research and possible ways to further this research.

Chapter 2

Literature Review

The three most common production stages are either primary, secondary or tertiary or also known as enhanced oil recovery (EOR). This research will be focused on one specific technique or technology that is part of the enhanced oil recovery mechanisms which is physical vibration.

The main target of this research is to see the relative effect that optimized parameters of the physical vibration have on the porosity, absolute permeability, relative permeability, and oil recovery factors when coupled together with the more well-known waterflooding technique. To do perform this research, optimized parameters of frequency, amplitude and applied time are to be used on the cores that will be tested. These optimized parameters are to be obtained from previous publications on the optimization parameters of physical vibration.

The paper that was published by myself and my professor was regarding the shortfalls found in all of the previous research that will be presented throughout this chapter. The main shortfalls that were found was the lack of consideration of the needed time of applying the physical vibration on the core samples. The time factor was the main novel solution provided by the publication as it was clearly seen that not only do the frequency and amplitude need to be optimized but also the time factor is also as crucial. Furthermore, other researchers, as will be presented, have discussed the concept of dominant frequency and amplitude without presenting a clear method of finding these dominant properties or the range of values to find them when dealing with the low frequency physical vibration method. We were able to identify a clear scientific method of how to reach these optimal or dominant frequency and amplitude and also provided the ranges of both properties of which we worked on.

2.1 The Basis of the Research – Optimization of Frequency, Amplitude and Time Factors

The Vibroseismic technology is a subject of interest for researchers, as it aims to enhance reservoir rock and fluid properties, increasing reservoir productivity. This technology involves vibrating rock formation with a pre-determined frequency and energy using either an acoustic wave or a physical vibrator. Previous laboratory work has not fully investigated the effect of vibration time (duration) on reservoir properties, and no previous work has discussed the optimum combinations of these parameters.

This research conducted laboratory measurements on multiple core plugs, both field, and outcrops, using various combinations of parameters, frequency, amplitude, and time to determine the optimum combination that ensures the enhancement of porosity and absolute permeability of the reservoir rock. The duration (time) in the measurements varies between continuous and time-steps, with the vibrating frequency and amplitude kept constant for the entire period of the vibration process. The vibration stopped after every time step, and measurements of the properties are taken to determine the optimum time that generated the maximum positive impact on both porosity and absolute permeability.

The research also aims to answer the question of whether the damaged property due to the vibration can be reversed or partially reversed by repeating the vibration with a better set of parameters. The laboratory work demonstrates the importance of optimizing vibration parameters before starting field trials, as the wrong combination of the three parameters can result in damaging rock properties, especially rock permeability.

A significant finding in this work is that the damaged parameters can be totally and/or partially recovered if the vibration is repeated with the optimum set of vibration parameters. This research also highlights the importance of optimizing vibration parameters before starting field trials and ensuring the optimal combination of parameters for optimal reservoir rock and fluid properties. For the outcrop cores tested, the optimal frequency was found to be at 10 Hz with an amplitude of 4 mm to be conducted for 15 minutes. While for field cores, the optimal frequency was to be at 10 Hz with no amplitude (zero amplitude) done for a time of 20 minutes. (Oraby et al., 2022)

2.2 Physical Vibration and Waterflooding Pivotal Previous Research

2.2.1 Physical Vibroseismic and Waterflooding Applications Combined

The writers believe that it is crucial to consider a number of aspects before deciding on a field. These considerations include the location of the land, the amount of oil that is currently there, the geology, the mechanics of the well, the availability of water, and the operating procedures. The land situation covers the leasing of the land and the availability of additional land should it be required for the project's completion. The oil that is now in use calculates the volumetric volumes of oil to determine how much can be generated. The geology examines the reservoir's architecture and conductivity in order to predict flooding. The mechanics of the well relate to whether or not new wells need to be drilled, together with their specific shapes and lengths, or if existing production wells need to be converted to injection wells. Finding an appropriate water source for injection involves the water source. Last but not least, the operating conditions address the ongoing operational problems that require solutions, for instance, facilities. When examining the Belcherville field, it was clear that the waterflooding project was effective because it was able to complete all of the procedures and checklists suggested by the writers. With 475 barrels produced per day, in 2008 it had the highest production.

When waterflooding is used, Mohammadian et al. (Mohammadian, 2011) tested the impact of an ultrasonic wave on the recovery of oil as well as the potential mechanisms. Two different generator types were employed, one with a power range of 100–500 watts and the other with a power of 110 watts, both operating at a frequency of 40 KHz. The experiments were performed on using normal and de-aerated 3 percent NaCl brine applied to a sand pack with initial porosity of 30-34 percent and permeability of 4 Darcy. Along with the main experiment done, two other experiments were performed to show the temperature change and pressure change that occurs due to the ultrasonic wave. According to Mohammadian et al. the two most significant mechanisms for recovery improvements were due to viscosity reduction due to temperature increase and emulsification due to pore pressure increase.

According to earlier research conducted by other authors, there was an increase in temperature of 4 to 16 degrees with an increase in power of 100 to 400 watts, respectively. Additionally, the pore pressure was raised from 2.1 psi to 2.3 psi by the application of the ultrasonic wave. The pore pressure dropped to 1.8 psi following the experiment, which is in agreement with earlier authors once more. These two occurrences are among the primary causes of the rise in oil production brought on by Vibroseismic with ultrasonic waves. The main experiments showed an increase of oil recovery by 16 percent due to the use of ultrasonic waves compared to conventional waterflooding.

Any field must be technically and economically feasible to launch a water flooding operation. A method was established, using the Belcherville field in Montague County, Texas, as an illustration. The field was developed with a total of 9 producing wells, which were able to produce 3 million barrels of oil in the field's initial production phase after it was discovered in 1946. The process consists of six steps, with "prospect identification" being the first. This means that the prospect must be located in a geological area that has a history of effective production. The next step is “prospect qualification” which comprise of all technical studies that need to be done to ensure that the field will produce efficiently in this project. These studies usually come from trustworthy geological, reservoir and production data of the field collected by the operators. The following step is the “economic analysis” which, as the name suggests, provides an analysis of whether or not the project will return money or not. As the oil and gas business like any other business is dependent on making money and so the waterflood project needs to make money. This involves making forecasts of production and reservoir models to see the relative production profile. After finishing the financial analysis and agreeing to perform the project, here comes the role of actually properly planning the project or as was termed “transforming the prospect to a program.” All data of all departments are collected such as geological, reservoir and production data in order to create a cohesive and holistic reservoir model to confirm the best waterflooding method or plan that needs to be applied to maximize the oil production. From this a re-development plan is made to start implementing the new waterflooding project. The “implementation” phase or step is focused on transforming the re-development plan from paper to reality in a safe and effective manner. The last step is “validation” which a constantly repeating step where more information collected with production and water injection is collected to enhance or improve the existing reservoir models previously created. In addition, the data collected will improve on the production forecasts which in total will improve the vision of the operators on the field production and economic analysis.

The effect of Vibroseismic application on waterflooded cores was tested to see if there was any improvement in the production of oil. The study was performed based on the usage of strong surface operated Vibroseismic generators. The experimental work was done on both natural core samples in addition to sand-packs. The main measurement to see the performance effect of Vibroseismic was via the rate of oil displacement by water with the presence and absence of the Vibroseismic source. This oil displacement by water was brought by calculating the oil/water relative permeability to see the oil displacement rate and residual saturation percentage. The tested samples were natural sandstone cores, sand-packs composed of quartz sand only with another composed of quartz sand and bentonite. The Vibroseismic waves applied has a frequency range

between 100 to 200 Hz which meant that the waves could affect a range of up to 2 kilometers without much affect from rock attenuation. The oil used in this experiment was kerosene with viscosity of 820 kg/m3 and water. The initial water saturation was 5 percent with permeability of the natural core being 1 μm2 and the sand-packs of 9.3 μm2 respectively. There were two methods of how the water was flooded; the first was having the water being injected in the same direction of the kerosene flow while the other was having them being injected in opposite directions. For the direct or same direction flow, the recovery increased from 32 percent before Vibroseismic to 60 percent in a lower time of 51 hours after Vibroseismic compared to 300 hours in the case of without. In the inverse direction flow, the Vibroseismic caused an incredible increase of recovery from the natural core and almost full recovery from the sand-packs (96 percent). In the lack of the Vibroseismic, the gravitational distribution of oil and water occurred during 20 days while with the vibro-energy the distribution was much quicker at a rate 500 times faster than without.

For the degassing, before the Vibroseismic was applied the rate of carbon dioxide production was approximately 0.2 percent per minute while after the rate increased to 3 or 4 percent per minute. Once the maximum amount of free gas was produced (40 percent), the rate decreased once more to 0.2 percent per minute. This would mean that there will be an increased rate of oil recovery compared to water recovery due to decrease in the relative permeability of water in the presence of the gas. When experiments were done of both gas free and carbon dioxide saturated water, it was found that in general the oil recovery by the use of carbon dioxide saturated water was greater than the use of regular gas free water. In addition, the application of the Vibroseismic energy to the sand-packs resulted in even greater oil recovery in both cases of water used. The proposed mechanisms that the Vibroseismic application operates by are that the application causes the molecules of both water and oil to adhere less to the pore walls allowing for more mobilization of the trapped fluids inside the pores. Moreover, the application increases the pressure gradient which thus will greatly reduce the water films that block the pore throats leading to a reduction in the relative permeability to both water and oil phases. This would then allow for more fluid to be able to exit the pore as the pore throat size has now gotten bigger. As the relative permeability of both oil and water decreases then this would ultimately mean that the relative permeability of water and oil also is reduced and so the interfacial tension is lowered. (Kouznetsov et al., 1997)

2.2.2 Physical Vibroseismic and Its' Effect on Different Rock Formations

How earthquakes affect the rock and its properties is very important to understand as it is the basis of how the vibrational Vibroseismic operates. Earthquakes work in much the same way as the Vibroseismic technique in affecting the rock. Energy is stored in the form of elastic energy in the rocks neighboring the rock in question. With the earthquake occurring, tectonic forces load the brittle rock. Once the fault strength threshold is reached, the fault will begin to slide and the previously stored elastic energy is then converted into heat due to the friction that occurs as well as surface energy that transpires due to rocks being crushed. An unstable condition may arise if fault strength threshold is reduced quicker than the driving force of stress. The fault then slips dramatically and can then cause an earthquake causing the stored elastic energy to be sent out as seismic waves hence the 'seismic' in Vibroseismic. The elastic energy when turned to seismic waves can then lead to a decrease in the net stress of the area around the origin of the earthquake.

The strength of the rocks decreases with the passing of time as well as displacement. The stress changes that have happened because of the seismicity and elastic energy release will affect the pore pressure and the relative change is determined by how much the stress has been altered. (Lockner and Beeler, 2002)

Further reduction in enrichment of the rock and fluid properties was acquired for the carbonate core but also with maximum deflection at optimal frequency of 10 Hz. Regarding the amplitude, once the maximum value is found to improve the properties further increase in the amplitude yields no further improvement.

It was concluded that frequency has a more influential effect on changes in formation properties compared to amplitude. Also, the maximum improvement in these formation properties occur at an optimal frequency. A similar experiment was performed at a larger frequency to see the effect this had on clean sand packs and sand packs with bentonite under confined pressure. Similar results were found that the vibration enhances the permeability due to grain redistribution and also that production can be enhanced as parameters of porosity and permeability combined allows for more oil production.

2.2.3 Physical Vibroseismic Effect on Rock and Rock-Fluid Properties

Several aspects can change from the application of vibration on the formation. Experimental efforts have been made in order to better understand these alterations and the frequencies needed to be used. A lab experiment was conducted to better understand the effect of the frequency and amplitude only of the vibration applied on a rock on certain rock and fluid properties being: porosity, permeability, relative permeability, capillary pressure and residual oil saturation. The trials were done on synthetic, field sandstone, and field carbonate cores. Major improvements were found for synthetic cores in all of the above-mentioned rock and fluid parameters at specific or optimal frequency, in this case it was found to be 10 Hz. The actual field cores also showed maximum enhancement of rock and fluid properties at an optimal frequency of 15 Hz; however, the improvement was not as profound as in the case of synthetic cores.

The research by Ariadji has made an effort to provide the first understanding of the actual impact of Vibroseismic waves on the improvement of both rock and fluid properties. The first production forecast study on the impact of seismic waves on oil-bearing strata was done in the lab or through reservoir simulation by Ariadji (T. Ariadji, 2005). The impact of the seismic waves on formations was presented for the first time using actual lab work. This research was crucial because it offered a much less expensive capital method to be used because the typical secondary and tertiary recovery mechanisms, like water flooding, steam injection, and chemical flooding (using surfactants and polymers), are all used around the world and require a significant initial capital investment. Additionally, Ariadji detailed a case study of a prior pilot and revealed encouraging findings with an increase in field output in addition to a number of studies that all indicate in the direction that the seismic waves will enhance the rock and fluid properties in turn. Additionally, Ariadji was the first to explore the optimization of frequency and amplitude parameters for various core types and shown that improvements outside of or prior to this range were negligible.

Investigations have been done into how permeability and porosity are affected by earthquake cycle periods. The experiment was carried out using a "spring-slider dashpot model" and numerical model simulators. The purpose of this model is to quantitatively depict the whole cycle of the seismic wave, or "earthquake wave," and its interaction with the rock, or more precisely, faults. Due to the fact that the authors specifically focus on faults as one of the main causes of fluid pressure, rock-fluid characteristics and interactions are largely dependent on the action of faults or tectonics size of the slipping zone and hydraulic diffusivity are the two key variables that control the evolution of the fault movement in the "thermal pressurization model" adopted in the numerical models included in this research (Bizzarri, 2011). Variations in porosity, permeability, or both have an impact on hydraulic diffusivity. The highest differences occur during the dynamic unsteadiness time window, which is accompanied by significant changes in the state variable and effective normal stress. Additionally, consequences are not just mechanical but also chemical. As an example, consider the mending or sealing of a fault brought on by mineral precipitation. The “rheology of the fault” (Bizzarri, 2011) and earthquake recurrence time (controls both rock stiffness and capacity to hold elastic energy) are both influenced by permeability changes in the rock. Furthermore, it has been found that permeability changes have a much greater impact on both hydraulic diffusivity and earthquake instability when compared to the porosity changes. The permeability variations in the rock have an impact on both the "rheology of the fault" (Bizzarri, 2011) and earthquake recurrence time (controls both rock stiffness and capacity to hold elastic energy). Furthermore, it has been discovered that, when compared to porosity changes, permeability changes have a far higher influence on both hydraulic diffusivity and earthquake instability.

Heterogeneity can affect how waterflood in a reservoir can react and effectively produce the oil in place. A numerical investigation was completed in order to see the relative effect that heterogeneity has on waterflooding applications especially in terms of relative permeability. The tested heterogeneity types tested were: stratification both in series and in parallel; vugs; and single and multiple lenses with varying permeability. The interfacial tension between oil and water, which was set at 50 dynes per centimeter, was one of the initial hypotheses. It led to significant mistakes in the waterflood relative permeability data for lens systems, but only minor errors for water-wet systems. This is mostly caused by the constrained permeability channels that lenses produce. Additionally, it has been demonstrated that small and evenly distributed lenses, regardless of their permeability, have essentially little impact on the performance of waterfloods. For layered systems, the results are suitable as long as the ratio between the layers goes to unity (one). High permeability channels or powerful capillary pressure crossflows may cause evident mistakes to emerge when ratios start to rise, such as in the case of a 10:1 layer permeability ratio. It was decided to test vugs and wormholes in a laboratory setting since vugs are extremely difficult to replicate due to rapid changes in permeability as well as discontinuity in the rock contact and relative permeabilities. Vuggy and wormhole simulation systems were implemented using glass bead packs and mesh screens. When employing field rates instead of lab rates, capillary pressure played a significant effect and occasionally caused the oil to become trapped within the vugs. At lab rates, the water washed the oil regardless of its wettability. This would imply that waterflooding would not be the best choice in strong water-wet vuggy systems. As the water-oil interface changed until all the oil had left the system, water relative permeability in the direction of flow was zero at high

water flow rates. When the vugs were small in size and properly distributed provided the best results according the author as there are no high permeability channels. In general, “According to the author, the greatest results were obtained when the vugs were small in size and evenly dispersed since there are no channels with a high permeability. According to one study, "well distributed heterogeneities have little effect on waterflooding results, but as the heterogeneities become channel-like, their influence on flooding behavior becomes pronounced.” (Huppler, 1970)

Wettability is one of the fluid-rock characteristics that has a significant impact on recovery. For the purpose of demonstrating the impact that wettability has on waterflood recovery, 50 slow rate experiments have been carried out. The Berea sandstone from the West Virginia Berea area served as the source for the used cores. To "identify the dominant variables that control wettability of the crude-oil/brine/rock (COBR) systems" is the main goal of this study (Jadhunandan and Morrow, 1995). Additionally, research the connection between wettability and waterflooding-assisted oil recovery. All of the Berea sandstone cores were taken out in advance of the experiment and submerged in the brine solutions for ten days. To test the permeability and replace the used brine, the cores were placed in the Hassler sleeve core holder. Using the Hassel sleeve core holder and oil flowing through the core under constrained pressure, the initial water saturation was also determined. The cores were aged in the crude oil for 10 days (Blends of Soltrol 130 and paraffin oil). Some cores aged at ambient temperature, and others did so between 50 and 80 degrees Celsius. Furthermore, some cores were left to age for up to 20 and 40 days to see the effect of aging on wettability. Once the cores were aged, they were placed back into the Hassler sleeve core holder and 20 PV of brine was injected and recovered oil volume was recorded. It was shown that the wettability is affected by the type of crude oil, the brine used, the initial water saturation and the aging time of the cores with crude oil. With the increase in aging time and decrease in the water content (initial water saturation) before aging causes the cores to be less water-wet. Moreover, the oil recovery increased with alteration of the wettability from strong to a maximum at neutral wettability.

The idea of colloidal mobilization is one of the first ways that output can grow as a result of transient stress. The term "colloid" refers to any particle with a diameter between one nanometer and 10 micrometers, which includes many of the particles found inside the pores of rocks. The filtration process that takes place as a result of the colloids passing through the rock pores results in "colloidal deposition," (Manga et al., 2012) which in turn reduces permeability. But if these colloids are mobilized rather than deposited, the result will be the opposite, increasing the permeability. The same results have been clearly demonstrated in studies using low-frequency stimulation with frequency ranges of 26 to 150 hertz. The enhanced transportation of fines or colloids through the pore structures as well as mobilization of deposited colloids inside the pores. Another method that transient stress can improve production is through the mobilization of non-wetting phase droplets and bubbles. Non-wetting phase fluid, either gas or liquid, usually exists as an emulsion of droplets inside the continuous wetting phase fluid. Flow is affected due to difference in interfacial tension between both fluids as well as the pore structure of the rocks.

An additional force known as an "inertial body" (Manga et al., 2012) with an oscillatory force and a specific amplitude is added inside the pores by the oscillatory wave brought on by the vibrating of the pore walls. The fluid can flow out of the pore if the new force enables the pressure

inside the pore to reach the threshold capillary pressure. It has been discovered that the oscillatory force and frequency are negatively correlated, with lower frequency waves causing stronger oscillatory forces. In addition, the value of the "mobilizing acceleration amplitude" (Manga et al., 2012) has found to increase with increasing frequency of the wave. These relationships show that the mobilization of droplets rises with increasing wave frequency but decreases with increasing wave amplitude. The increase in the permeability happens almost instantly but the recovery of the permeability to its original state can take an extended period of time. The slow recovery of the permeability occurs due to the slow depressurization of the pore system and fractures which is the main reason for the increase in the permeability.

Permeability variation was put into question under the influence of a transient disturbance that usually occurs due to earthquakes or enhanced oil recovery mechanisms like the Vibroseismic application. The permeability variation was measured before and after vibration disturbance for both intact and fractured core samples of both Kushiro Cretaceous sandstone and Shikotsu welded tuff. Regarding the sandstone sample, it was saturated with water for 3 days after initial cleaning and drying and three confining pressures were applied to it which were 3, 10, and 15 MPa. The transient disturbance that was operated was at 0.5 Hz frequency; amplitude of 11 MPa and performed for 200 seconds. For the welded tuff, also 3 other confining pressures were applied at 0.1, 0.5 and 5 MPa with the axial stress having a frequency of 0.05 Hz; 2 amplitudes of 0 and 8 MPa and also done for 200 seconds. What was found was that there was an initial decrease in permeability for the intact cores which was thought to be because of "consolidation over time under the confining pressure." As the confining pressure increased so did the reduction of permeability for the intact sandstone cores; however, the results were different in the fractured cores. In the case of the fractured sandstone, the permeability was almost constant with reduction of permeability increasing as the disturbance amplified. On the other hand, for the pore pressure disturbance higher permeabilities were found with the intact cores with an increase in the disturbance in pore pressure. However, the opposite occurred for fractured sandstone with the permeability reduction increasing with higher pore pressure disturbance. For the Shikotsu welded tuff, the same exact results were found for the intact and fractured rock samples. Overall, what was found that there is an initial decrease in permeability, but after some time the stress disturbance would increase the permeability. The only downfall was if there was high clay content which would be offset because of the increased consolidation of the clays. The consolidation effect was more profound in fractured samples due to the "plastic and viscous deformations" which occurred alongside the "elastic deformations, of the mineral particles on and near the ruptured surface." The pore pressure disturbance had a more imminent effect when compared to the transient stress disturbance as the axial stress only affects in the axial direction; however, the pore pressure disturbance would increase water flow paths allowing for a larger effect. The stress disturbances have showed both increasing and decreasing effect on the permeability depending on the rock type but mainly the time of it was applied. (Boeut et. al, 2019)

The relationship between the Poisson's ratio and permeability has been put under investigation especially in areas around faults where a seismic wave has been applied. Core samples were taken from Well-A located along the Chelungpu fault in central Taiwan. The core samples were taken from the fault zone at depths ranging from 482 until 1316 meters. The

Chelungpu fault movement was the reason behind the Chi-Chi earthquake that took place in 1999. The core samples were different in composition with some of them containing silt content than others (more silty-sand) and even the grain diameters were found to have been ranging from 40 up to 160 micro-meters. The different grain sizes cores were placed into two categories 'Type-A' and 'Type-B' according to their respective distributions. Seismic velocity measurements were made using a "gas-medium high pressure and high temperature deformation apparatus." This device produces required confining pressures and pore pressures. The permeability as well as the Poisson Ratio was measured under varying effective pressures. What was found was that there does exist a relation between the seismic velocity and permeability for some of the core samples. In the silty-sandstone and sandstone with a large percentage being fine in nature the correlation between both parameters changes with the controlling factor being the clay content as well as the degree of sorting. Sandstones with well-sorted grains displayed small permeability-related variations in the Poisson ratio. Additionally, silty-sandstone-type rocks' permeability is largely dependent on pore pressure. The permeability and Poisson's ratio both rise along with the increase in pore pressure. Furthermore, it was discovered that the water content of the rock pores and the nearby water supply, if any, were related to the fault's strength. (K. Kitamura et al., 2010)

The influence of a brief disturbance, which typically results from earthquakes or increased oil recovery techniques like the Vibroseismic application, called into question permeability fluctuation. For intact and cracked core samples of both Kushiro Cretaceous sandstone and Shikotsu welded tuff, the permeability variation was studied before and after vibration disturbance. After initial cleaning and drying, the sandstone sample was submerged in water for three days, and then three confining pressures of 3, 10, and 15 MPa were applied to it. The transient disturbance ran for 200 seconds at a frequency of 0.5 Hz and an amplitude of 11 MPa. Moreover, 3 additional confining pressures were applied to the welded tuff at 0.1, 0.5, and 5 MPa for 200 seconds each, with an axial stress frequency of 0.05 Hz and 2 amplitudes of 0 and 8 MPa. It was discovered that the intact cores' initial decrease in permeability was due to "consolidation over time under the confining pressure," according to what was discovered. As the confining pressure increased so did the reduction of permeability for the intact sandstone cores; however, the results were different in the fractured cores. (K. Kitamura et al., 2010)

The permeability was nearly constant in the case of the cracked sandstone, with the drop in permeability increasing as the disturbance grew more intense. On the other hand, as pore pressure disturbance increased, higher permeabilities were discovered in cores that were still intact. For fractured sandstone, on the other hand, the permeability reduction increased with more pore pressure disturbance. The complete and fragmented rock samples from the Shikotsu welded tuff yielded exactly the same results. (K. Kitamura et al., 2010)

Overall, it was discovered that whereas permeability initially decreased, it eventually increased as a result of the stress disruption. The sole drawback was a high clay percentage, but it would be offset by enhanced clay consolidation. Due to the "plastic and viscous deformations" that took place alongside the "elastic deformations, of the mineral particles on and near the ruptured surface," the consolidation effect was more pronounced in fractured samples. The pore pressure disturbance had a more imminent effect when compared to the transient stress disturbance as the axial stress only affects in the axial direction; however, the pore pressure disturbance would

increase water flow paths allowing for a larger effect. The stress disturbances have showed both increasing and decreasing effect on the permeability depending on the rock type but mainly the time of it was applied. (Boeut et. al, 2019)

2.2.4 Physical Vibroseismic and Improved Recovery

Low frequency seismic wave creation from the surface has been demonstrated to yield the greatest results, allowing other researchers to pursue this theory further (Roberts et al., 2002). The Department of Energy and numerous institutions collaborated on a research initiative to monitor field downhole tests when seismic was used, conduct lab experiments, and simulate theoretically the seismic EOR phenomena. Applying 25 Hz with a 150-psi amplitude causes changes in the pore pressure, which in turn causes a rise in fluid pressure decrease. The authors connected this to two logical explanations. An increase in oil's ability to flow through pores that were previously filled by brine was one of the explanations given. Due to the high oil viscosity and increase in oil's relative mobility to water, pressure will rise. The other factor is the immobilization of one or both fluid phases, which lowers permeability but raises pressure, causing the transition from wettability to non-wettability. When applying the vibration during a flood, the same thing happened. The vibration that occurs during waterflooding was discovered to boost water output while decreasing oil production. Production increases by around 20 percent during the field testing. A generalized elastic porous media balancing equation was created using these data.

Zhang and his colleagues similarly discovered the same outcomes (Zhang et al., 1999). On a field that could only previously recover 17.2 percent after using water injection, low frequency physical vibration was used. To better depict the effects that occurred in the reservoir, a geo-mechanical model was developed using the vibrational experience and data. Due to a rise in the differential pressure in the oil layer and a decrease in the interfacial tension between the water and oil phases, it was discovered from these that vibration can improve the flowing velocity of fluids inside the formation. As gas is discharged, the idea of fluid redistribution has also been discovered to exist, with redistribution taking place due to density differences that favor oil production. Additionally, the stress relaxation on the rock grains increases permeability, and the stress wave generated by the propagation of the vibration wave may result in micro-fractures. Moreover, depending on the frequency employed, vibration can diminish the interfacial tension that exists between the grain surface inside the pores and the remaining oil present in the system. In benefit of oil production, this would have an impact on both the capillary pressure and relative permeability curves. In rare circumstances, the oil coating can be broken, lowering the viscosity of the fluid.

The impact of seismic vibration properties specifically amplitude and frequency in freeing trapped oil (diesel) in a pore model structure was investigated. The advantage known regarding seismic vibration is in “mobilizing trapped oil droplets that otherwise cannot be produced with existing technologies.” (Kanjirakat et al., 2022). This is mainly due to the wettability forces especially in oil-wet reservoirs, the permeability and porosity of the rock itself. The observe the relative effect of the vibration, an experimental approach was undergone. The experimental approach was conducted by using a vibration generator or seismic excitor which main function is to vibrate the model under test with set amplitude and frequency. To see the effect of the vibration

itself, the tested model is placed above an LED pad to allow for imaging of the core to be taken place. The vibration applied is in the horizontal direction i.e., parallel to the tested model. The water level is kept constant through a reservoir tank pumping water at the same inlet pressure and the overflow outlet of the model at a certain height keeps the water level constant. A definite volume of diesel (approximately 15 micro liters) is injected into the test area via a syringe and through controlling of the inlet pressure the droplet is entrapped. To know the effect of the vibration, the test model is imaged before and after. To differentiate between the phases, the water is colored blue.

A 3D printed model is used to represent the pore structures of a rock and is used throughout the experiment. The model is created to have a pore throat size of 0.2 millimeters. What was found was that for the same input voltage utilized by the vibration generator an increase in the frequency causes a severe (exponential) reduction in the amplitude especially for high voltage inputs. The displacement amplitudes produced are lesser than 1.5 millimeters for all the frequencies tested except the 5 hertz. To place into perspective, an amplitude of 1.5 millimeters is the same as an earthquake with strength of 3 on the Richter scale. The diesel flows after injection into the 3D model via the aid of the injection pressure of the water and trapped through adjusting the level of the model to a critical point. Once the diesel is stuck in the middle section, no more flow will occur. Several amplitudes and frequency combinations were applied to the pore model for a time of 5 seconds each. It was found that frequencies lower than 20 Hz show no noteworthy enhancement of the dislodgment of the diesel from the middle chamber. For frequencies of 40, 60, and 80 Hz higher than 5 percent improvement was noted when combined with an amplitude of 0.5 millimeters. Moreover, below the amplitude of 0.5 millimeters once again no notable difference was noticed in the pore model structure. Furthermore, for the frequency range of 40 to 80 Hz, improved acceleration rates were seen reaching higher than 40 m/s2 which is capable of mobilizing the diesel injected. Interestingly, for 100 Hz the fluid acceleration was even higher with no observable change to the diesel injected which the authors described was due to the very high speeds not being able to be conveyed to motion of the pore walls. Also, the slip factor of the walls while vibrating at high frequencies. It was found that the best frequency ranges were between 40 to 80 Hz with amplitudes higher than 0.5 millimeters. (Kanjirakat et al., 2022)

A study was conducted in order to find an analytical model of the Vibroseismic stimulation application in order to describe the mechanism of how more residual oil can be mobilized. The model is aimed at providing the basis to efficiently use the Vibroseismic application. The model itself is composed of blocks of different sizes that is meant to represent oil-saturated rock formations. The large blocks consist of several smaller sized blocks and the block sizes depend on the geological structures and processes of the formation. The correlation between the rock sizes is dependent on core measurements and photographic measurements from the open hole. When applying the Vibroseismic stimulation to the model created, low frequency energy is shifted from the larger size blocks to the smaller size blocks. This in turn will produce high frequency vibration in the smaller size blocks of 10 to 20 kHz along with an external low frequency of 120 Hz. The high frequency vibration affects the oil in the smaller size blocks by affecting the capillary forces interaction between the oil and the formation rock allowing more oil to be made to move freely inside the pore structures. In addition, heat energy is created when the frequency alters from low

to high also increasing oil mobility. The now free to move oil can now be able to exit the pore at a higher volume (higher recovery) as more oil is now mobile. When comparing these results with the results obtained from the experimental noise produced from pilot tests of the Vibroseismic application in different fields in Russia, it can be seen that the results are in agreement. 3 wells: 2035, N471, and N331 located in the Pavlovskoe, Byrkinskoe, and Chernushinskoe fields respectively were used for the experimental testing. (Lopuchov, 1999)

2.2.5 Latest Physical Vibroseismic Field Application

Vibroseismic applications were most recently used in Indonesia's Tempino Field (Sitompul et al., 2021). The authors were the first to address the subject of capital and operational investment in EOR projects. Vibroseismic is a more cost-effective application strategy since it does not require the large financial and operational commitments required by the current conventional EOR methodologies. Additionally, it reacts rapidly; is environmentally friendly; and can readily be moved to other locations. The optimal frequency to use before beginning the field pilot test was found to be 20 Hz after lab studies were conducted to establish the best frequencies to be used. A similar test was carried out once more in the field prior to starting the yield test to establish the optimal frequency and amplitude, which was found to be 20 Hz. After six weeks, there was a 25 barrels oil per day (BOPD) increase in oil production rates following the vibration, or around 14 percent for the first area. Over the course of the subsequent four months, production grew rapidly and peaked at 225 BOPD, up 50 BOPD from the initial 175 BOPD or around a 30 percent increase. The output in the second region under investigation also improved, rising from 39 to 48 BOPD, or about 23 percent, in total. For both sites, these effects remained for around five to six months.

Vibroseismic methods, as the name suggests, is the utilization of vibrational source of energy via seismic wave propagation or physical vibration in order to enhance the production of oil. The seismic wave propagation and thus stimulation depends on several rock parameters which are: compressibility factor, elasticity, size of the grains, and their densities (Irfan et al., 2016). The effect of earthquakes has been compared to the use of seismic wave propagation in order to influence rock properties alteration. When the seismic wave is applied at the dominant or optimal frequency to a formation, the wave will convert to ultrasound. This dominant frequency is dependent on fluid saturation of oil and water and both the size and tightness of the of the grains. This approach is more applied more in cases of low permeability zones that have been depleted and also contain bypassed or trapped oil.

It has been discovered that strain amplitudes as low as 10^{-6} can improve reservoir output by increasing the flow of streams and springs, raising the water level in wells, and other natural system parameters. The permeability as well as the fluid mobility of formation rocks can be improved by stress-induced oscillations, such as those that come from earthquakes. When closely looking at earthquakes, it can be made clear that the vibration occurring due to these earthquakes have altered the fluid-rock properties and relations in the rocks around the area of the earthquake.

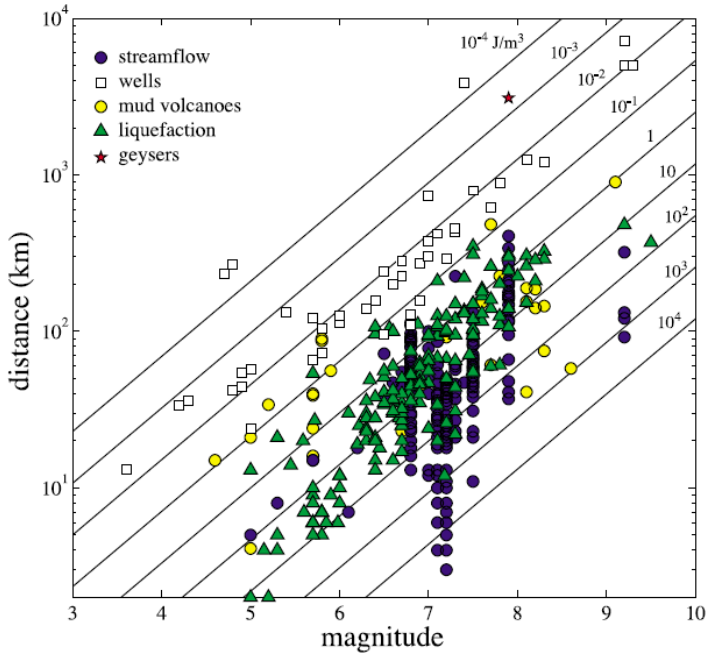

Fig 2: Relation between earthquake magnitude and epicenter distance along with the changes in the fluid-rock properties (Manga et al., 2012)

From figure 1, it is apparent that the earthquakes have a large-scale effect over a great distance reaching up to hundreds and thousands of kilometers. What is also clear here is that the lower energy densities produce a more profound effect as they influence a larger distance from the epicenters of the earthquakes. The authors claim that it is neither rational nor reasonable for static stress generated by fault movements or slips to result in such a consequence across such vast distances. The authors postulate that the effect of dynamic stress is what causes the shaking effect. This idea can be further solidified as there is no sign of permeant damage and therefore, the wave propagation must occur through the transient stress which in turn change both the rock and rock-fluid properties. Furthermore, it can also be inferred that small shift in the transient stress is capable of producing short-term or long-term variations to the rock and fluid-rock properties. The main changes that were found to have changed was the permeability of the rock along with the mobility of fluid through the rock. This entire concept can then be used further as an engineering tool to alter both properties through applying low-amplitude transient stress which is the entire basis of the Vibroseismic approach. (Manga et al., 2012)

2.2.6 Physical Vibroseismic Field Application Tools

Another plausible method that will allow for the wave effect propagation to reach a larger radius is through the use of downhole vibration tools. These tools are aimed at producing the needed vibration downhole instead of on surface. A tool was patented in order to produce the

vibration downhole (Westmark et al., 2001). One of the ways that vibrational method can be applied in the wellbore is through the use of backwards whirl occurrence. This is when a small cylindrical mass rotates in a larger cylindrical mass in that the center of rotation at any one instant is the location of contact between the two cylinders. The tool uses the backwards whirl into its own advantage in three ways. First of all, it allows for a realistic rotations per minute (rpm) at low frequency to produce a much more amplified frequency in the formation. Second of all, the gravitational effect that the tool has on the formation is much higher and so the force that is applied with each contact is large and effective. Last but not least, the effect of backwards whirling is very similar to an eccentric orbital vibrator which will create both shear and compressional type was in the formation. The authors suggest that the permeability will increase due to the differential velocity of both types of waves as compressional waves better in fluids and also due to the varied propagation speeds causes the permeability to increase. However, one of the conclusions made was that the downhole vibration tools may be successful sometimes; however, surface vibration generators have a much higher success rate.

Similar results were found using ASR tool (Kostrov and Wooden, 2008). It was found that both the API gravity and gas to oil ratio (GOR) affect the success of the downhole vibration methods. One of the field cases used two downhole in-situ seismic generation tools. The vibration generator was applied for a grand total of 20 months in 47 production wells. There was an increase in total oil production of 215,000 barrels with a decrease in oil saturation by more than 50 percent. Also, the radius of response was much more than the anticipated 1 mile. The same technology was applied for a carbonate reservoir with permeability range of 1 to 20 md. and being one of the lowest recoveries in the entire Permian Basin. The same two tools were installed at a difference of three quarters of a mile apart. The production data showed that the two tools were able to increase production in the entire field of approximately 100 wells with simulated radii of more than 1 mile each. This technique was able to increase the production decline from 14.5 percent to 12 percent with incremental growth of oil production by above 100,000 barrels. It was made clear that seismic simulation does not affect only one well but affects a larger radius around it being at least three quarters of a mile in sandstone and 1 mile in carbonates

2.3 Ultrasonic Wave Application and Its Application with Waterflooding

Nikolaevskiy (Nikolaevskiy, 1992) shown that vibration enhances oil recovery by restoring permeability. The author hypothesized that this may be achieved in a real-world setting by vibrating from the surface and continuing production at specific, ideal vibrational frequencies that are unique to each type of formation. Nikolaevskiy asserted that low frequency seismic vibrations and earthquake impacts were related and that both had an impact on the characteristics of the formation. It was found that the ultrasonic vibrations produced by the low frequency seismic waves can have an impact on the small oil droplet due to their short wavelengths. Additionally, the vibration of the oil droplets redistributes the two phases of water and oil inside the pores, making it easier to produce oil.

An application of ultrasonic waves was implemented for a waterflooding case study in Nigeria (Abdulfatah, 2018). The research was aimed at showing the improvements in fluid properties of traditional waterflooding compared to waterflooding coupled with ultrasonic

application. The work was divided into sections; experimental work and simulation. The experimental section of the research included applying classical waterflooding to an oil sample from a local field, Niger Delta with a range of frequencies ranging from 24 to 54 KHz. The simulation part was used for performance prediction with MATLAB models to analyze the results. The results of both portions of the work shows an improvement in the critical oil saturation of 0.09 which is equivalent to approximately of 25 percent. In turn, this reduction would mean an increase in the overall recovery of the oil by around 50 percent. The ultrasound application also lowered the connate water saturation to 0.27 at a relative permeability of 1 which entails that the waterflooding as exceedingly effective which connects to the 50 percent rise in oil recovery. Abdulfatah has provided not only technical information on the success of the combination of the waterflooding and ultrasonic application together but has also provided some awareness on the commercial aspect. Most other EOR applications require large initial capital and operational costs while this application has proven to enhance the oil recovery without the requirements of large investments making it a more economically feasible method to be implemented.

An investigation was performed on the ability of ultrasound waves in mobilizing higher oil recovery. To do this, an experimental approach was used where core flooding was done in two different dimensions both horizontally and vertically. In order to see the actual effect of the ultrasound waves, oil/water relative permeability was done before and after the ultrasound waves as well as the total oil recovery to measure the waterflooding performance. Moreover, to measure the waterflooding performance fractional flow curves where also drawn to see the average water saturation before and after the use of ultrasound waves. Furthermore, this investigation was not only done on consolidated cores but the effect of ultrasound waves on unconsolidated cores was also tested. The main purpose of the ultrasonic waves is to "provide continuous energy to create hydrodynamic waves downhole for dislodging trapped oil at a distance from the source." (Alhomadhi et al., 2013) The experiment's main apparatuses are vessels to store fluid (oil and water); displacement pump connected to the fluid vessels; core holder to house core being tested; collector of outlet fluid; and the acoustic wave generator. The core type used for the consolidated section of this investigation was Berea sandstone and the oil used throughout this experiment is Saudi Arabian crude oil (Arabian light) with viscosity between 13 to 16 cp and an API gravity of 31.2°. The ultrasonic wave generated for this experiment at an elevated frequency at 50 kHz and power of 300 watts applied in two ways either by several short pulses of a few minutes per pulse or by continuous waves. Regarding the horizontal core floods, the wave stimulation allowed an increase in the total recovered original oil in place from 54 to 59 percent. Improvements of relative permeability in the case of ultrasonic waves application is clear at water saturations higher than 60 percent of the total pore volume which may suggest that this application can be more advantageous in the early stages of the production rather than later. Furthermore, the average water saturation in the wave stimulated compared to without is higher with earlier breakthrough. In the case of the vertical core floods, the presence of the wave also increased the total oil recovery from 49.9 percent to 58 percent. However, what was interesting was that the breakthrough in this case was delayed than the original case. When testing lower permeability samples, it was found that longer wave stimulation times were needed in order to mobilize the oil. Furthermore, the maximum improvement in oil recovery occurred in the intermittent cycled wave stimulation as the level of oil separation in the pores was reduced. The continuous wave application between 30 to 45 minutes

did increase the recovery but to a lesser extent when compared to the cyclic application and also caused earlier breakthrough of the water due to the separation of oil that occurs in the pores. In the unconsolidated cores, they were only flooded with brine as oil cannot be applied in this case. The wave stimulation application caused sand production as well as flow resistance of the injected brine inside the pores. This is due grain motion and movement from the ultrasound waves. (Alhomadhi et al., 2013)

Further research on the same notion concentrated on how the ultrasonic vibrational energy affected the redistribution of water and oil in the pore space. This concept was put to the test in actual scenarios where vibration was utilized to halt the distribution of both oil and water during the water pumping phase of a flooded reservoir. These results unambiguously show that the application of ultrasonic waves can alter the relative permeability curves of the two phases by causing mild seismic wave amplitude vibration. Seismic waves that move the grain in a way that provides the required ultrasound waves can be used to generate these ultrasonic waves. A number of field trials were presented for approval by the study. (Salem and Snousy, 2015)

2.4 Classical Waterflooding Application

Usually when waterflooding is performed, the chances of the recovery being different than the prediction are low. However, in the case of West Virginia Richardson Berea, Calhoun and Roane fields the recovery was higher than expected. What was interesting in their cases was that when waterflooding was performed, the low permeability 'non-pay' zone was actually a main contributor to the overall recovery of the respective fields. The author's motivation was to showcase these three cases in order to present the idea that ignoring the low permeability zones could be a mistake as it was proven in these cases.

The Richardson Berea can be regarded as an average reservoir of the Appalachian kind with average primary recovery of approximately twenty percent of the original oil in place. The Upper Berea was found to have a horizontal permeability of 0.2 md with the vertical permeability being about fifty percent of the horizontal (0.1 md). The Lower Berea on the other hand was found to be coarse sand or conglomerate sand with noticeably much higher rock properties in terms of porosity and permeability which made the initial consideration of this layer being the pay zone. Several wells were drilled throughout the Berea field and were perforated in the Lower Berea section (considered the pay zone) with a regular five-spot injection pattern.

Injection was performed using shallow produced fresh water and the estimated recovery was supposed to be at an average of 1583 barrels of oil per acre. What was found was that the calculations performed for specific patterns showed larger recoveries than anticipated and occurring at early stages of the fill up phase (lower than fifty percent). This phenomenon would imply that either there was more oil or water in place than initially calculated. After the production continued, it was very evident that the Upper Berea non-pay zone was contributing to the refill of the depleted Lower Berea formation. Due to the contribution of the Upper Berea formation, the overall recovery increased from the initial twenty percent estimated from just the Lower Berea to thirty-five percent. The main factor that allowed for the production of large amounts of oil from the Upper Berea was that the waterflooding in the Lower Berea was postponed for some time allowing for the flow of oil from the low permeability Berea over time. (John R. Blomberg, 1997)

2.5 The Basis of Wave Propagation

Biot was the first to describe the notion of wave propagation in rock formations (Biot, 1956). Biot was able to build mathematical models that could explain and anticipate the influence of vibrational elastic waves on a porous material for any frequency range. Other scholars were able to deduce from these equations that elastic waves had some form of influence on porous solid materials.

Beresnev and Johnson (Beresnev and Johnson, 1994) investigated the influence of wave excitation on fluid mobility and permeability in porous saturated formations. The summarized laboratory tests demonstrated that applying vibration to saturated rock samples increased oil permeability and mobility. The increased mobility was due to a variety of factors, including decreased oil viscosity, increased percolation rates, and reduced capillary pressures. Furthermore, they provided a 6-hour experiment at low frequencies of 30, 50, and 60 Hz that demonstrated that the mobility of oil increased while the mobility of water decreased. The results of the field tests were consistent with those of the experiment; however, because the number of field tests undertaken was restricted, the data became insufficient to make a decisive conclusion.

2.6 Measuring Permeability and Relative Permeability to Perform Research

It is critical to choose the sort of instrument that will offer the most accurate results for measuring permeability for this experiment and others. The use of gas or water permeability devices to test the permeability of sandstone was investigated. Following the rupture of the Wenchuan earthquake in China in 2008, three samples of almost identical size were used. The lithology ranged from tight sandstone with 9.9 percent porosity to other cores with 21 percent porosity. However, because the permeability is so low, the investigations had to be carried out using ultra-low permeability apparatus. Pore pressure oscillation with a certain frequency and amplitude was utilized to evaluate the permeability in such low permeability cores. The permeability may be calculated using the received wave from the opposite end of the core, namely the amplitude attenuation and phase difference. Furthermore, another way for measuring permeability was to employ "gas steady state flow" (QingBao and XiaoSong, 2014) at certain confining pressures. Permeabilities steadily decrease with increased injection pressure between injection cycles. The cycles were carried out to lessen the compaction influence of the cores on the permeability measurements. Figure 2 depicts the five cycles used by the authors in this experiment.

Pressure cycles[a)]	Method	Pore media	Pore pressure (MPa)	Confining pressure (MPa)[b)]
Cycle-1	Steady state flow	Nitrogen	4	10→180→10
Cycle-2	Steady state flow	Nitrogen	4	10→180→10
Cycle-3	Steady state flow	Nitrogen	0.3, 0.6, 1, 2, 4	10→100
Cycle-4	Oscillation	Nitrogen	15	20→180→20
Cycle-5	Oscillation	Water	15	20→180→20

Fig 3: The 5 cycles run to find permeability of the 3 cores (QingBao and XiaoSong, 2014)

Furthermore, as restricting forces are applied to the device, the permeability decreases more profoundly. In cycle 5, the injection medium was changed from gas to water to test the effect

of water on permeability. The Klinkenberg effect of gas accounted for the variation in permeability measurement between the two approaches. There was a 20 to 60 percent disparity in the results of the water and gas permeability measurements. As a result, the recommendation was made that it was "essential to employ liquid as pore medium to test the transport characteristics of fracture rocks" (QingBao and XiaoSong, 2014).

To measure the relative permeability and recovery in the lab, it is important to first understand the device theory and mechanism to produce the needed data as well as the meaning behind the produced data. The device used for the measurement of the relative permeability is of constant rate nature with its schematic shown in figure 4.

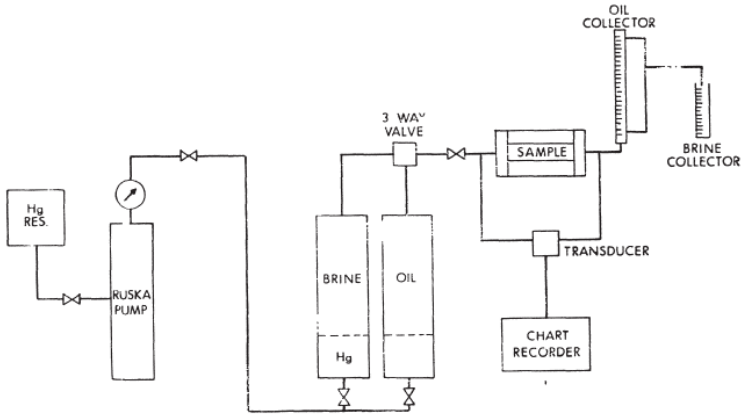

Fig 4: Schematic of Steady Flow Relative Permeability Apparatus (Archer and Wall, 1994)

Based on the fractional flow of displacing water of the oil inside the core, the gadget generates relative permeability data for the required core or sample. The first occurrence of "fractional flow is the displacing phase's breakthrough time" (water). The flow rate of the displacing phase must be set carefully such that no capillary pressure effect occurs. This test is often performed on core samples that have a significant wetting preference (oil or water) and homogeneous cores. The relative permeability data provided by heterogeneous cores is quite erroneous. The process happens when the displacing and displaced fluid is completely displaced, at which point no more fluid can enter and the ratio of input and output fluids is equal. Furthermore, the pressure ratio of the intake and output is even in this scenario, and Darcy rule may be used. Because the capillary pressure impact is so little, it is often overlooked. An effective relative permeability curve requires five to ten phases to be developed. (Archer and Wall, 1994)

Chapter 3

Research Gap and Hypothesis

3.1 Research Gap

The paper prepared by our team has all of the needed components that is needed when discussing the topic of physical vibration. The paper is novel in that it discusses the need to not only optimize the frequency and amplitude but also the time the physical vibration will be applied for. We were able to not only show how the optimal values were reached in a scientifical manner but also provided the required optimal values of frequency, amplitude and time for both synthetic and field cores. It was found that both cores need a frequency of 10 Hz but the synthetic cores require an amplitude of 4 mm applied for 15 minutes while the field cores necessitate an amplitude of 0 mm applied for 20 minutes. Furthermore, we were able to show that the optimal parameters when applied were able to partially and/or totally recover the porosity and absolute permeability of the cores. The paper is capable to fill all of the research gaps that the other literature failed to mention.

The period of application of the Vibroseismic was one of the major gaps in the research performed until now. Until yet, no studies have specified how long the vibration or ultrasonic Vibroseismic application has been used for any of the experiments or even the field testing. There is usually a mention of the application in all of the articles in the literature, but no indication of how long the vibration was performed for. Furthermore, no study was done to demonstrate the influence of application time on the attributes of the cores until our paper. Furthermore, no debate was held to determine whether or not there is a dominating time for the application, similar to the frequency and duration.

Only one publication focused on the relative influence of frequency and amplitude on rock core samples of various types, whether synthetic cores or field cores of both sandstone and carbonate types. When compared to amplitude, frequency had a more substantial influence on improvement in core parameters tested, porosity and permeability. The most crucial thing was that the optimal or "dominant frequency" (Irfan et al., 2016) and amplitude, as described in the literature study, were not found. According to the literature, the dominating vibration parameters must be used in order to best enhance the rock properties of the core in issue.

Another gap in the research was comparing the waterflooding capacities with and without the Vibroseismic. No study was conducted to determine if the application of optimum physical vibration on a core will improve the waterflooding application or whether the waterflooding application alone is adequate. This will be the major foundation of the research as well as the central emphasis of what this research is about.

The majority of the material described has comparable qualities and outcomes. One of the most profound elements shared by practically all of the literature or study conducted to date is the

use of either a single frequency or amplitude of either ultrasonic or vibration, or a range of these frequencies or amplitudes. These frequencies and amplitudes are not optimum for the cores and so will not offer the most effective outcomes when it comes to core improvement.

3.2 Filling in the Research Gap

To close the research gap, it was critical to first undertake research to determine the ideal vibrational parameters of the physical vibration that was used. The term "optimum vibrational conditions" refers to the frequency, amplitude, and duration that was used.

The first portion of the research on optimal vibrating conditions has already been finished. This is reference to a study written by my professor and myself in which we discovered the best vibrating conditions of frequency, amplitude, and time. Because the cores I'll be employing in this research are synthetic, I'll used a frequency of 10 Hz, an amplitude of 4 mm, and a duration of 15 minutes for this study. As there were previously no ideal circumstances for the vibration, this takes care of the first important portion that was absent in all of the other publications cited earlier.

The second way for filling the research gap, which is the focus of this study, was to execute classical waterflooding alone and compare it to when the Vibroseismic is combined with the waterflooding. The major goal was to determine whether or not coupling vibration with traditional waterflooding improves the core's rock and fluid characteristics. Furthermore, the entire recovery of oil from waterflooding may be compared to determine the relative influence of the combination.

According to the literature, there are a range of parameters that are affected by the vibration such as porosity, permeability, and wettability as examples. For this research, the comparison of whether or not the coupling of vibration and waterflooding compared to just waterflooding was done by evaluating the core porosity, absolute permeability, relative permeability, and total recovered oil after waterflooding is performed. These are the main parameters that are not only affecting the injection of water but also control the production rates of the oil inside the core.

3.3 Hypothesis

From the literature review in the previous chapter and from the preceding discussion of the main gaps found in the literature found, a hypothesis was formed in order to incorporate all of the above points. The hypothesis that was reached was built upon the fact that an optimum frequency, amplitude and time have already been found for the same rock type as the ones to be applied in this research.

The theory obtained was based on two distinct notions. The first is based on the results of the literature review. It is obvious that vibration, whether physical or ultrasonic, improves the characteristics of the core or sand packs to which it is applied, even when no waterflooding is used. As a consequence, it is obvious that the Vibroseismic application, when used alone, produces favorable results in the lab or even in the field, according to the literature study.

For the second idea, waterflooding has been proved in many situations in the literature study to boost oil recovery in the lab and in the field. Furthermore, waterflooding is one of the

most well-known strategies of enhancing oil recovery and has demonstrated several times that it is capable of increasing or at least sustaining output.

Therefore, through clear deduction of the impact that each of these methods separately has on production increase and in specific the rock and fluid property alterations that have been reported by researchers in the literature review, the following hypothesis has been reached:

The optimization of frequency, amplitude and time of the physical vibration application coupled with waterflooding can improve the rock and rock-fluid properties (porosity, absolute permeability, and relative) and the overall hydrocarbon recovery compared to classical waterflooding alone

Chapter 4

Research Methodology

4.1 Research Background

The hypothesis reached was that combining optimal Vibroseismic and waterflooding can improve porosity, absolute permeability, and relative permeability, hence increasing oil recovery from cores. The results are to be contrasted with the usage of only waterflooding application. The optimization of the Vibroseismic has already been accomplished in a previous study conducted. The previous study was able to reach the ideal frequency, amplitude, and duration for both synthetic and field cores.

To test this hypothesis, a comparison of particular quantitative qualities of the core must be made. These measurements must be taken with the same instruments on the same core, once when just classical waterflooding is used and once when vibration combined with waterflooding is used. Porosity, absolute permeability, and relative permeability was measured, and the total recovered oil from waterflooding was determined. These qualities have been mentioned in all of the material studied in chapter 2 to change in some way when vibration, either physical or ultrasonic, is applied.

The primary goal of this experimental approach is to compare the findings of the above-mentioned measured parameters, namely porosity; absolute permeability; relative permeability; and total recovered oil. The comparison is to be made of these parameters before and after vibration when waterflooding is used. The sole difference between the two procedures is the vibration stage that was used on the core, with its effect being the deciding element.

4.2 Research Design and Data Collection

The cores that were tested upon are consolidated synthetic surface cores that were cut from several different rock slabs. Initially fifty core samples were cut and sanded and then their length and diameter measured. Each core length and diameter were measured 3 times and the average values of each parameter was then calculated.

The cores were cleaned using Soxhlet apparatus and dried in an oven prior to the initial measurements. Over the course of this study, this same step was done twice. Before any work was done on the cores, it was done the first time, and the second time it was done, it was done before the second step before the vibration application. The cut cores were designed to be cut from a variety of rock slabs in order to maximise the variation in the values of the different properties.

Certain cut-off ranges were used to form the groups for the porosity and absolute permeability groupings. In terms of porosity, any core with a value of 30 pu or more is considered a high porosity, whereas any number less than that is considered low porosity. In terms of absolute

permeability, anything greater than 500 md is called high absolute permeability, while anything below is termed low absolute permeability.

The four categories that this research was completed on are as follows:

1. High absolute permeability and high porosity
2. High absolute permeability and low porosity
3. Low absolute permeability and high porosity
4. Low absolute permeability and low porosity

The porosity was measured using a helium porosimeter throughout, and the absolute permeability, relative permeability, and total recovery were calculated using a permeameter. The Helium Porosimeter determines effective porosity, whereas the liquid permeability determines absolute permeability. Furthermore, because there would be two unique fluids, brine and synthetic oil, the relative permeability was determined during the first and second stages of the research during the waterflooding experiment. The first stage occurred prior to vibration, whereas the second occurred following optimum vibration of the cores. The synthetic oil used is paraffin oil with properties described in table 1.

Oil Properties	Value
Density (g/cc)	0.83
Viscosity (cP)	52.56

Table 1: Synthetic oil properties

These were measured before and after the vibration to see the effect of the vibration. The same paraffin oil and brine salinity were used throughout the entirety of this research. The water properties are to be reported in table 2.

Water Properties	Value
Salinity (ppm)	35,000
Density (g/cc)	1.11
Viscosity (cP)	1.12

Table 2: Brine properties

The brine prepared for this research had the salinity reported above and was prepared using only salt (sodium chloride) as the sole mineral added. The brine is used for the saturation of the cores before any measurements are performed as well as the measurements of the absolute and relative permeability in the permeameter device.

The original values of these samples were tested to assess the effect of the vibration augmentation or damage after they were set and cleaned using the Soxhlet and oven. The helium porosimeter was used to acquire the first measurements of effective porosity. The permeameter is then used to determine the absolute permeability of each core. Following that, traditional water-flooding was performed, which began with oil saturation and continued with brine injection until breakthrough and then total brine production.

After that, the total recovered oil was measured, as well as the intake pressures, oil volume, and water volume collected at each pressure step. This data was utilized to determine the relative oil and water using the unsteady state approach, from which the relative permeability curves may be constructed. In addition, the total amount of recovered oil was gathered and measured. The same methods were done after the vibration to determine the effect of the vibration. The sole variable in this strategy was the vibration. Furthermore, this strategy is as near to the actual scenario used in the field as possible.

After the first properties of porosity, absolute permeability, relative permeability, and total recovery were finished and the core was cleaned and dried, the vibrational stage began. In the first stage, porosity was assessed before saturating the same cores used in the previous phase with the same brine. The absolute permeability was measured, and the core was put in the vibrating device with the optimal settings.

Following completion of this process, the core absolute permeability was re-measured to determine the influence of vibration, followed by relative permeability measurements. Because of the nature of the cores, the absolute permeability and porosity are re-measured after cleaning and drying. Because the cores are consolidated and synthetic, there is a strong possibility that some damage or alterations to the core effective porosity and absolute permeability will occur, altering the study and experimental outcomes. As a result, in order to adequately monitor the outcome of vibration on the cores, the porosity and permeability are re-measured in the second phase of the investigation (immediately before vibration).

4.3 Optimization of Vibroseismic Parameters

4.3.1 Optimization of Parameters

For the physical vibration, which is the core essence of this research, the optimized parameters are going to be used directly from prior research on the optimization of vibration parameters. The research was able to provide the frequency, amplitude and duration that are needed to successfully increase the rock, rock-fluid and oil recovery of the synthetic cores in question. As the cores used in this research and from the former research are very similar then the parameters would be the same.

The previous study was carried out in order to determine the ideal frequency, amplitude, and duration required to best boost core porosity and absolute permeability. It was also tried to determine if the damage could be reversed by using the improved conditions. As previously stated, a setup was created and utilized to determine the optimal values. Frequency ranges of five to twenty hertz, amplitude ranges of zero to eight millimeters, and time ranges of five to twenty minutes were all examined to determine the best settings based on the literature research.

Sandstone field samples and synthetic outcrop consolidated samples were the two types of samples investigated. The optimal parameters for the outcrop samples were found to be ten hertz, four millimeters in amplitude, and fifteen minutes in duration. The frequency of the field samples was the same as that of the outcrop samples, but the optimum amplitude was zero and the time required was twenty minutes.

It took several steps to optimize the frequency, amplitude, and time for the outcrop samples. The optimization results of optimization of time and frequency are as presented first. After, the optimization results of the amplitude will also be presented to show how the results were selected.

Frequency (Hz)	Time (min)	Porosity (pu)	K (md)	% Porosity Diff.	% K Diff.
5	10	22.69	36.30	0.22	3.71
5	20	23.07	37.50	1.9	7.14
5	30	22.72	36.90	0.39	5.6

Table 3: Results of Five Hz Frequency vibration on core (Oraby et al., 2022)

Frequency (Hz)	Time (min)	Porosity (pu)	K (md)	% Porosity Diff.	% K Diff.
10	10	22.67	30.96	1.8	-4.8
10	15	23.21	31.01	4.3	-4.7
10	20	23.64	35.37	6.2	9.9
10	25	22.88	31.42	2.8	-3.4

Table 4: Results of Ten Hz Frequency vibration on core (Oraby et al., 2022)

Both tables 1 and 2 present the results of the optimization of the frequency and time parameters of vibration. The best results when comparing both results was the 10 Hz at a time of 20 minutes; therefore, the following step was to optimize the amplitude. Frequency was kept at 10 Hz as it showed to be the optimum but different time periods were also tested. The results of the optimization are as follows.

Frequency (Hz)	Time (min)	Porosity (pu)	K (md)	% Porosity Diff.	% K Diff.
10	10	30.75	55.05	0.31	10.00
10	15	31.29	68.09	0.46	-15.68
10	20	30.86	33.44	0.65	21.45

Table 5: Results of Ten Hz Frequency and Zero mm Amplitude (Oraby et al., 2022)

Frequency (Hz)	Time (min)	Porosity (pu)	K (md)	% Porosity Diff.	% K Diff.
10	10	29.55	13.21	0.81	72.24

10	15	30.30	12.52	2.44	12.52
10	20	29.73	23.73	0.45	-72.90

Table 6: Results of Ten Hz Frequency and Four mm Amplitude (Oraby et al., 2022)

Frequency (Hz)	Time (min)	Porosity (pu)	K (md)	% Porosity Diff.	% K Diff.
10	10	31.68	127.69	1.05	4.02
10	15	31.78	55.51	2.32	-32.46
10	20	30.83	96.35	-0.32	-1.81

Table 7: Results of Ten Hz Frequency and Eight mm Amplitude (Oraby et al., 2022)

Under the optimized parameters, the porosity of the outcrop samples rose by 2.44 percent, while the absolute permeability increased by 12.52 percent. In terms of field samples, the porosity and absolute permeability rose in all samples under the optimum settings, with damage visible beyond or before the optimized values. Furthermore, rock property repair was done on a damaged field sample that had received unoptimized vibration during our testing. The adjusted parameters were able to restore the porosity and relative permeability to their previous values. (Oraby et al., 2022)

Previous study on the optimization of Vibroseismic parameters revealed that the optimal values change for distinct consolidations of sandstone rock cores. The optimum parameters for synthetic surface consolidated cores, comparable to those employed in this study, were a frequency of ten hertz, an amplitude of four millimeters, and a duration of fifteen minutes. As a result, the vibration was performed utilizing these parameters in the second part of this investigation.

4.3.2 Apparatus Setup

This study's setting was designed to get the best results possible. The sample setup and measurement stages can be simply copied, allowing it to be easily repeated. Furthermore, the approach and setup employed are strikingly similar to the actual scenario of waterflood and Vibroseismic application in the field.

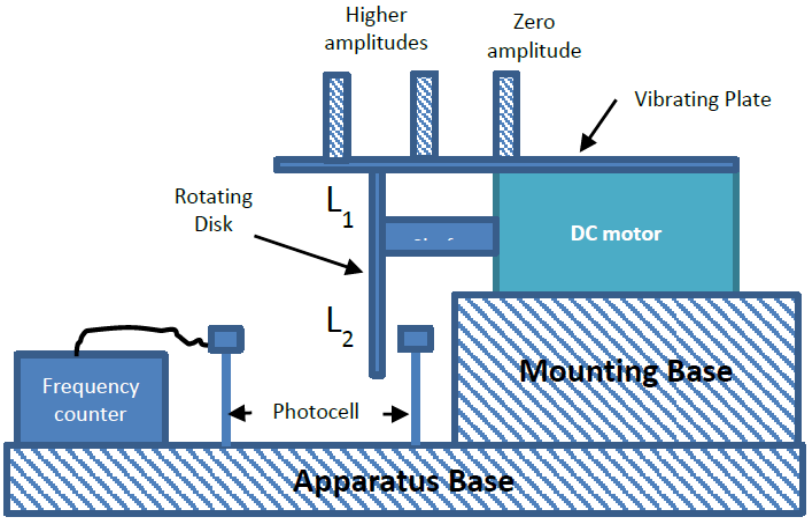

Fig 5: Schematic of Vibration Tool (Oraby et al., 2022)

The equipment pictured comprises of a DC motor with a voltage regulator to control the motor's speed. This apparatus's sole source of power is the motor, which rotates the spinning disc through the shaft placed between the motor and the rotating disc. Figure 5 depicts a revolving disc that is nearly completely circular except for a sliced portion. The vibration is caused by this sliced portion. When the spinning disc rotates and the sliced piece collides with the vibrating plate, the missing section causes the vibrating plate to descend from the disc radius to the vibration section. The core is placed inside the metal container that is filled with sand in order to protect it and also act as the surrounding formation. The core itself is protected from the sand through the use of cling film in order for it not to be plugged from the loose sand around it.

The two photocells are used to sense the rotations of the rotating disk which is then displayed on the frequency counter. As shown in figure 6, the location of the sample box with the sample inside differs according to the needed amplitude. The closer the sample box and sample to the end of the vibrating plate toward the motor the lower the amplitude of the sample was and vice versa.

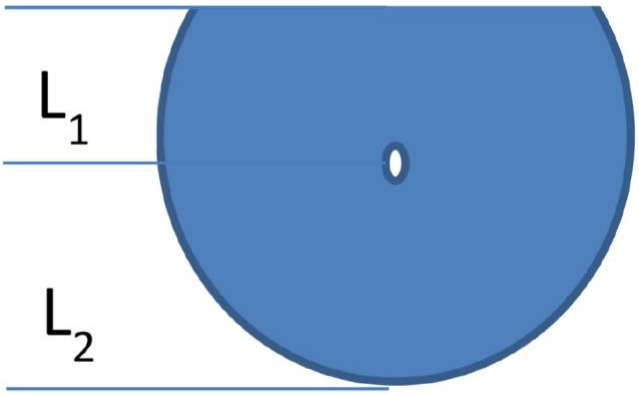

Fig 6: Schematic of Rotating Disk (Oraby et al., 2022)

The difference in lengths between lengths 1 and 2 (L1 and L2) is used to regulate the varied amplitudes required for the experiment. The difference between the entire distance between the highest point the core will reach, which is the second length (L2), and the chopped section distance where the vibrating plate is at its lowest position is used to place the core in the right connection. The core box and core were set in a specified location to guarantee the proper amplitude was applied, and the suitable rotating disc with the correct amplitude was installed. Figure 7 shows a simplified pictorial way for demonstrating how the amplitude was measured or may be measured for this device.

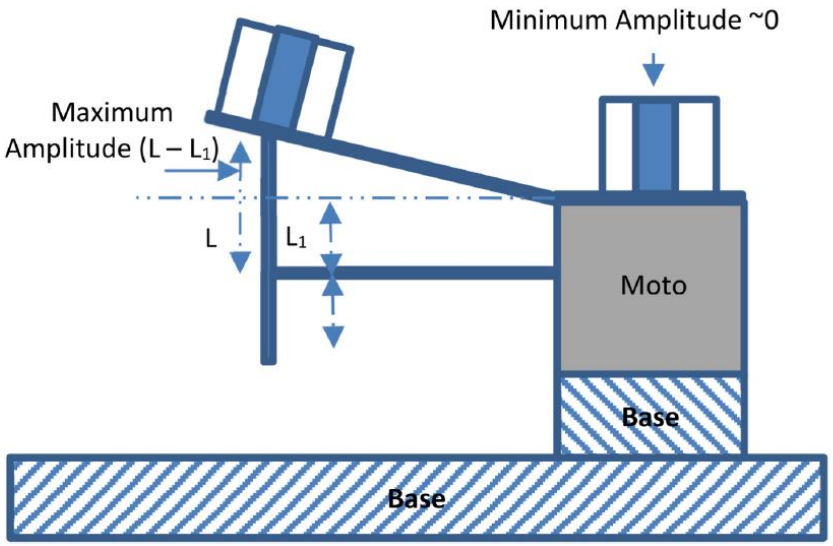

Fig 7: Schematic of Method for Amplitude Calculation and Positioning (Oraby et al., 2022)

4.4 Waterflooding, Absolute, and Relative Permeability Measurement

In this study, the waterflooding portion is performed before and after the optimum vibration step. Waterflooding is performed in the liquid permeameter in the same manner as the relative permeability experiment. The core is first completely saturated with a brine solution with a salinity of 35,000 ppm. The next stage is to saturate the brine-soaked core with oil (paraffin oil) until the core can no longer be injected with oil and has attained irreducible water saturation (Swi).

Because the pore spaces are mostly filled with oil and irreducible water, the oil saturated core now resembles the reservoir prior to water injection in any field situation. The core is then injected with the same brine water that it was originally saturated with until no more oil is generated from it. At this stage, the total amount of oil produced is gathered. Furthermore, the input pressures, as well as the water and oil quantities, are recorded at each time step and used to generate the relative permeability curves for each core. Since the back pressure is held constant at zero, only the inlet pressure is measured, not the delta pressure through the core holder or Haussler sleeve.

The total oil collected indicates the overall recovery from the core, while the relative permeability curves represent the production relationship between the two phases. Using the unsteady state calculation approach, the relative permeability data is then utilized to determine the relative oil and relative water permeabilities with varied water saturations. These data are then gathered and drawn to create the relative permeability curves for each core before and after the vibration application. The brine injection rate is kept constant at one centimeter cubed per second in all tests performed while doing the relative permeability experiment.

Depending on the expected input pressure, the confining pressure for all cores was set to be between 700 and 1000 psi. The greater the intake pressures obtained when injecting both the oil and the brine in the first and second phases, the tighter the core is in terms of absolute permeability. The manufacturer recommends that a differential of at least 200 psi be maintained between the inlet and confining pressure for reliable results.

Fig 8: Liquid Permeameter for Waterflooding and Relative Permeability

The liquid permeameter contains two accumulators on the left side of figure 4 that retain the oil and brine to be injected and may be switched by shutting and opening valves on each accumulator. The injected fluid enters the device through the pipelines on the left side and passes through the core in the Haussler sleeve in the center. The fluid created by the Haussler sleeve or core holder is subsequently collected in any beaker or graduated cylinder on the apparatus's right-hand side. Figure 9 depicts the internal dynamics of the Haussler sleeve as well as the injection of various fluids into the permeameter device.

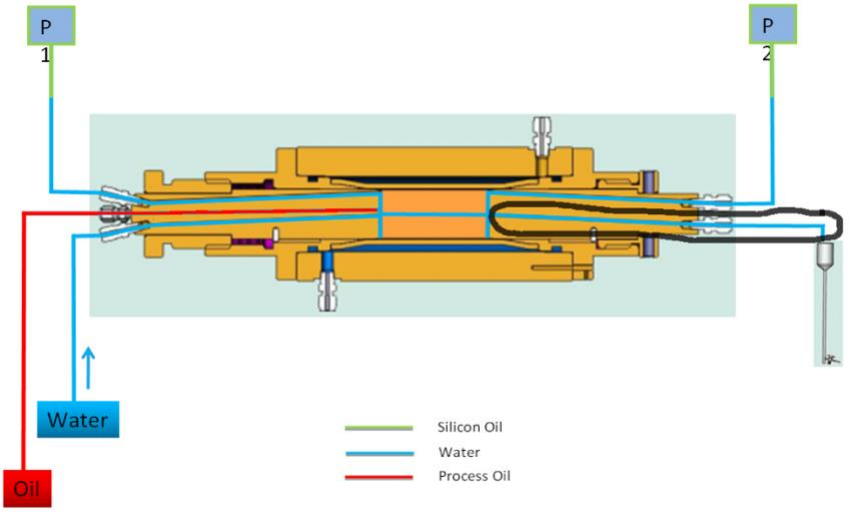

Fig 9: Inner Dynamics of the Liquid Permeameter

In this case, there is no back pressure making the value of the outlet pressure or back pressure (P2) is equal to zero. Therefore, the delta pressure across the core inside the Haussler sleeve is the same as the inlet pressure (P1) and hence why it is the only pressure that is recorded. The collection nozzle has also been presented in figure 9 and has been highlighted by the black circle. This is the path of the produced fluid to be collected which is vital when in both the waterflooding and relative permeability experiments. There are some dead volumes that must be accounted for when performing the relative permeability experiments. The dead volume must account the unused volume of oil that leaves the accumulator but does not actually pass through the cores but instead is located in the piping of the device. The dead volumes for the brine/water are 2.6 cubic centimeters while for the oil it is 1.3 cubic centimeters, respectively.

4.5 Porosity Measurement

The Helium Porosimeter was used to test porosity for this research. The equipment can determine the porosity of any core sample based on its size as well as the type of rock it is comprised of. After entering this information, the accompanying software may calculate the bulk volume of the core itself using the core's dimensions. The next step is to utilize helium gas to determine the pore volume of the core, which is accomplished by expanding helium gas into the chamber in which the core is put.

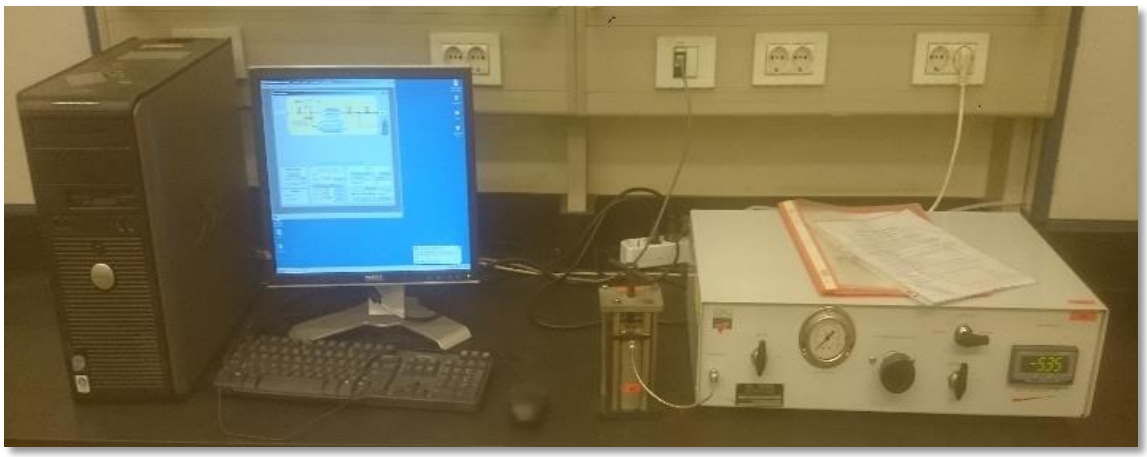

Fig 10: Helium Porosimeter and Accompanying Software AppiLab

The idea of the expansion of helium gas is based on Boyle's Law which states.

$$Pressure_1 * Volume_1 = Pressure_2 * Volume_2$$

The helium porosimeter, which can be used to determine any core's porosity, was created on the foundation of this equation. According to figure 11, the core is put within the cup holder of the matrix, which is the initial volume according to Boyle's equation.

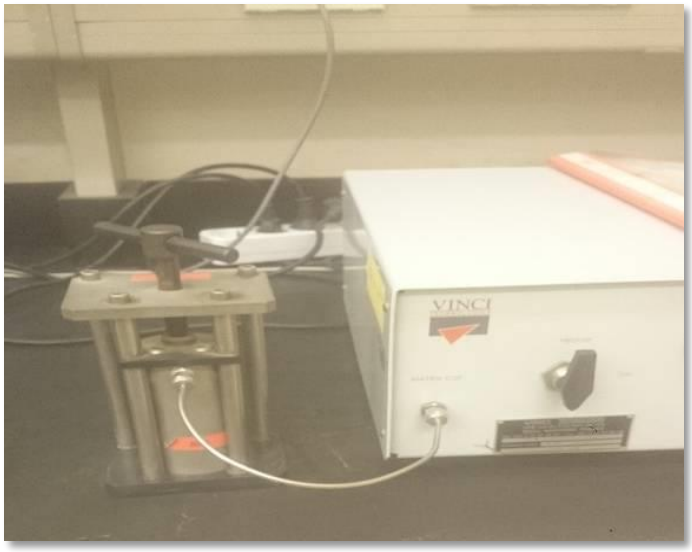

Fig 11: Matrix Cup Connected to Helium Porosimeter

The second volume is a chamber with a known volume that is housed within the instrument itself. The device's initial phase is to expand the helium gas within the device's reference chamber and build up pressure until the pressure stabilizes at a predetermined amount. Once the pressure within the reference chamber has stabilized, the gas is allowed to expand into the matrix cup where the core is placed, and this is repeated until the pressure stabilizes.

The volume of the matrix cup is calculated using the equation, and the excess volume of the cup is first subtracted from the length of the core. The grain volume and pore volume make up the remaining volume. The grain volume is computed using the bulk volume and information of

the kind of rock from which the core is formed. The pore volume of the core sample being examined is what remains of the volume. After calculating the pore volume from all of the foregoing, the porosity is derived by dividing the pore volume by the bulk volume, as stated in the equation below.

$$Porosity = \frac{Pore\ Volume}{Bulk\ Volume}$$

4.6 Viscosity Measurement

The rolling ball viscometer was used to determine the viscosity of the synthetic oil. To determine the viscosity, the rolling ball viscometer employs the principle of the time it takes an item to travel through a liquid as well as correlations of previously studied viscosity ranges. The apparatus comes with a variety of balls of various sizes for varying viscosity ranges. As seen in Figure 8, the instrument itself comprises of an interior chamber to store the liquid being measured, in this case synthetic oil, and two laser indicators on opposite ends of the device.

Fig 12: Rolling Ball Viscometer

The rolling ball was placed in the barrel, which contains the liquid chamber and two lasers. But first, the appropriate ball must be selected based on the range of viscosity suspected by the user. The 7.7-inch ball is utilized for our research measurements for viscosities ranging from 5 cP to 200 cP. Because the instrument incorporates a heater, it can measure viscosity at different temperatures; however, because all of the research experiments are done at room temperature, the measurements were likewise done at room temperature. The rolling ball is held in place by a latch at the top of the barrel, and the time it takes for the rolling ball to move through the synthetic oil to reach the bottom when the device is tilted at an angle is recorded by the apparatus itself. The program is able to create the viscosity of the synthetic oil, which in this example was 52.56 cP, based on the time taken and previously calibrated correlation supplied by the accompanying

software. The tests were repeated numerous times, and the most frequent value, in the case of the research outcome, was picked.

Chapter 5

Results

5.1 Core Preparation

To prepare for the entire research, cores needed to be cut and sanded prior to any work being done. 6 synthetic slabs or rock pieces were collected from around university to be used to cut cores from. The pieces are consolidated synthetic rock that are made with a variation of components that are unknown but with varying initial looks which made them suitable for some variation between the initial parameters of porosity and absolute permeability.

Each of the rock pieces was used to cut 9 cores except for 2 rock pieces could only cut 7 and 3 cores respectively due to their smaller size compared to the other 4 rocks. The cores were cut with a 1-inch cutter and were cut at almost the same length. Once all 53 cores were cut, they needed to be sanded down to make sure that both ends of the cores were straight. Once sanding was done, the cores were then labeled with a 2-code numbering system. Each rock was banded to be in one group respectively making them 6 different groups. The groups were named group R, S, T, U, V, and X. Each group consisted of several cores depending on the number of cores that could be cut from each rock piece initially collected. The cores were then numbered 1 through 9, except for the 2 groups with lower number of cores cut, and each of these cores was marked using ink and left to dry in the oven. Once dry, all of the cores had their length and diameter measured which are data required for the remainder of the research. Each length and diameter were measured 3 times and an average value for each was calculated, respectively. Regarding the diameter, it was measured from the top, middle, and lower part of each core. Table 1 in appendix will present the measurement of all the cores with each of the respective groups with their respective color coding.

5.2 Collection of Initial Data

5.2.1 Initial Porosity of Cores

To begin and categorize the cores according to the 4 categories mentioned before, the porosity was the simpler route to take. The porosity of all 53 cores were measured using the helium porosimeter as well as the dimensional data of each of the respective cores. The dimensional data that was inputted was the average length and average diameter of each core. Table A2 in appendix presents the initial porosity of each of the 53 cores before any further research was performed.

From the porosity data it is clear that the difference in porosity was unfortunately not large due to the nature of the rock and thus core samples themselves. The fact that they were unconsolidated means that the porosity will be on the higher end of the spectrum when compared to consolidated core samples for example. The range of porosity difference is around 10 pu with the maximum porosity obtained from core 7T with a value of 33.13 pu while the lowest porosity was obtained from core 3X with value of 23.51 pu, respectively.

5.2.2 Saturation of Selected Cores

From these results, 21 cores (almost half of the total number of cores) were selected for the next step which is measure the absolute permeability. These cores were selected to represent the entire range of porosities that were found from the 53 cores. The porosities that were selected ranged from the highest value to the lowest value which members of each group to allow the research to be as inclusive to all of the cores as possible. The cores selected are 1, 3, 4, 7, and 8 from group T; 2, 3, 5, 6, and 7 from group R; 3, 7, and 9 from group S; 4, 6, and 9 from group V; 1 and 5 from group U; all of group X. All of these cores were then measured by the permeameter after being saturated in brine. The saturation occurs by soaking the cores in the brine solution for several days to a week to make sure that the cores have been saturated. Then the weights of when they are dry to after saturation are compared to make sure that they have reached maximum saturation. The weight comparisons are presented in the table 3 in the appendix for these 21 cores.

The saturation ranges are very acceptable for this research as at least more than 7 grams of brine has filled the pores of the cores with water saturation reaching up to around 11 grams. These figures create a range of weight increase from around 10 percent up to just shy of 17 percent. The cores were left to soak for about 1 week which is more than enough time for saturation and were done under vacuum. Each group was done separately due to the nature of apparatus being used for saturation not being able to handle all 21 cores at the same time.

From the difference in weight increase, the percentage of filling of the pore volume has also been calculated. There are discrepancies in the saturation percentage filled of the pore volume for each group with most of the cases being 80 percent or higher which is very acceptable. There are some cores which could not have any higher increase in saturation with saturation percentages from 60 to just under 80 percent which is acceptable also but not the best results that can be obtained. However, all of the cores were left in the same conditions for saturation and so any difference in saturation percentages are based solely on the capability of the core to be saturated.

5.2.3 Initial Measurement of Absolute Permeability of Selected Cores

All of the cores were measured using the liquid Permeameter and were measured using the same brine solution that was used for saturation of the cores. The inlet pressure data was collected at different flow rates of 1 to 6; however, in some cases only to 5 cubic centimeters per minute (cc/min). This was usually because the values were awfully close to each other in the case of high permeability cores and so an increase in the flow rate would not have produced any different results. Table 8 will present the liquid permeabilities of the 21 cores that were measured along with their porosities.

Sample Name	Liquid Permeability (md)	Porosity (porosity unit – pu)
2R	4.32	27.58
3R	4.68	29.92
5R	5.28	28.20

6R	5.76	27.45
7R	5.40	27.50
3S	52.44	27.01
7S	59.52	27.02
9S	55.08	26.45
1T	544.08	31.99
3T	364.68	32.55
4T	357.24	32.91
7T	880.44	33.13
8T	1218.96	30.95
1U	55.32	28.60
5U	64.68	29.66
4V	15.96	26.43
6V	19.92	26.75
9V	25.32	26.53
1X	4.92	24.81
2X	5.52	23.51
3X	4.08	26.14

Table 8: Selected Cores Liquid Permeabilities and Porosities

There are several combinations of porosity and permeabilities that can be seen from these results. In group ‘R,’ it is clear that the porosity is medium range according to the range found before; however, the cores are not connected effectively making the permeability quite low in all of the cores. Group ‘S’ has some of the same traits as in group ‘R,’ but the permeabilities in group S are much higher than group ‘S’. On the other hand, Group ‘T’ has both high porosity and permeability for all of its members with a wide range of permeabilities also. All other groups have small ranges of permeabilities with a maximum difference of around 10 milli-Darcy (md) but in this group the permeability range is between 357.24 md to 1218.96 md which is a difference of 861.72 md, respectively. Moreover, group ‘U’ has even worse grain distribution than both groups ‘S’ and ‘R’ as the porosity ranges is higher than this group but on the other hand the permeability figures are similar to group ‘S.’ The same can be said about group ‘V’ with even lower permeability with medium porosity according to the range of porosities of all the cores. Group ‘X’ has the lowest porosity and permeability values than all of the other groups.

5.2.3.1 Core 2R Initial Absolute Permeability

The first absolute permeability measured was core 2R in the 'R' group. The first step was to measure the inlet pressure with every increase in brine flow rate. The table A5 in appendix will present this datum. From that, a graph of ΔP/L and Q/A are drawn to find the slope of the trendline between the points. The slope will then be multiplied by the viscosity of water to find the permeability.

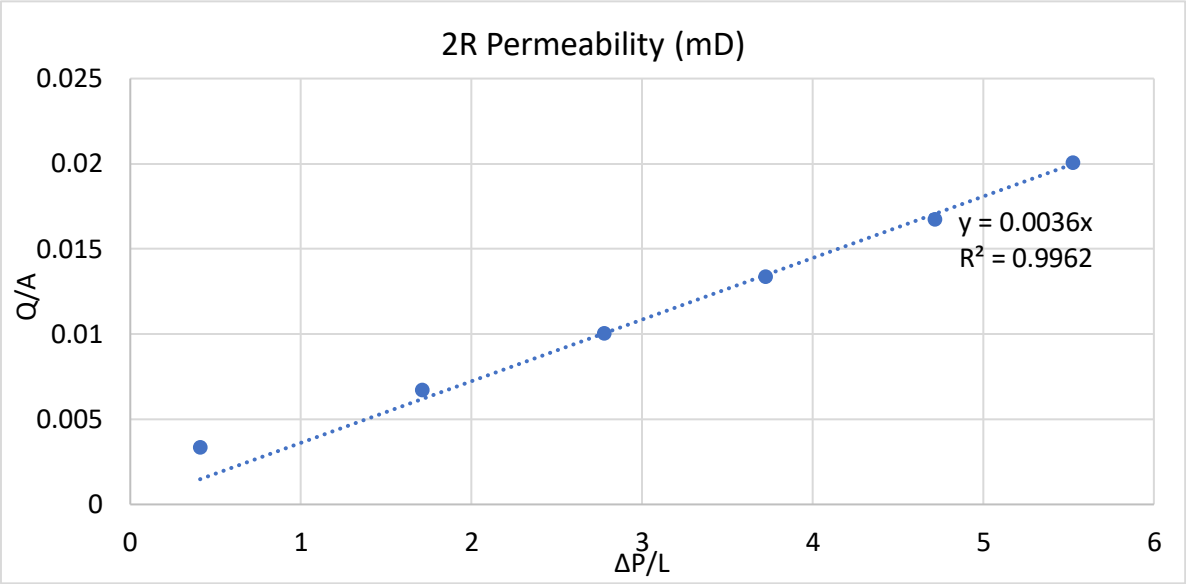

Fig 13: Absolute Permeability Curve of Core 2R

From the graph, it can be seen that the values are close together meaning that the values that have been collected are accurate. The trendline or slope is very close between the points which is reinforced with the R2 or trendline reliability with a rating of 0.9962 from 1 which means the trendline is exceedingly accurate.

5.2.3.2 Core 3R Initial Absolute Permeability

The second absolute permeability measured was core 3R in the 'R' group. The first step was to measure the inlet pressure with every increase in brine flow rate. The table A6 in appendix will present this datum. From that a graph of ΔP/L and Q/A are drawn to find the slope of the trendline between the points. The slope will then be multiplied by the viscosity of water to find the permeability.

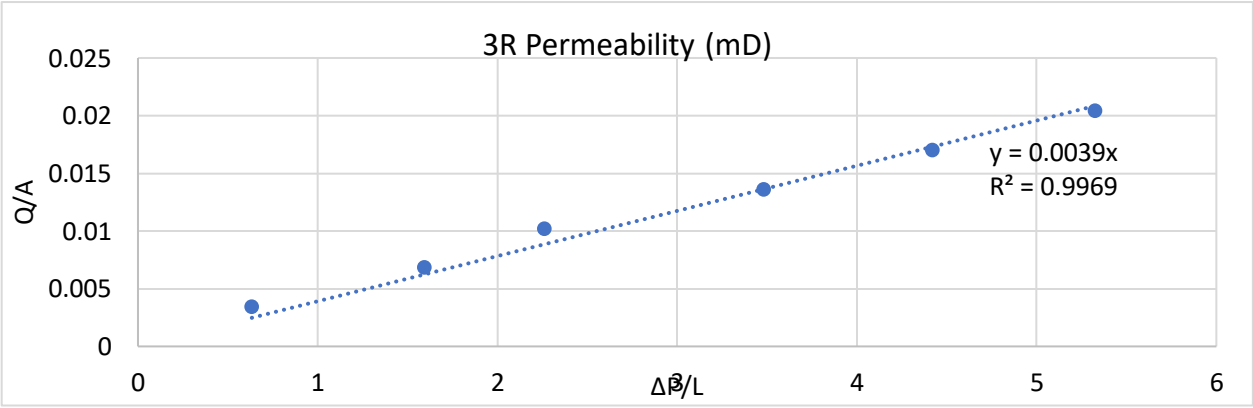

Fig 14: Absolute Permeability Curve of Core 3R

The values in relation with one another is close meaning that the values that have been collected accurately. The trendline is remarkably close between the points which is reinforced with the trendline reliability with a rating of 0.9969 from 1 which means the trendline is exceedingly accurate.

5.2.3.3 Core 5R Initial Absolute Permeability

The next core to have its absolute permeability measured was core 5R in the 'R' group. The first step, once again, was to measure the inlet pressure with every increase in brine flow rate. The table A7 in the appendix will present this data collected. From that a graph of ΔP/L and Q/A are drawn to find the slope of the trendline is to be found which will then be multiplied by the viscosity of water to find the permeability.

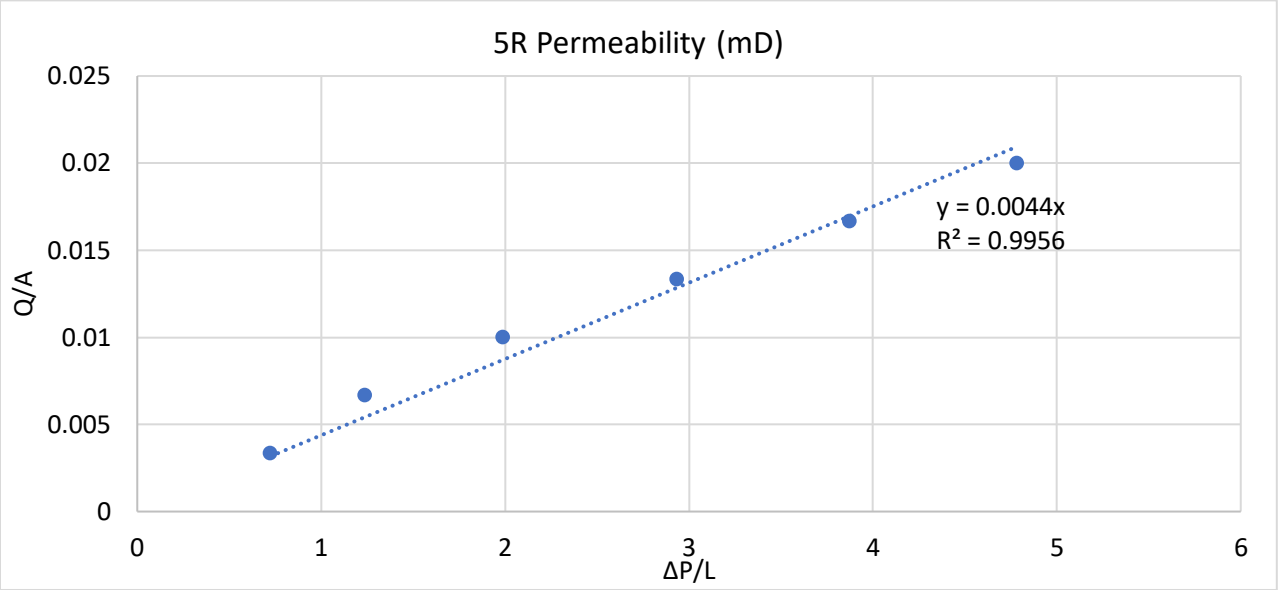

Fig 15: Absolute Permeability Curve of Core 5R

Once more the values of each flow rate are near one another meaning that the values that have been collected accurately. The trendline is again remarkably close between the points which is reinforced with the trendline reliability with a rating of 0.9956 from 1 which means the trendline is exceedingly accurate.

5.2.3.4 Core 6R Initial Absolute Permeability

Core 6R in the 'R' group was the following core to have its initial absolute permeability measured and the penultimate core in this group. The first step, once more, was to measure the inlet pressure with every increase in brine flow rate. The table A8 in the appendix will present this data collected. From that a graph of ΔP/L and Q/A are drawn to find the slope of the trendline is to be found which will then be multiplied by the viscosity of water to find the permeability.

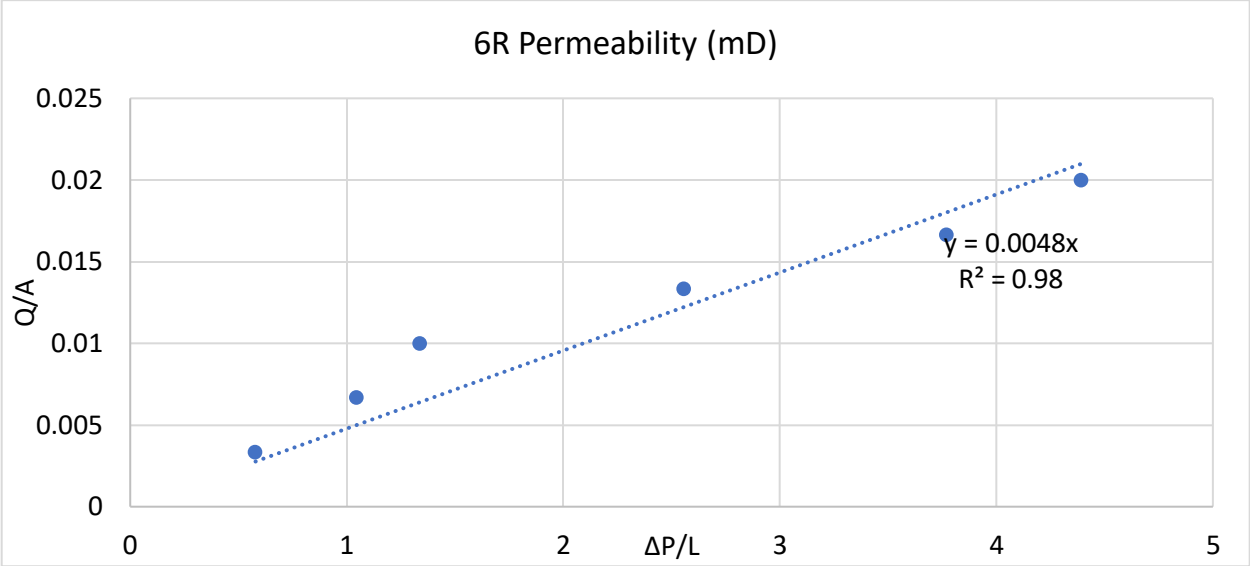

Fig 16: Absolute Permeability Curve of Core 6R

The individual values for this core may a bit more scattered than the previous members in its group. However, the trendline reliability value is the amongst the highest in this group with a value of 0.98 from 1 making the slope accurate and the results reliable.

5.2.3.5 Core 7R Initial Absolute Permeability

Core 7R in the 'R' group was the following core to have its initial absolute permeability measured and the last core in this group. The first step, once more, was to measure the inlet pressure with every increase in brine flow rate. The table A9 in the appendix will present this data collected. From that a graph of ΔP/L and Q/A are drawn to find the slope of the trendline is to be found which will then be multiplied by the viscosity of water to find the permeability.

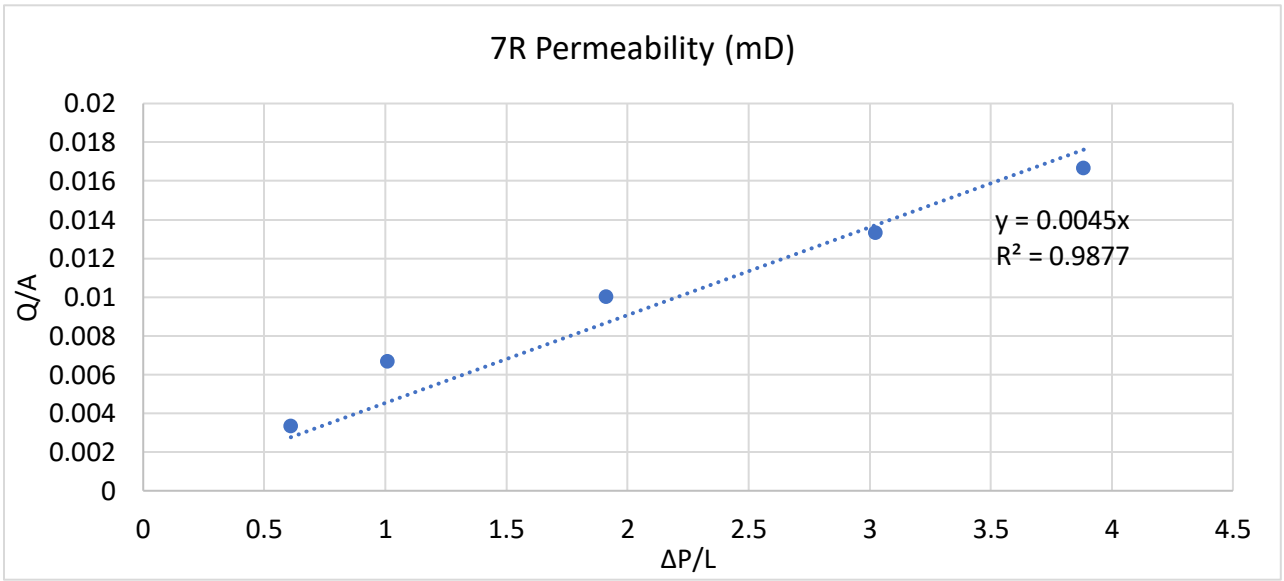

Fig 17: Absolute Permeability Curve of Core 7R

The individual values for this core may a bit more scattered than the other members in its group but a bit less than core 6R. However, the trendline reliability value is the highest amongst this group with a value of 0.9877 from 1 making the slope accurate and the results the most reliable.

5.2.3.6 Core 3S Initial Absolute Permeability

The first core in the 'S' group was core 3S to have its initial absolute permeability measured. The first step, once more, was to measure the inlet pressure with every increase in brine flow rate. The table A10 in the appendix will present this data collected. From that a graph of ΔP/L and Q/A are drawn to find the slope of the trendline is to be found which will then be multiplied by the viscosity of water to find the permeability.

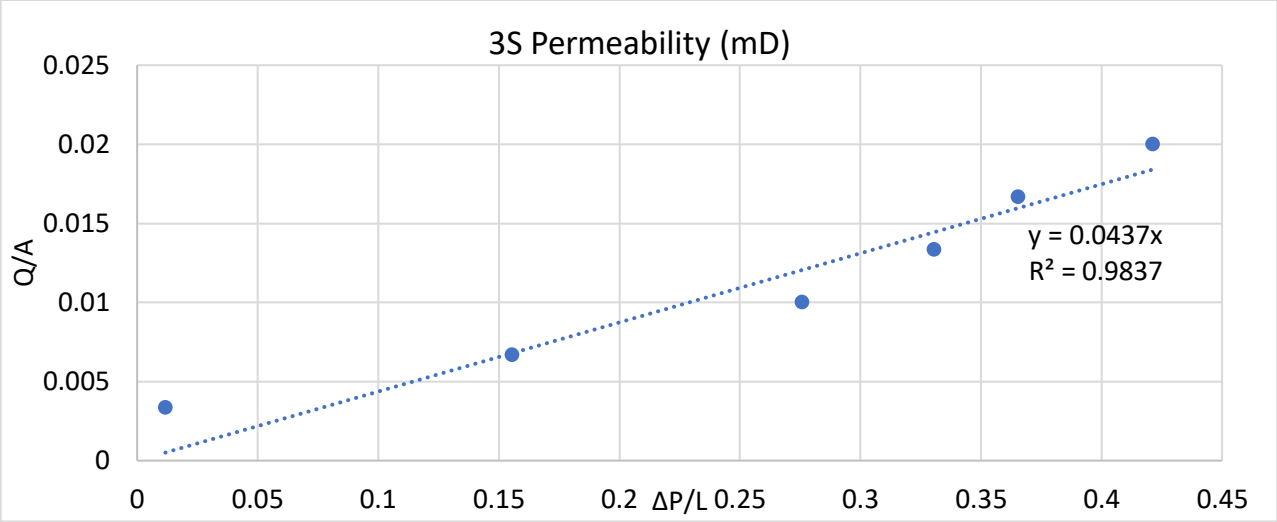

Fig 18: Absolute Permeability Curve of Core 3S

The individual values at the beginning were close together but seem to separate slightly as the brine flow rate increases. However, the trendline reliability value is the is quite high at a value of 0.9837 from 1 making the results accurate and reliable.

5.2.3.7 Core 7S Initial Absolute Permeability

The second member in the 'S' group was core 7S to have its initial absolute permeability measured. The first step, once more, was to measure the inlet pressure with every increase in brine flow rate. The table A11 in the appendix will present this data collected. From that a graph of ΔP/L and Q/A are drawn to find the slope of the trendline is to be found which will then be multiplied by the viscosity of water to find the permeability.

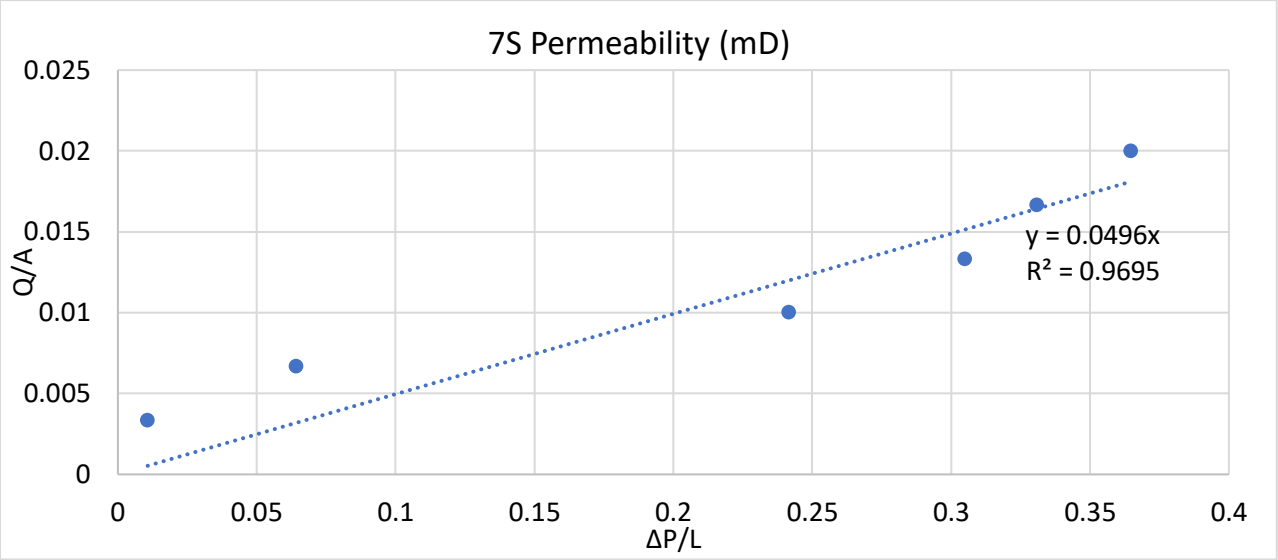

Fig 19: Absolute Permeability Curve of Core 7S

At lower brine rates, the values began to be scattered as can be seen from the chart while with progression of flow rates the scattering is reduced. The trendline reliability value is still high making the confidence in the results also high.

5.2.3.8 Core 9S Initial Absolute Permeability

The last member in the 'S' group to have its initial absolute permeability measured was core 9S. The first step, once more, was to measure the inlet pressure with every increase in brine flow rate. The table A12 in the appendix will present this data collected. From that a graph of ΔP/L and Q/A are drawn to find the slope of the trendline is to be found which will then be multiplied by the viscosity of water to find the permeability.

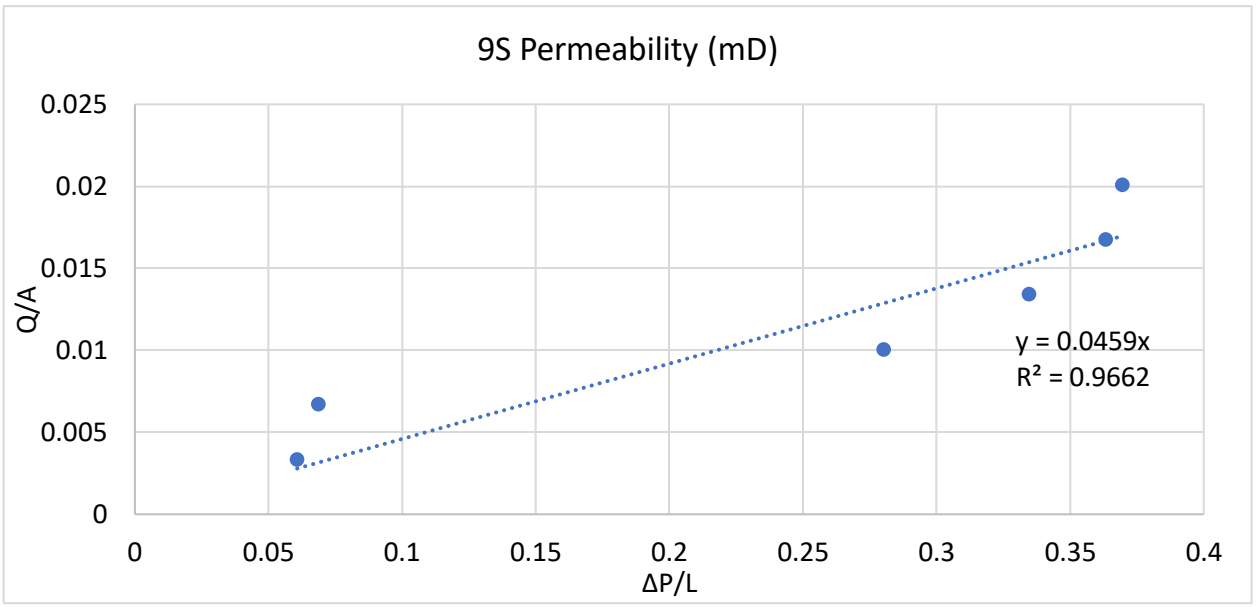

Fig 20: Absolute Permeability Curve of Core 9S

The scattering at the beginning is quite small but at higher flow rates the scattering begins to increase but still the relative range of values is not enough to lower the trending and hence the trendline reliability value still making the permeability reliable and accurate.

5.2.3.9 Core 1T Initial Absolute Permeability

The first member in the 'T' group to have its initial absolute permeability measured was core 1T. The first step, once more, was to measure the inlet pressure with every increase in brine flow rate. The table A13 in the appendix will present this data collected. From that a graph of ΔP/L and Q/A are drawn to find the slope of the trendline is to be found which will then be multiplied by the viscosity of water to find the permeability.

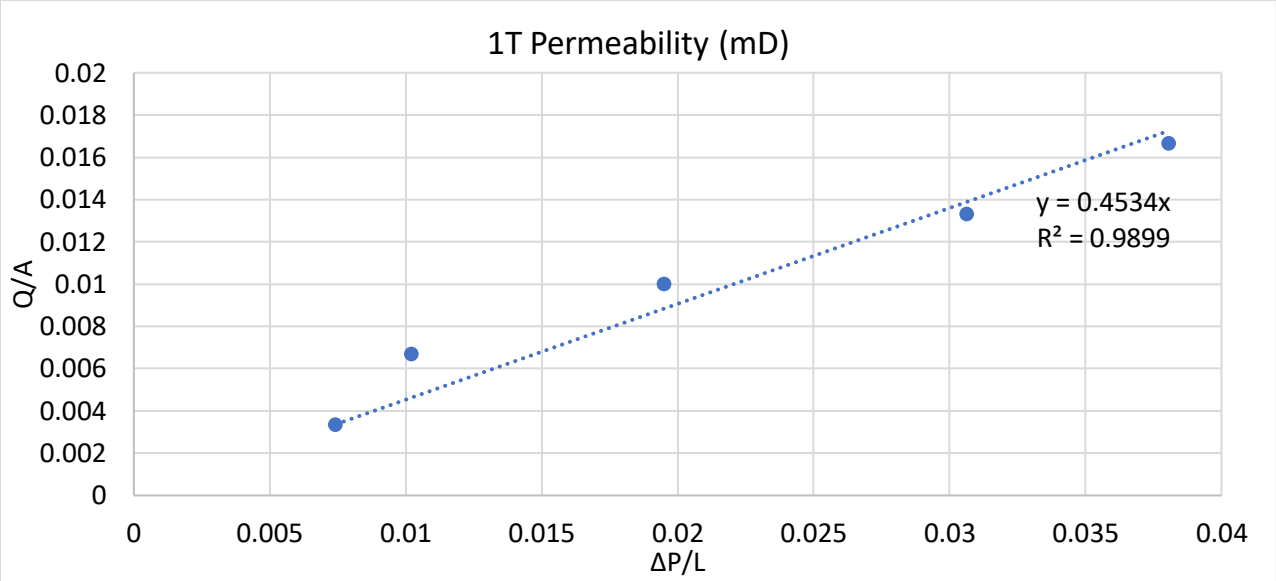

Fig 21: Absolute Permeability Curve of Core 1T

The scattering throughout the entirety of the graph is very minimal when compared with the points and one another and their closeness to the trendline drawn. This is reflected in the high trendline reliability value.

5.2.3.10 Core 3T Initial Absolute Permeability

Core 3T is the second member in the 'T' to have been measured to find the absolute permeability. Therefore, the first step was to measure the inlet pressure with every increase in brine flow rate. The table A14 in the appendix will present this data collected. From that a graph of ΔP/L and Q/A are drawn to find the slope of the trendline is to be found which will then be multiplied by the viscosity of water to find the permeability.

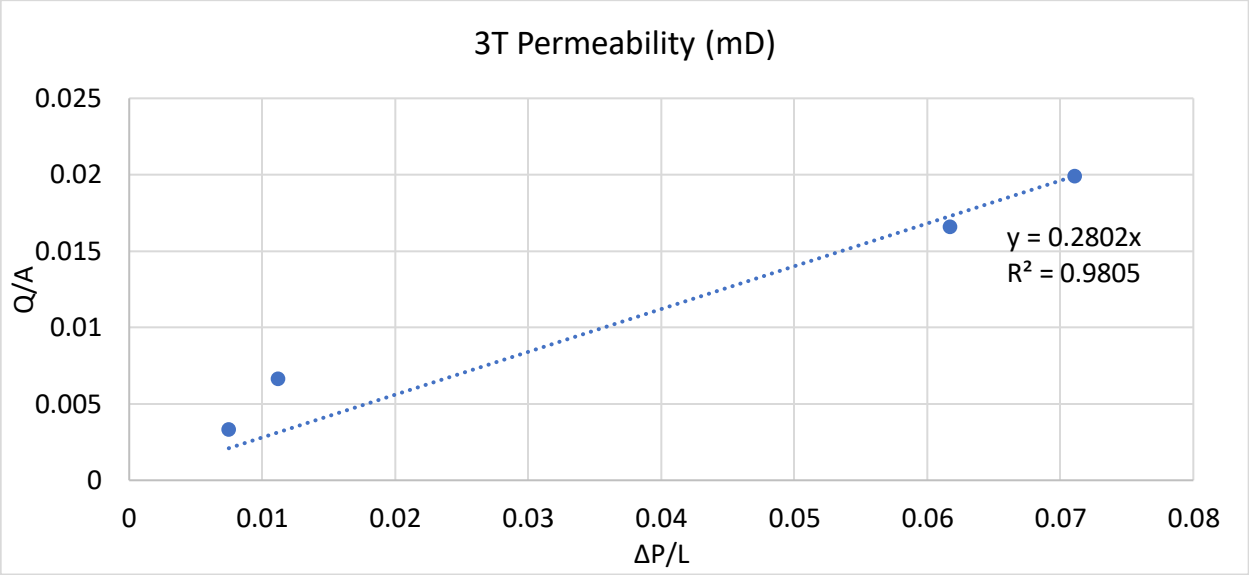

Fig 22: Absolute Permeability Curve of Core 3T

The scattering in this case has been highest amongst all other cores for most of the flow rates as made clear by the trend of the first 4 points. The last 2 points are reasonably scattered but overall, this has reduced the trendline reliability value; however, the value is not low enough to distrust the results or its accuracy.

5.2.3.11 Core 4T Initial Absolute Permeability

Core 4T is the third member in the 'T' to have been measured to find the absolute permeability. To begin with, one must measure the inlet pressure with every increase in brine flow rate. The table A15 in the appendix will present this data collected. From that a graph of ΔP/L and Q/A are drawn to find the slope of the trendline is to be found which will then be multiplied by the viscosity of water to find the permeability.

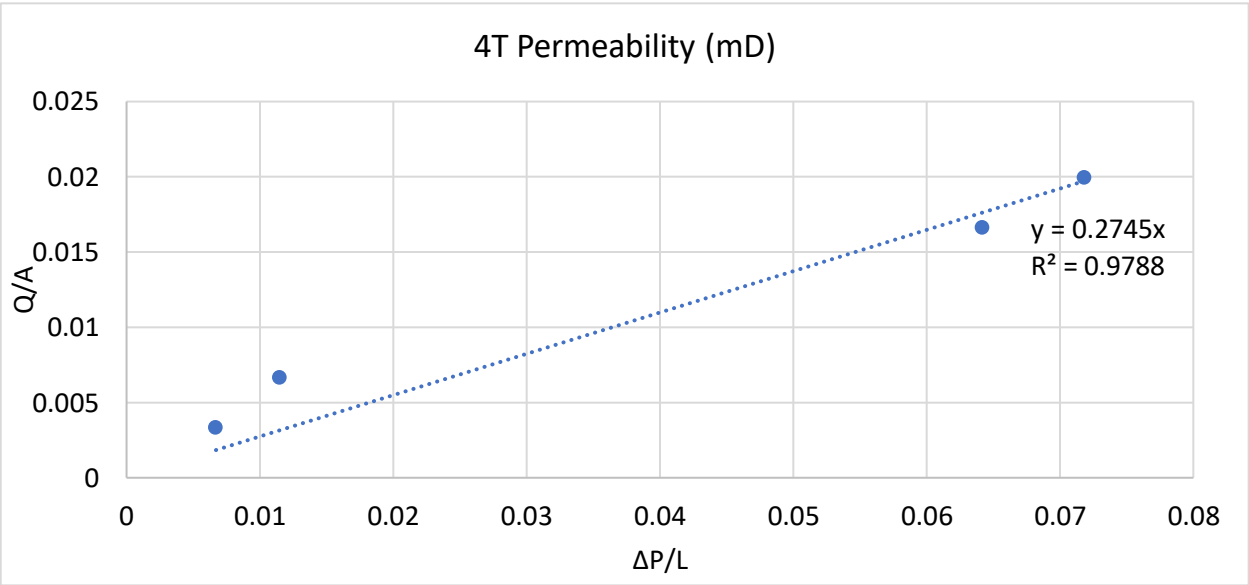

Fig 23: Absolute Permeability Curve of Core 4T

The scattering in this case, the same as core 3T, is highest amongst all other cores for most of the flow rates as made clear by the trend of the first 4 points. The last 2 points are reasonably scattered but overall, this has reduced the trendline reliability value; however, the value is not low enough to distrust the results or its accuracy.

5.2.3.12 Core 7T Initial Absolute Permeability

Core 7T is the fourth member in the 'T' to have been measured to find the absolute permeability. To begin with, the measurement of the inlet pressure with every increase in brine flow rate is be taken. The table A16 in the appendix will present the data collected. From this a graph of ΔP/L and Q/A are drawn to find the slope of the trendline is to be found which will then be multiplied by the viscosity of water to find the permeability.

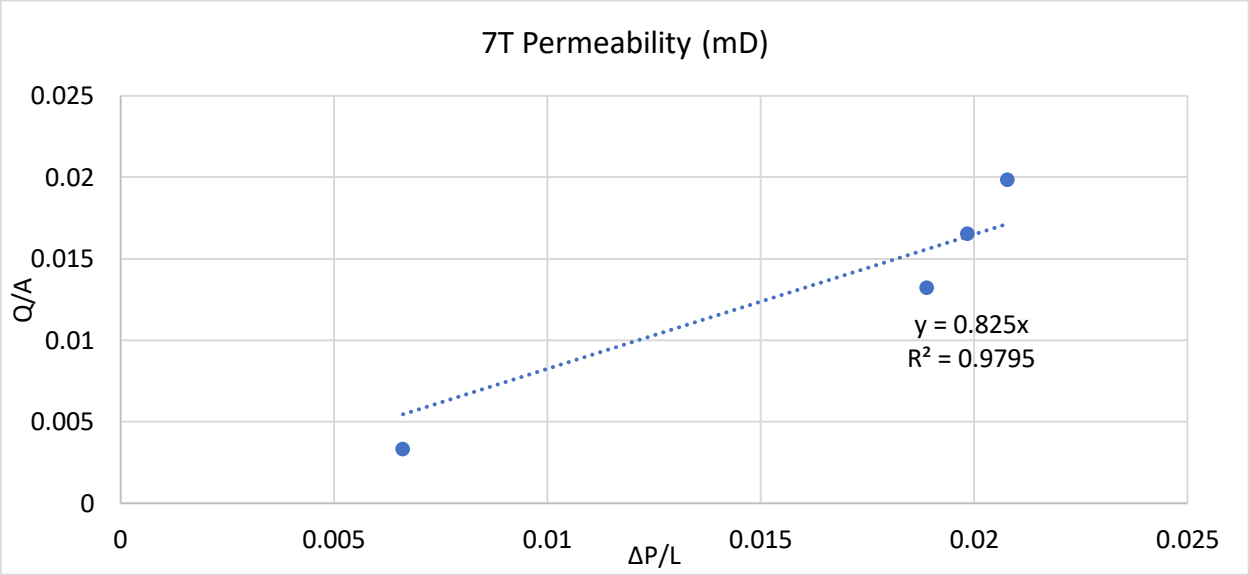

Fig 24: Absolute Permeability Curve of Core 7T

The scattering in this case, the same as core 3T, is highest amongst all other cores for most of the flow rates as made clear by the trend of the last 4 points. The first 2 points are reasonably scattered but overall, this has not greatly reduced the trendline reliability value and so the results and accuracy are still high.

5.2.3.13 Core 8T Initial Absolute Permeability

Core 7T is the fifth and last member in the 'T' to have been measured to find the absolute permeability. To begin with, the measurement of the inlet pressure with every increase in brine flow rate is be taken. The table A17 in the appendix will present the data collected. From this a graph of ΔP/L and Q/A are drawn to find the slope of the trendline is to be found which will then be multiplied by the viscosity of water to find the permeability.

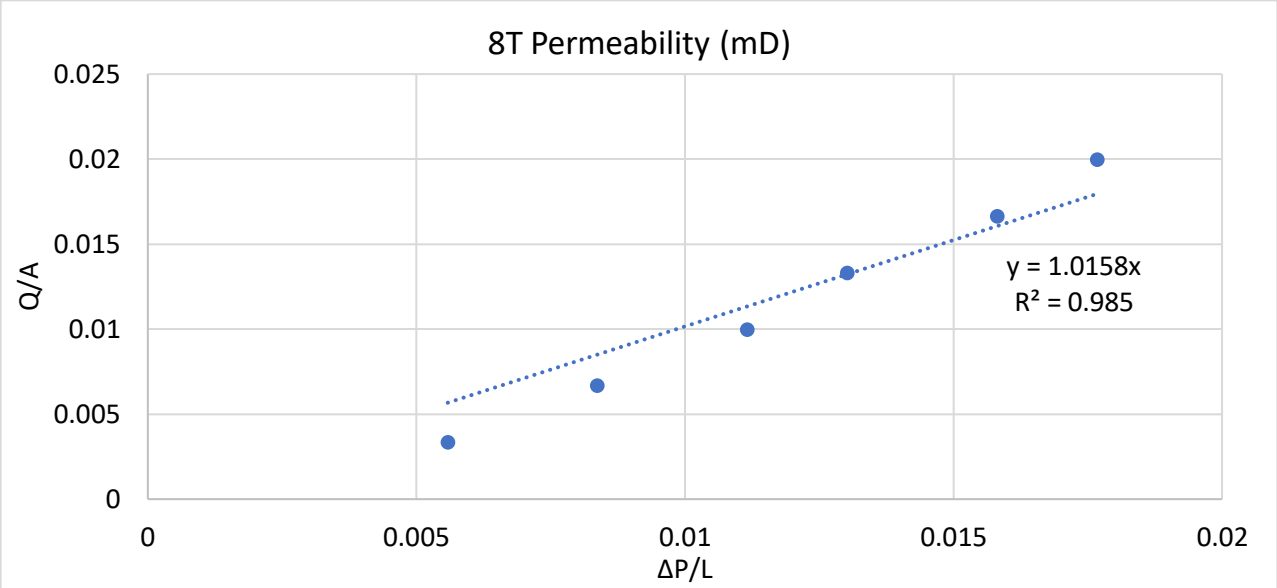

Fig 25: Absolute Permeability Curve of Core 8T

The scattering in this case is the lowest in amongst all of the members in this group. The scattering between the different flow rates is minimal and the relative distance between each of the respective points and the trendline is also exceedingly small. This is reflected by the high value of the trendline reliability value ensuring that the accuracy and reliability of the results is high.

5.2.3.14 Core 1U Initial Absolute Permeability

Core 1U is the first of two members in the 'U' group to have been measured to find the absolute permeability. To begin with, the measurement of the inlet pressure with every increase in brine flow rate is be taken. The table A18 in the appendix will present the data collected. From this a graph of ΔP/L and Q/A are drawn to find the slope of the trendline is to be found which will then be multiplied by the viscosity of water to find the permeability.

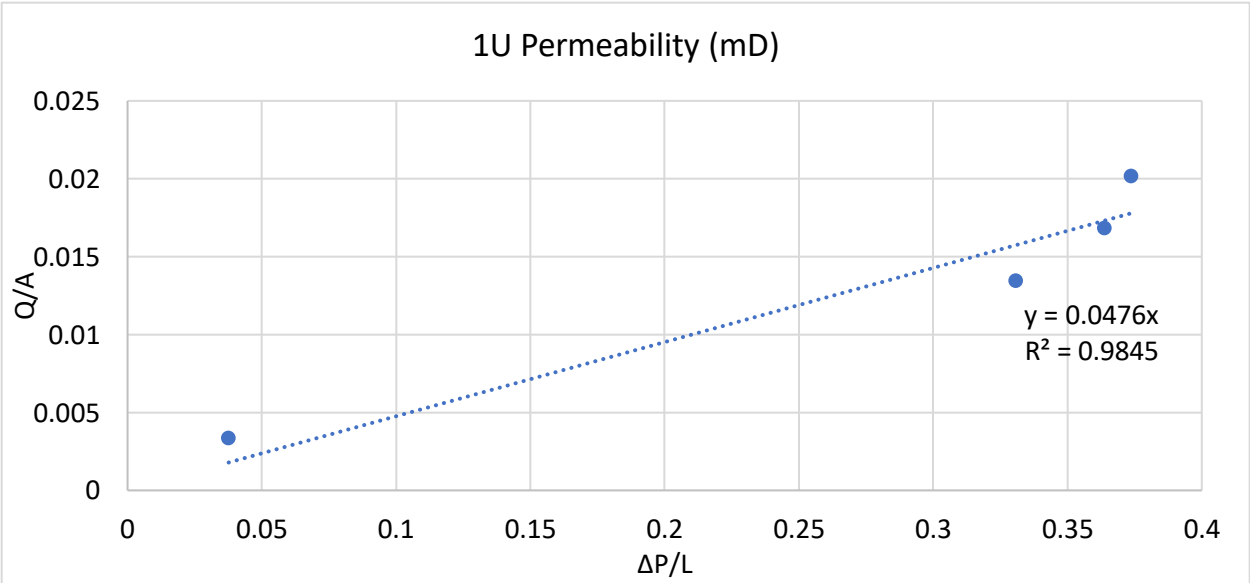

Fig 26: Absolute Permeability Curve of Core 1U

The scattering in this case is different again for the first 2 points than the other 4 points where the first 2 points are somewhat close together while the last 4 points have a similar upward pattern thar can be seen throughout the cores. The trendline reliability value has not been affected greatly with the scattering as the value is still high (0.965 from 1).

5.2.3.15 Core 5U Initial Absolute Permeability

Core 5U is the second of two members in the 'U' group to have been measured to find the absolute permeability. To begin with, the measurement of the inlet pressure with every increase in brine flow rate is be taken. The table A19 in the appendix will present the data collected. From this a graph of ΔP/L and Q/A are drawn to find the slope of the trendline is to be found which will then be multiplied by the viscosity of water to find the permeability.

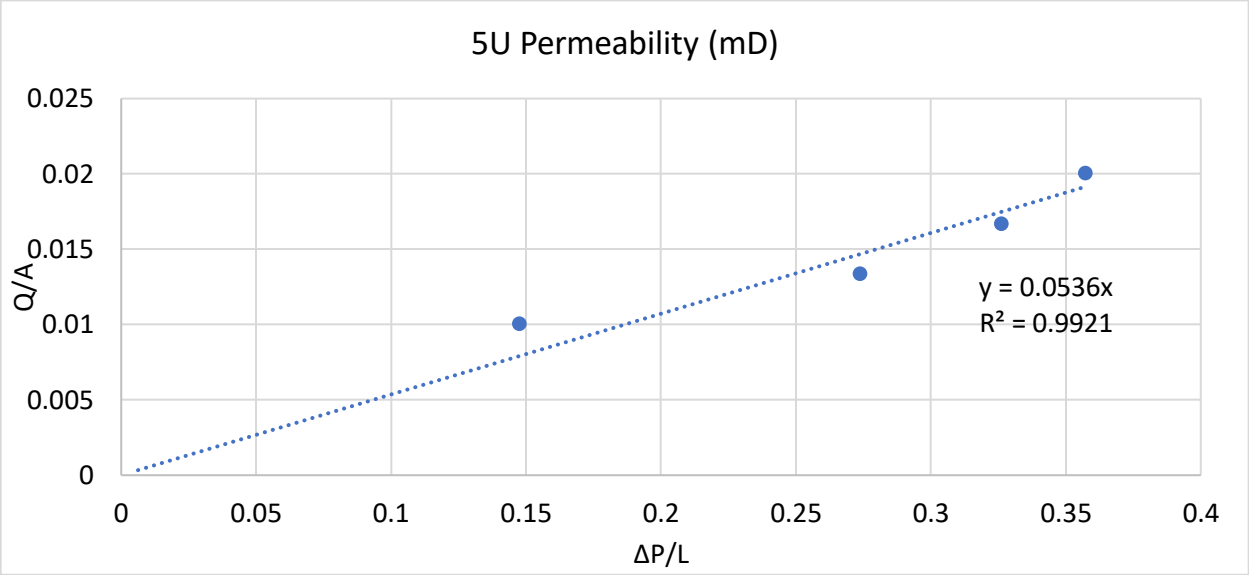

Fig 27: Absolute Permeability Curve of Core 5U

Only the first 2 points are not as close to the trendline when compared to the other 4 points which is why the trendline reliability value decreased slightly to 0.9475 from 1. However, the other 4 points are relatively close the trendline. The accuracy of the results according to the trendline and the trendline reliability value is high.

5.2.3.16 Core 4V Initial Absolute Permeability

Core 4V is the first of three members in the 'V' group to have been measured to find the absolute permeability. To begin with, the measurement of the inlet pressure with every increase in brine flow rate is be taken. The table A20 in the appendix will present the data collected. From this, a graph of ΔP/L and Q/A are drawn to find the slope of the trendline is to be found which will then be multiplied by the viscosity of water to find the permeability.

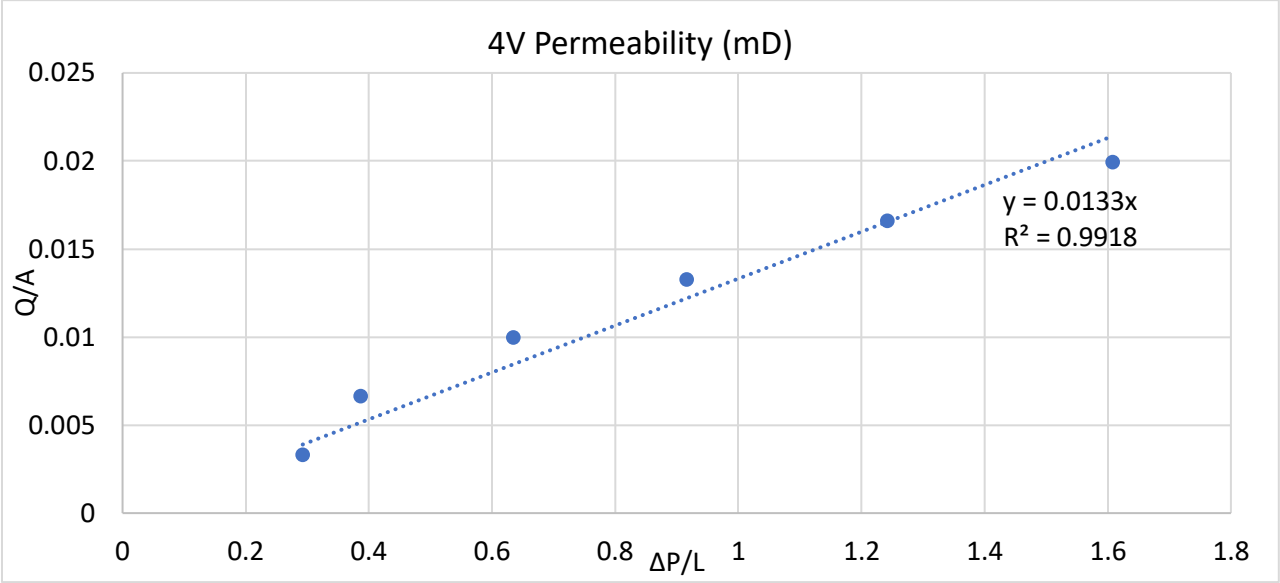

Fig 28: Absolute Permeability Curve of Core 4V

The scattering of the different points in this core in particular is almost zero as it can be seen from the closeness of the points to one another as well as the points and the trendline that has been drawn. Furthermore, the trendline reliability value is exceedingly high at a value of 0.9918 which is almost 1 i.e., perfect match.

5.2.3.17 Core 6V Initial Absolute Permeability

Core 6V is the second of three members in the 'V' group to have been measured to find the absolute permeability. To begin with, the measurement of the inlet pressure with every increase in brine flow rate is be taken. The table A21 in the appendix will present the data collected. From this, a graph of ΔP/L and Q/A are drawn to find the slope of the trendline is to be found which will then be multiplied by the viscosity of water to find the permeability.

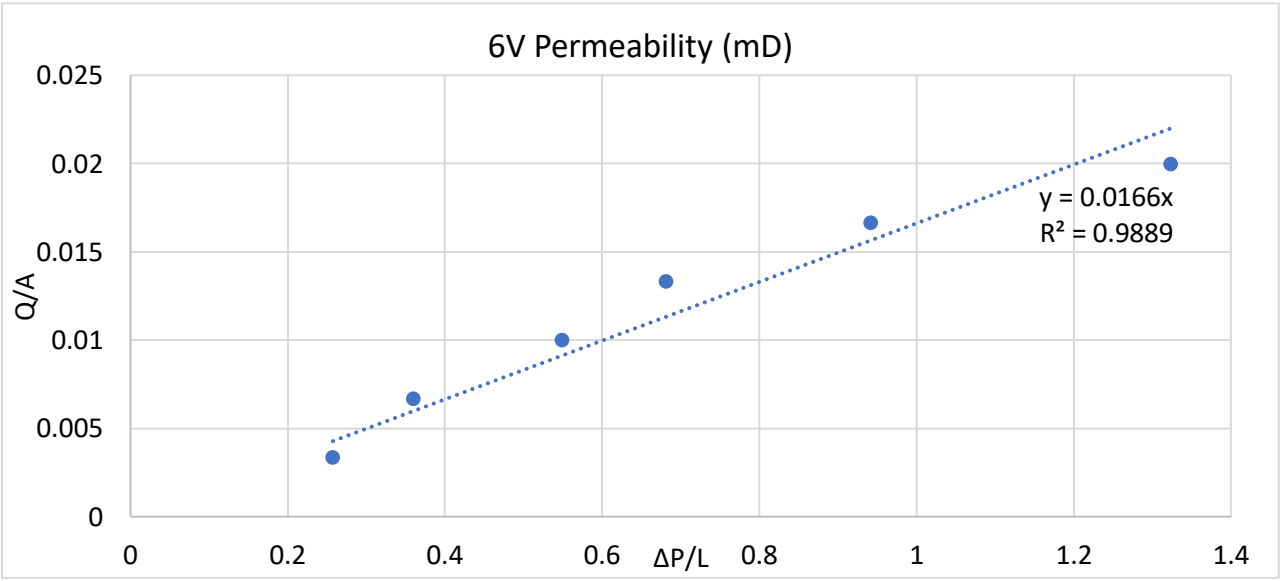

Fig 29: Absolute Permeability Curve of Core 6V

The same scattering effect can be seen in core 6V as the core before that in the same group, core 4V. The points are all close to each other and close to the trendline. Once again, the trendline reliability value is almost 1.

5.2.3.18 Core 9V Initial Absolute Permeability

Core 9V is the third and last member in the 'V' group to have been measured to find the absolute permeability. To begin with, the measurement of the inlet pressure with every increase in brine flow rate is be taken. The table A22 in the appendix will present the data collected. From this, a graph of ΔP/L and Q/A are drawn to find the slope of the trendline is to be found which will then be multiplied by the viscosity of water to find the permeability.

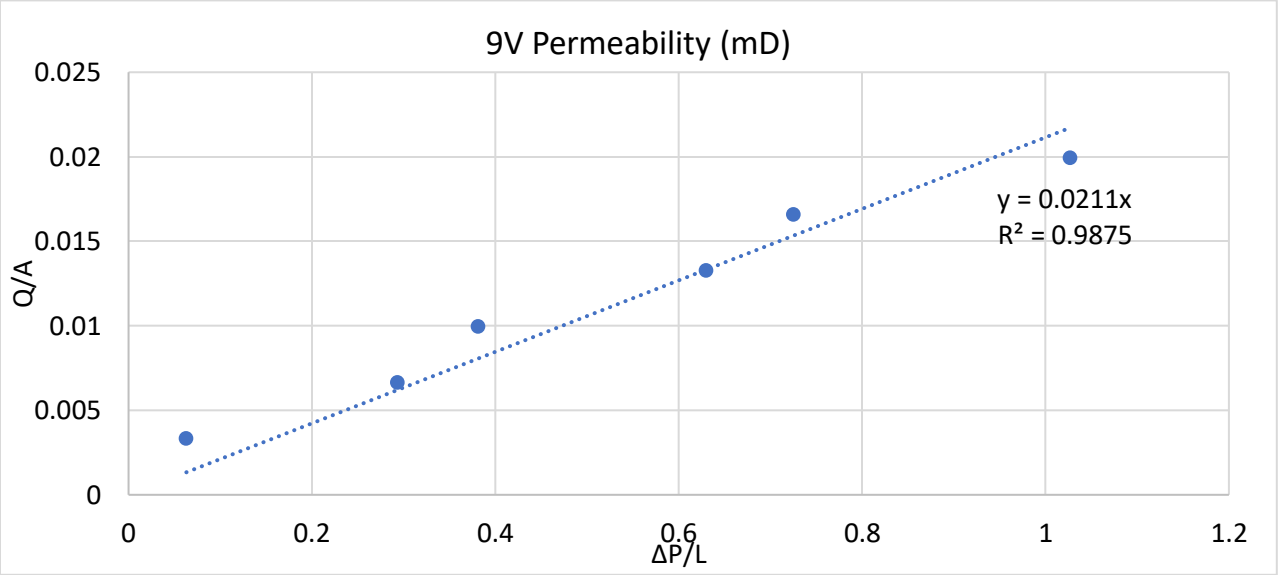

Fig 30: Absolute Permeability Curve of Core 9V

The same scattering profile here has occurred in the other two members of the same group where the points are close together. There are even two points which are the second and fourth flow rate that are perfectly on top of or awfully close to the trendline. Moreover, the trendline reliability value is also high reassuring the accuracy and reliability of the permeability.

5.2.3.19 Core 1X Initial Absolute Permeability

Core 1X is the first member in the 'X' group to have been measured to find the absolute permeability. To begin with, the measurement of the inlet pressure with every increase in brine flow rate is be taken. The table A23 in the appendix will present the data collected. From this, a graph of ΔP/L and Q/A are drawn to find the slope of the trendline is to be found which will then be multiplied by the viscosity of water to find the permeability.

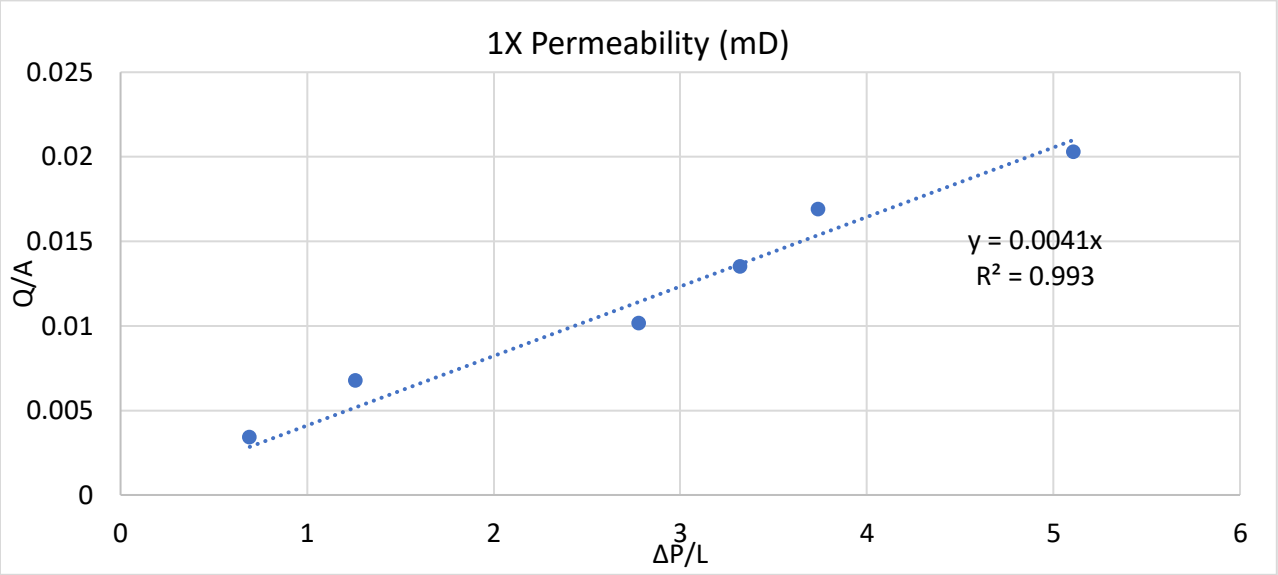

Fig 31: Absolute Permeability Curve of Core 1X

The points in this core are very close to one another and to the trendline making the accuracy of the results acceptable. Further, the trendline reliability value is almost equal to unity which reinforces the notion of accurate results.

5.2.3.20 Core 2X Initial Absolute Permeability

Core 2X is the second member in the 'X' group to have been measured to find the absolute permeability. To begin with, the measurement of the inlet pressure with every increase in brine flow rate is be taken. The table A24 in the appendix will present the data collected. From this, a graph of ΔP/L and Q/A are drawn to find the slope of the trendline is to be found which will then be multiplied by the viscosity of water to find the permeability.

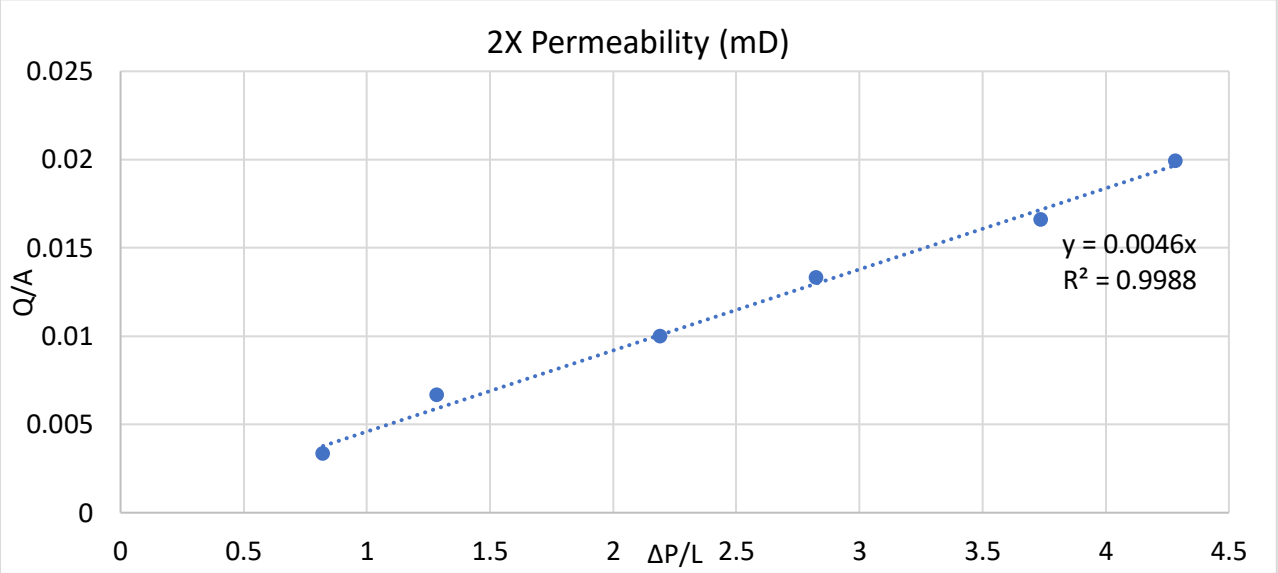

Fig 32: Absolute Permeability Curve of Core 2X

The points are almost perfectly aligned with one another and to the trendline that has been drawn accordingly. The value of the trendline reliability is amongst of all the cores tested in all of the groups. The reliability and accuracy of this core is under no question.

5.2.3.21 Core 3X Initial Absolute Permeability

Core 3X is the third and last member in the 'X' group as well as the last core to have been measured to find the absolute permeability. To begin with, the measurement of the inlet pressure with every increase in brine flow rate is be taken. The table A24 in the appendix will present the data collected. From this, a graph of ΔP/L and Q/A are drawn to find the slope of the trendline is to be found which will then be multiplied by the viscosity of water to find the permeability.

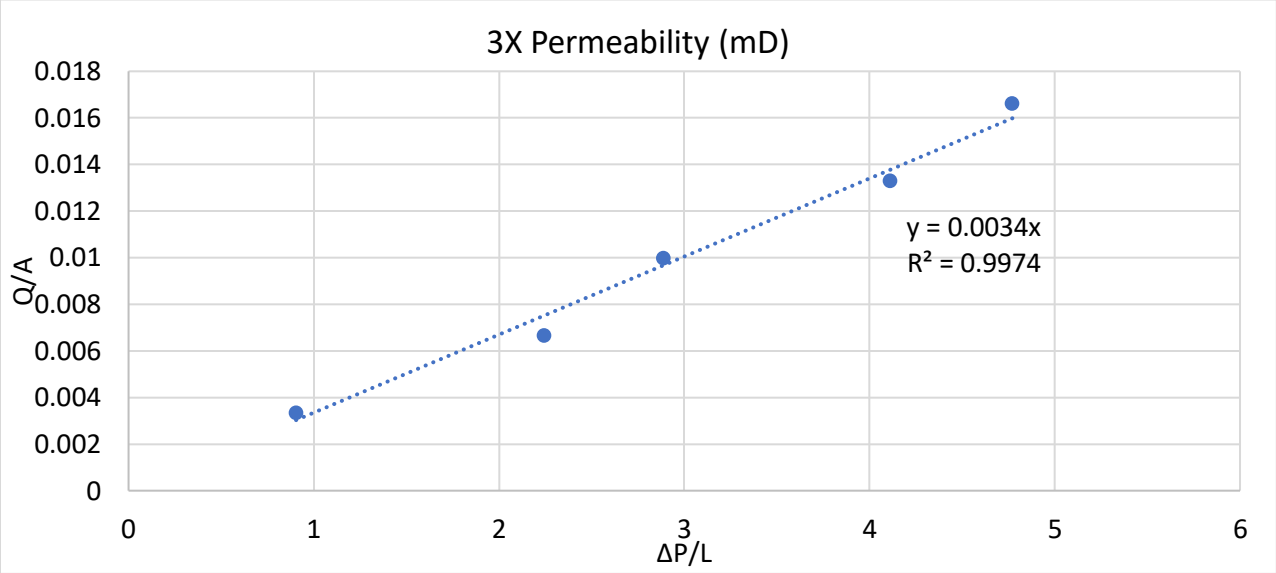

Fig 33: Absolute Permeability Curve of Core 3X

The points are almost perfectly aligned with one another and to the trendline that has been drawn accordingly. The value of the trendline reliability is amongst of all the cores tested in all of the groups. The reliability and accuracy of this core is under no question.

5.2.4 Selection of Cores for Remainder of Research

From the measurements taken of both porosity and absolute permeability, a selection of cores needed to be chosen to continue on further with the research. According to the methodology, 4 groups were to be chosen with a combination of porosity and permeability; however, the 4 categories were difficult to be obtained due to the nature of the cores themselves and the thus the rock property data collected so far. Therefore, 3 groups were chosen which are high porosity and high absolute permeability with cores 8T, and 7T to represent a wide range of absolute permeabilities. Then medium permeability with medium porosity relative to the range of porosities and permeabilities that were found with cores 9S and 7R to be tested for this category. Furthermore, the third group is low absolute permeability and low porosity also relative to the range of porosities and permeabilities that were found with cores 6V, 7R, and 3X being selected.

When starting to saturate the cores with oil, an issue was faced with the third group which is the low absolute permeability and low porosity. The cores could not even be partially saturated with oil due to the excessively low absolute permeability which would make any results after that unacceptable. Moreover, applying water injection on cores of just under 3 mD does not make much sense as formations in the field with such a low absolute permeability would not have water injection being applied to them in the first place. This led for a decision to only have the first 2 groups as oil saturation was achievable as well as the absolute permeabilities are close to actual cases where water injection can be used. Unfortunately, core 7R got broken as well during the testing (see figure 34) and so it was replaced by core 1U.

Fig 34: Broken Core 7R

In addition, core 4T was also added to make the range of permeabilities tested more representative with the absolute permeability of core 4T being in the middle of the first and second group. All of these alterations finally led to the selection of the following cores to be tested which are: 8T, 7T, 4T, 1U, and 9S. The table below will summarize the porosity and absolute permeability data of the 5 cores selected to be used for the remainder of this research.

Sample Name	Porosity (porosity unit – pu)	Absolute Permeability (mD)
9S	26.45	55.08
4T	32.91	357.24
7T	33.13	880.44
8T	30.95	1218.96
1U	28.60	55.32

Table 9: Summary of Selected Cores for Further Research

5.2.5 Initial Relative Permeabilities and Waterflooding of Selected Cores

As both waterflooding and relative permeability entails imbibition and drainage of two fluids with one being the wetting and the other the non-wetting then the relative permeability experimentation would also entail the waterflooding simulation. For the waterflooding simulation case, the amount of oil recovered at the end was collected and the recovery factor was calculated to see the percentage of oil recovered. The data collected as well as the relative permeability curves for the above five selected cores are to be presented in this section.

5.2.5.1 Core 9S Initial Relative Permeability and Waterflooding

Sample Name	Average Length (mm)	Average Width (mm)	Dry Weight (g)	Porosity (pu)	Cross Sectional Area (Cm2)	Saturated Weight (g)	Liquid Permeability (md)
9S	76.16	2.52	74.71	26.45	4.99	84.26	55.08

Table 10: Summary of Data Needed for Initial Relative Permeability of Core 9S

Recovered Volumes	Volume (cc)
Total initial recovered water	6.4
Dead Water Volume	2.6
Corrected initial water recovered	3.8
Pore Volume	8.52
Bulk Volume	36.31
Sw_i (%)	55.43
So_r (%)	55.2
Recovery Factor (%)	44.80

Table 11: Summary Data of Initial Relative Permeability for Core 9S

The saturation of oil was not as sufficient as was needed; however, the amount of oil saturated was as much as the core can withstand at that current time. Further time was allowed for the oil saturation to occur with no positive outcome and so the oil injection was stopped. The same has also occurred to the water injection and oil production with more than half of the oil still located inside the pores of the core.

Another issue faced was that the inlet pressure when performing the water injection was not stable and kept on increasing and decreasing between each step which did not create the best curve. The vibration should improve the injectivity of the oil and water in the later stages of the research.

The first time recorded is the water breakthrough which occurs when the first droplets of water start to emerge with the oil. This has occurred at four minutes and thirty-five seconds as per table 28 presented above. The difference between the inlet pressure from breakthrough till the end is only 28.9 psi which is not a lot. This is reflected also by the volume of connate oil saturation which is at 55 percent. This data is found in table A25 in the appendix.

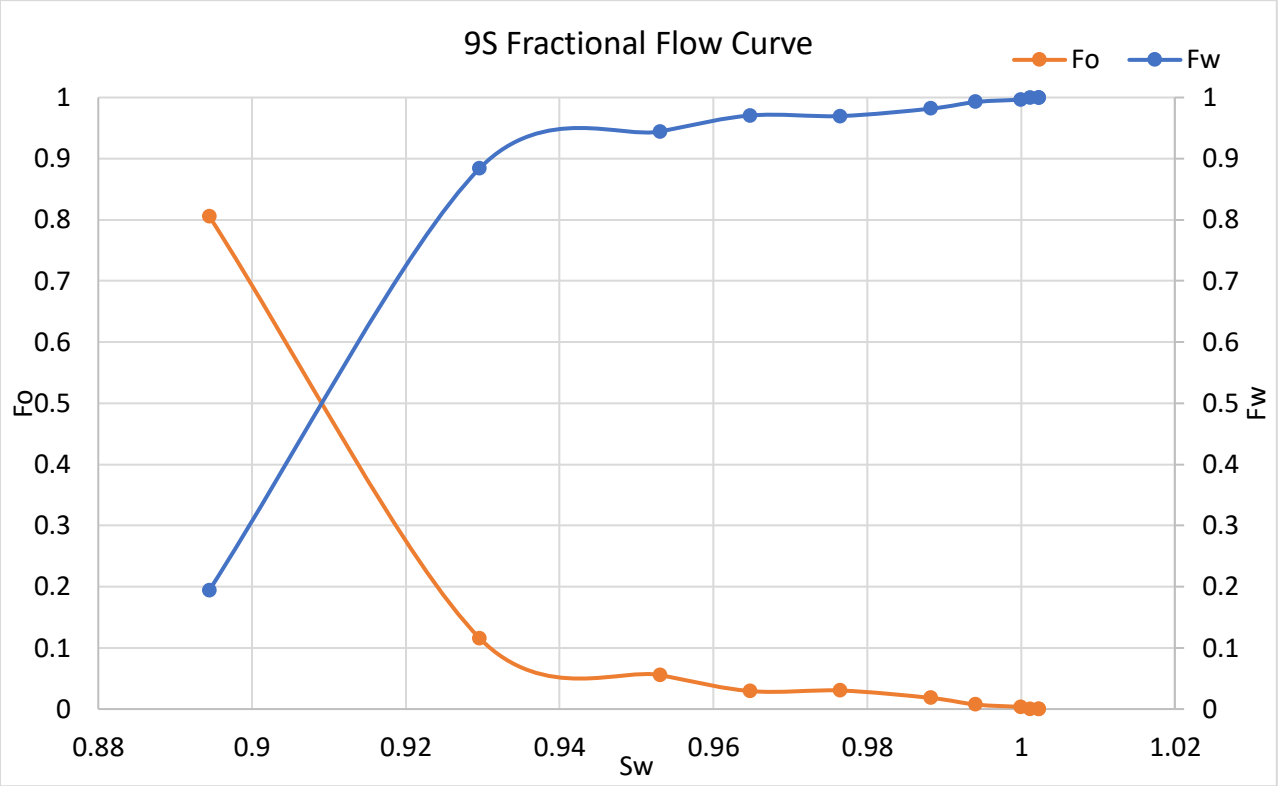

Fig 35: Initial Fractional Flow Curve for Core 9S

The fractional flow curve shows the imbibition and drainage process of core 9S. The core is very water wet as can be seen from the intersection point being at a water saturation almost at 1 (approximately at 0.91). This data will be found in table A26 in the appendix.

From the relative permeability data in table A27 in the appendix, the relative permeability curve can be drawn. Any data that is outside the typical range has been excluded due to it not being accurate or realistic when drawing the curve itself.

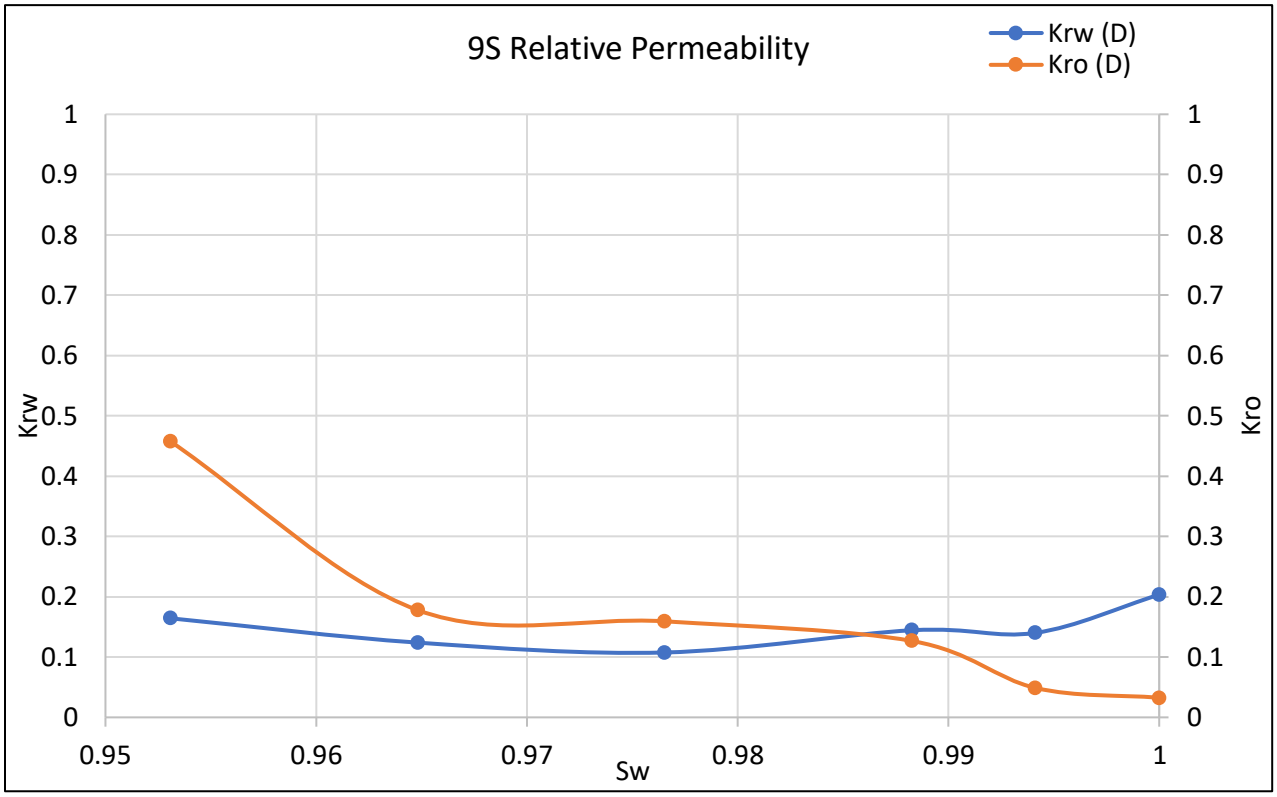

Fig 36: Initial Relative Permeability Curve of Core 9S

The relative permeability curve is unfortunately not an ideal one in this case specifically. Regarding the relative permeability to oil the curve should start from higher; however, it does not. For the relative permeability to water the curve should start from lower down and reach higher at the other end. These results would lead back to the nature of the core itself being is manufactured and not natural rock and so the components themselves may affect the flow of oil and water through the core. In addition, the permeameter apparatus as previously mentioned faced difficulties specifically with this core as the injection of both oil and water was not able to be completed as well as the struggle for the inlet pressure to become stabilized to make any readings. Furthermore, the inlet pressure kept increasing and decreasing for some of the time steps which made reading the accurate pressures tedious. All of these reasons are what led to the relative permeability curve to appear in the way that it does. Regardless of all of this, the recovery factor is around 45 percent which is very acceptable even though there were some troubles injecting both fluids. The effective oil permeability at breakthrough is around 0.8 Darcy.

5.2.5.2 Core 4T Initial Relative Permeability and Waterflooding

Sample Name	Average Length (mm)	Average Width (mm)	Dry Weight (g)	Porosity (pu)	Cross Sectional Area (Cm2)	Saturated Weight (g)	Liquid Permeability (md)
4T	7.10	2.53	64.61	32.91	5.04	73.918	357.24

Table 12: Summary of Data Needed for Initial Relative Permeability of Core 4T

Recovered Volumes	Volume (cc)
Total initial recovered water	9.4
Dead Water Volume	2.6
Corrected initial water recovered	6.8
Pore Volume	8.31
Bulk Volume	36.31
Sw_i (%)	18.18
So_r (%)	40.56
Recovery Factor (%)	59.44

Table 13: Summary Data of Initial Relative Permeability for Core 4T

The oil saturation in this case is very acceptable with the initial water saturation being at only 18 percent. Most of the water was recovered when initially injecting the oil which makes this core's relative permeability experimentation reliable to consider. However, the production of the oil through the waterflooding was regrettably not as successful. This was due to the large percentage of oil left behind in the core as it is made clear from the irreducible water saturation of around 40 percent even though the absolute permeability and porosity both being high to some extent relative to the ranges of each, respectively.

The first time recorded is the water breakthrough which occurs when the first droplets of water start to emerge with the oil. This has occurred at three minutes and seven seconds only. The difference between the inlet pressure from breakthrough till the end is only about 26 psi which is not a lot. This is reflected also by the volume of connate oil saturation which is at 40.5 percent. The production of water took a fairly large amount of time of nearly 7 hours to produce all of the oil that it can. This data can be found in table A28 in the appendix.

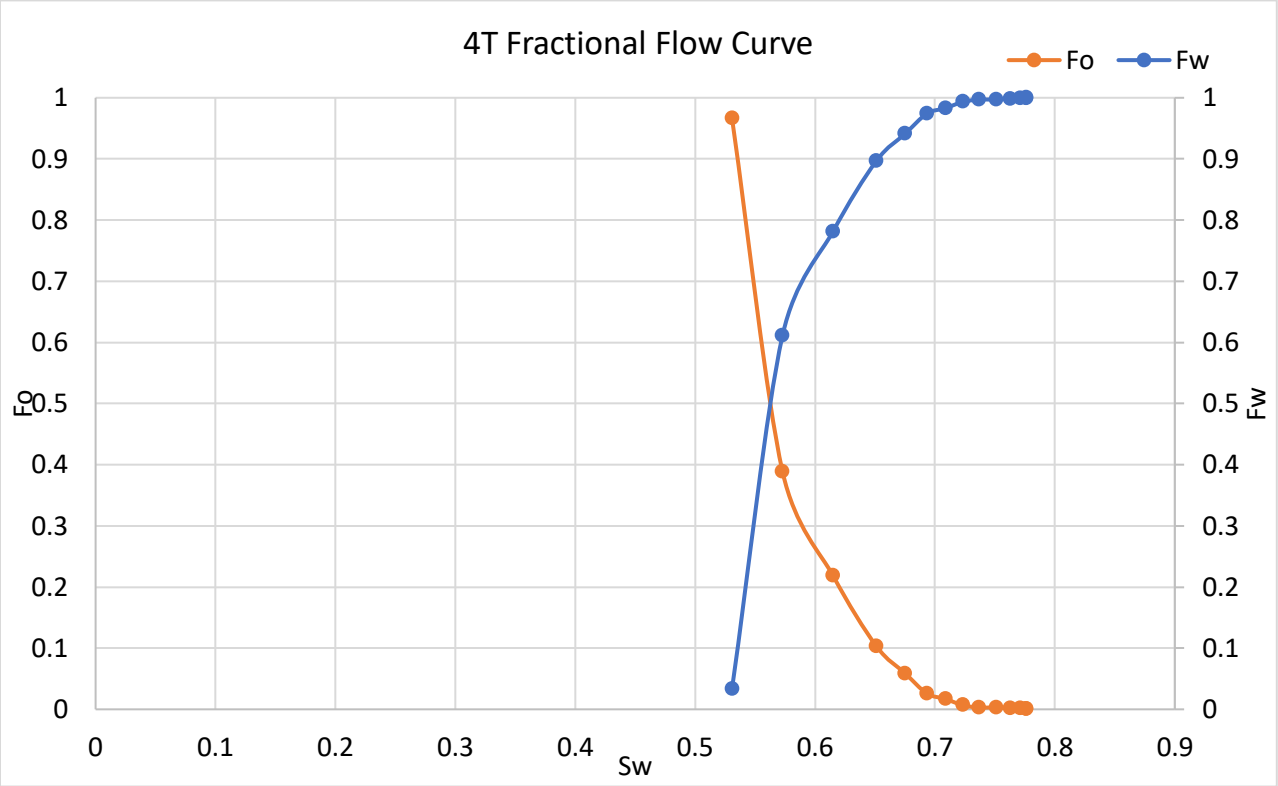

Fig 37: Initial Fractional Flow Curve for Core 4T

The fractional flow curve shows that imbibition and drainage process occurred relatively at the same rate as the saturation of water at the intersection point is almost at 50 percent (approximately at 55 percent). Moreover, the trends of both curves are almost identical meaning that the imbibition and drainage process occurred at almost the same. This would infer that the wettability is slightly water wet. This data can be found in table A29 in the appendix.

From the relative permeability data in table A30 in the appendix, the relative permeability curve can be drawn. All data is within the normal or typical limits of the relative permeability curve and therefore, all of the points have been included in the drawing of the curve.

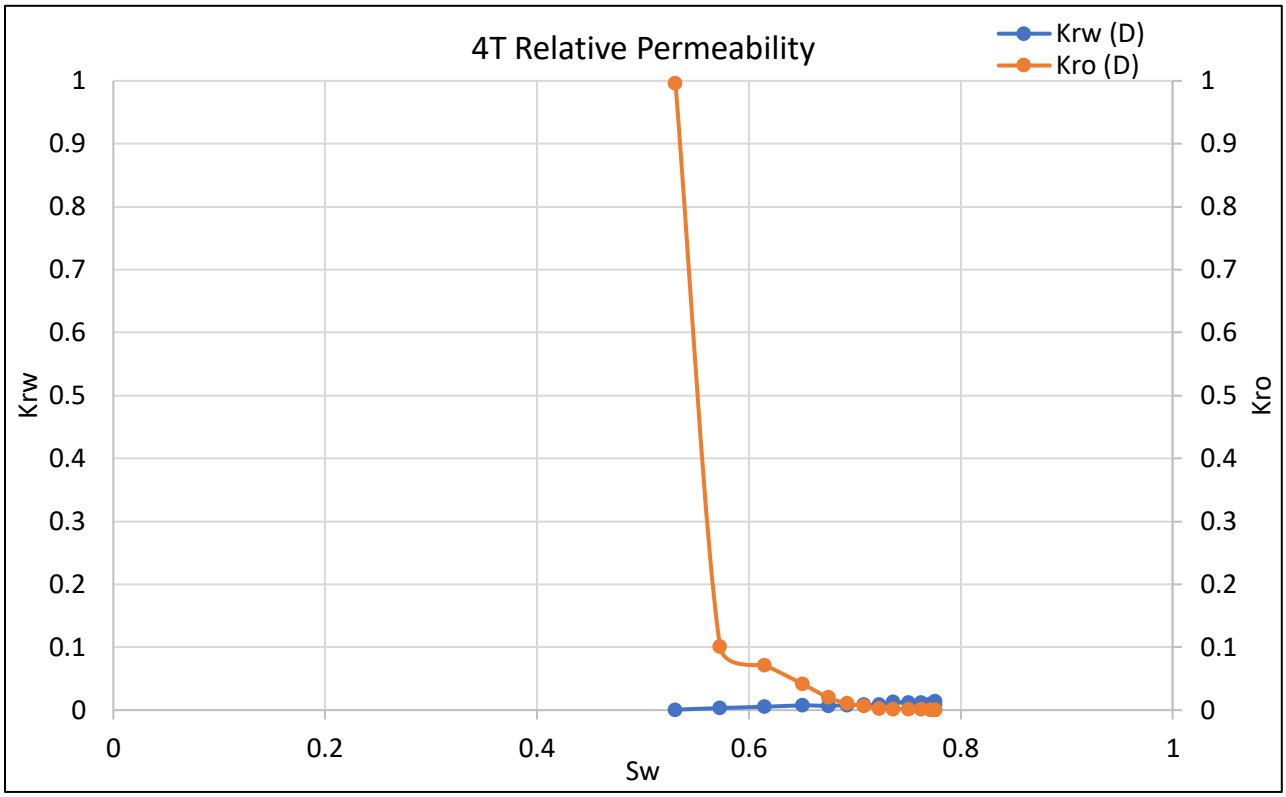

Fig 38: Initial Relative Permeability Curve of Core 4T

The relative permeability curve clearly shows that the core is water wet as the intersection point is at a water saturation of around 0.7 which is water wet. There is a massive drop between the breakthrough and the second time point when it comes to the relative permeability of oil. The effective oil permeability at breakthrough is 0.35 Darcy.

5.2.5.3 Core 7T Initial Relative Permeability and Waterflooding

Sample Name	Average Length (mm)	Average Width (mm)	Dry Weight (g)	Porosity (pu)	Cross Sectional Area (Cm2)	Saturated Weight (g)	Liquid Permeability (md)
7T	7.19	2.54	66.74	33.13	5.06	77.86	880.44

Table 14: Summary of Data Needed for Initial Relative Permeability of Core 7T

Recovered Volumes	Volume (cc)
Total initial recovered water	10
Dead Water Volume	2.6
Corrected initial water recovered	7.4

Pore Volume	9.93
Bulk Volume	36.31
Sw_i (%)	25.47
So_r (%)	49.14
Recovery Factor (%)	50.86

Table 15: Summary Data of Initial Relative Permeability for Core 7T

The initial water saturation is quite satisfactory with only a quarter of the total water being left behind in the core. On the other hand, the oil production due to the water injection was not as effective as it can be seen that the irreducible oil saturation is around 50 percent with only 50 percent of the oil recovered.

The breakthrough time had occurred at three minutes and forty-nine seconds only. The difference between the inlet pressure from breakthrough till the end is only about 41 psi which is higher than other cores but is clearly not sufficient enough to produce the majority of the oil. This is further shown also by the volume of connate oil saturation of around 50 percent. The production of water took a fairly large amount of time of just over 7 hours to produce just the 50 percent of oil. This data can be found in table A31 in the appendix.

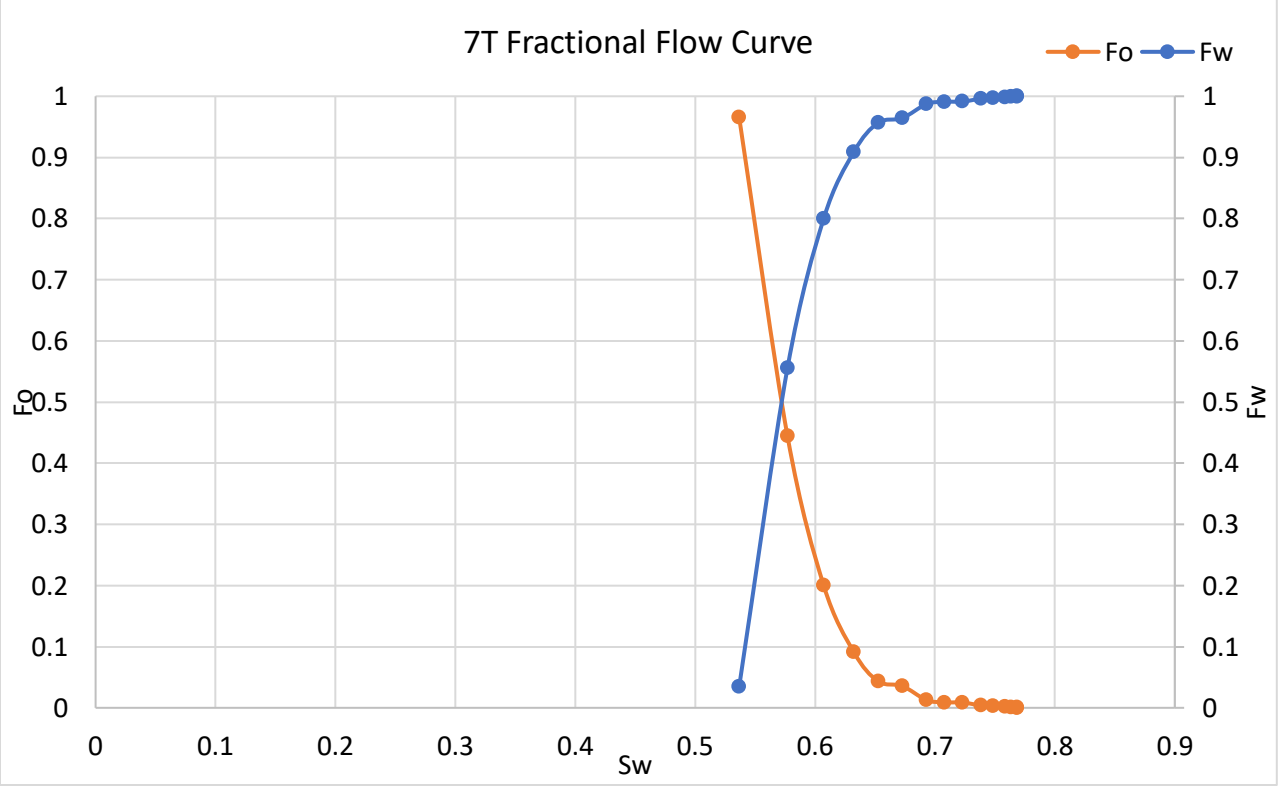

Fig 39: Initial Fractional Flow Curve for Core 7T

The fractional flow curve shows that imbibition and drainage process occurred relatively at the same rate as the saturation of water at the intersection point is almost at 50 percent (approximately at 58 percent). Moreover, the trends of both curves are almost identical meaning that the imbibition and drainage process occurred at almost the same. This would infer that the wettability is slightly water wet. This data can be found in table A32 in the appendix.

From the relative permeability data in table A33, the relative permeability curve can be drawn. All data is within the normal or typical limits of the relative permeability curve and therefore, all of the points have been included in the drawing of the curve.

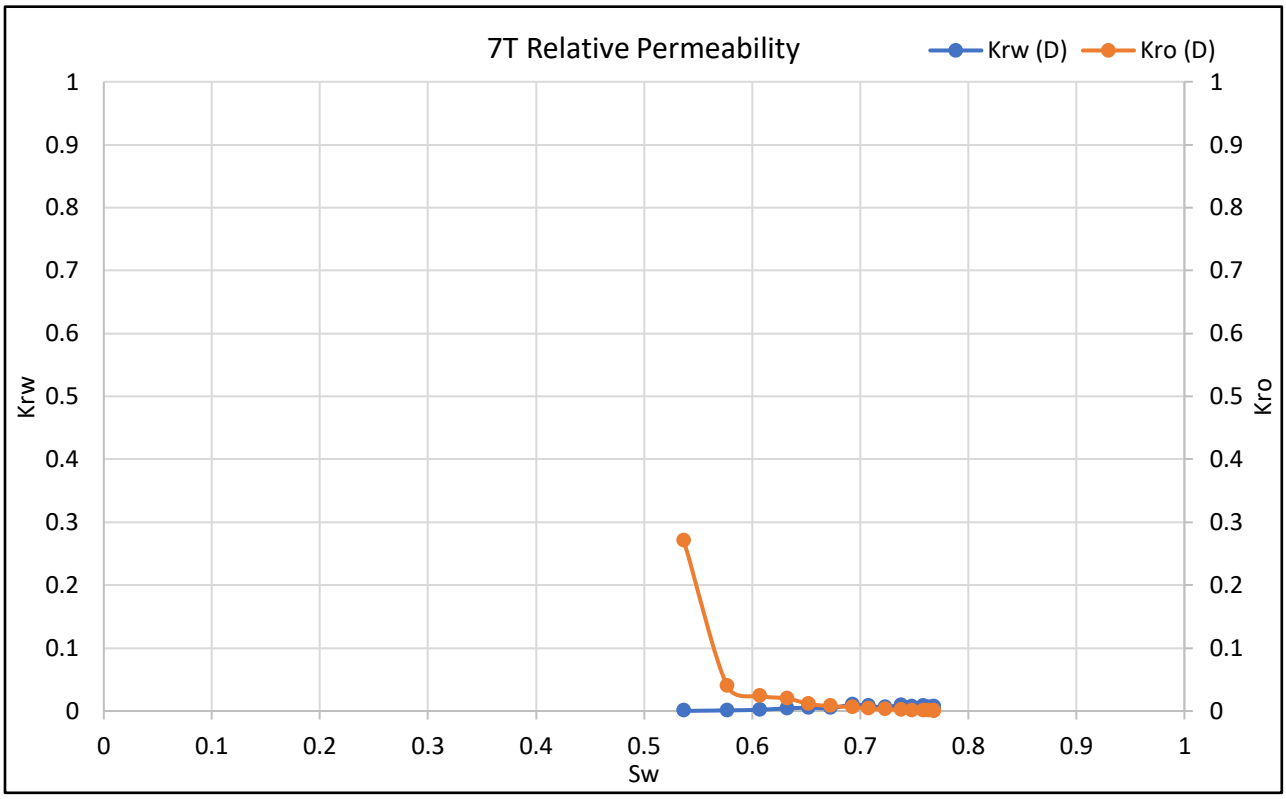

Fig 40: Initial Relative Permeability Curve of Core 7T

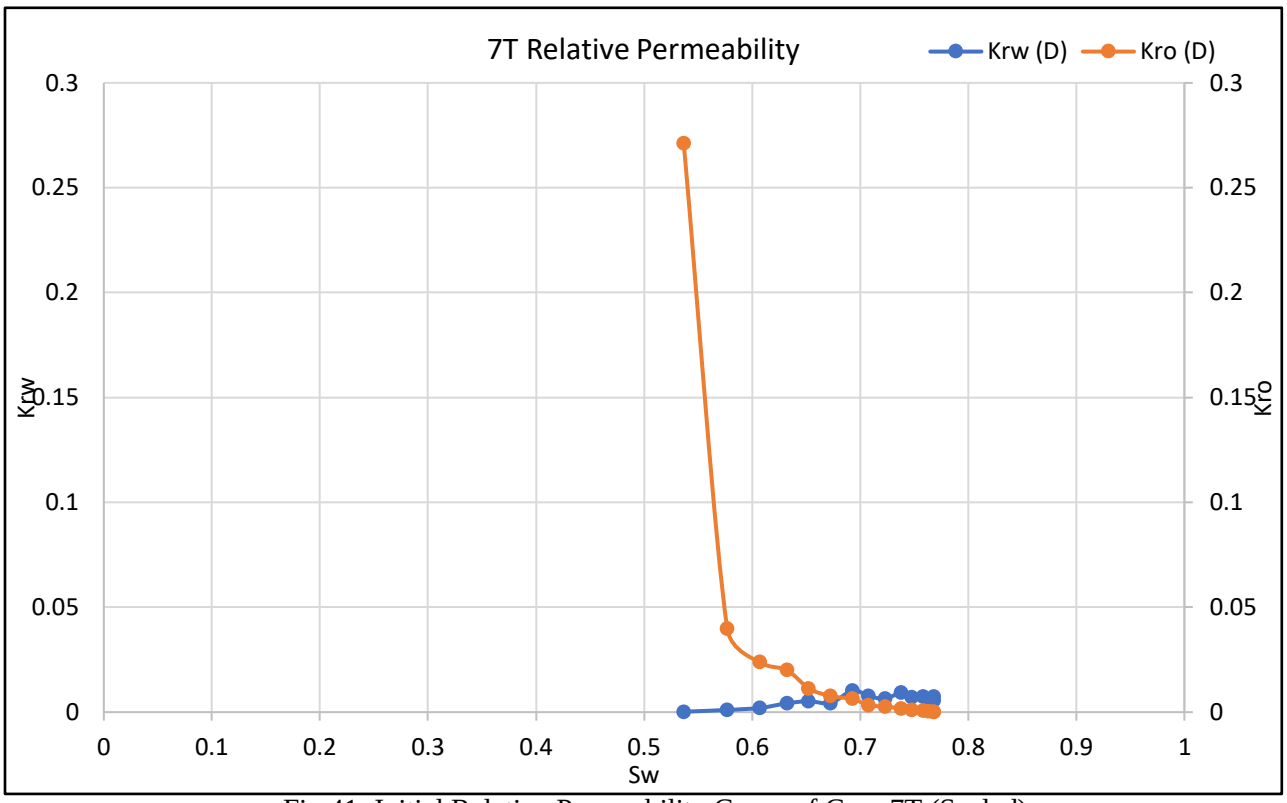

Fig 41: Initial Relative Permeability Curve of Core 7T (Scaled)

The core is water wet as the intersection is at around 0.7 water saturation (approximately 0.68). The ranges of both curves are very small with minimal with not much change in both saturations but a much higher change in saturation of oil. The largest drop in oil relative permeability occurred between the first 2 time points or right after water breakthrough. The effective oil permeability at breakthrough is 0.23 Darcy. The difference in water saturation from the beginning till the end of the relative permeability experiment is not a lot with a change of only 0.23 which explains the small scale of change on the x-axis. As the water injection did not produce around half of the oil inside the core, this would explain the low water permeability shown by the water relative permeability curve.

5.2.5.4 Core 8T Initial Relative Permeability and Waterflooding

Sample Name	Average Length (mm)	Average Width (mm)	Dry Weight (g)	Porosity (pu)	Cross Sectional Area (Cm2)	Saturated Weight (g)	Liquid Permeability (md)
8T	7.31	2.53	68.15	30.95	5.03	79.23	1218.96

Table 16: Summary of Data Needed for Initial Relative Permeability of Core 8T

Recovered Volumes	Volume (cc)
Total initial recovered water	10.3
Dead Water Volume	2.6
Corrected initial water recovered	7.7
Pore Volume	9.89
Bulk Volume	36.31
Sw_i (%)	22.17
So_r (%)	56.84
Recovery Factor (%)	43.16

Table 17: Summary Data of Initial Relative Permeability for Core 8T

The oil saturation is very acceptable as the initial water saturation is only at around 20 percent as this is experimental work. However, the water flooding in this specific case was not as successful as the oil saturation as the recovery of the oil is only just under 45 percent making it close to around 50 percent. Therefore, just under half of the oil saturated was able to be produced from the water flooding application for this core.

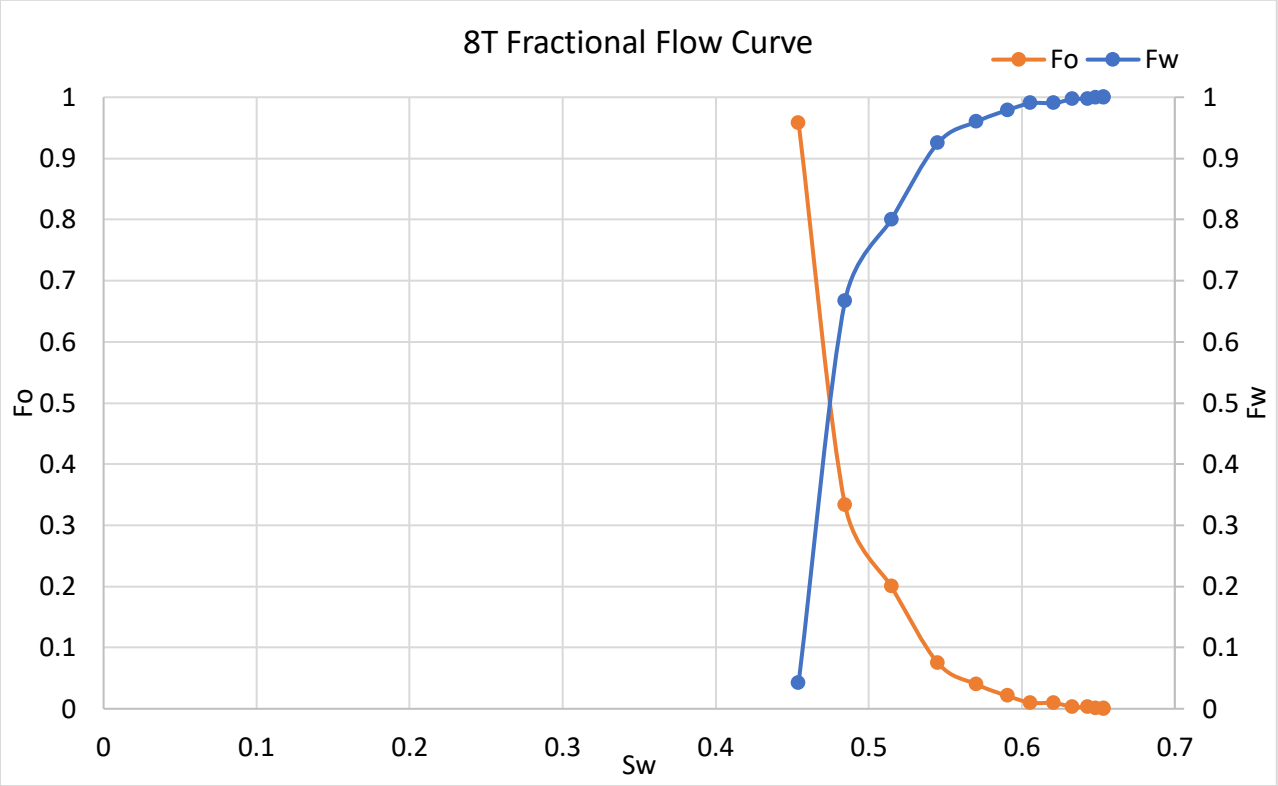

Fig 42: Initial Fractional Flow Curve for Core 8T

The fractional flow curves show the same idea as the table before that when it comes to the saturation of oil and water respectively. The oil saturation occurred very well as the fractional flow starts from 0.95 (almost 1) all the way to zero which means that the oil has entered and produced almost all of the water which can be confirmed by the low initial water saturation of 22 percent. The fractional water began at a slightly later stage and ended at 1. The slight delay as well as the large gap between the first 2 points once again approves the irreducible oil saturation over 50 percent and thus recovery of just under 50 percent. This data can be found in table A34 in the appendix.

The breakthrough time had occurred at two minutes and fifty-five seconds only which is one of the quickest times between the cores done. The difference between the inlet pressure from breakthrough till the end is only about 36.8 psi which is somewhat high compared to other cores but clearly not sufficient enough to produce the majority of the oil. This is further shown also by the volume of connate oil saturation of just over 50 percent. The production of water took a fairly large amount of time of just under 6 hours to produce less than 50 percent of oil. This data can be found in table A35 in the appendix.

From the relative permeability data in table 36, the relative permeability curve can be drawn. All data is within the normal or typical limits of the relative permeability curve and therefore, all of the points have been included in the drawing of the curve.

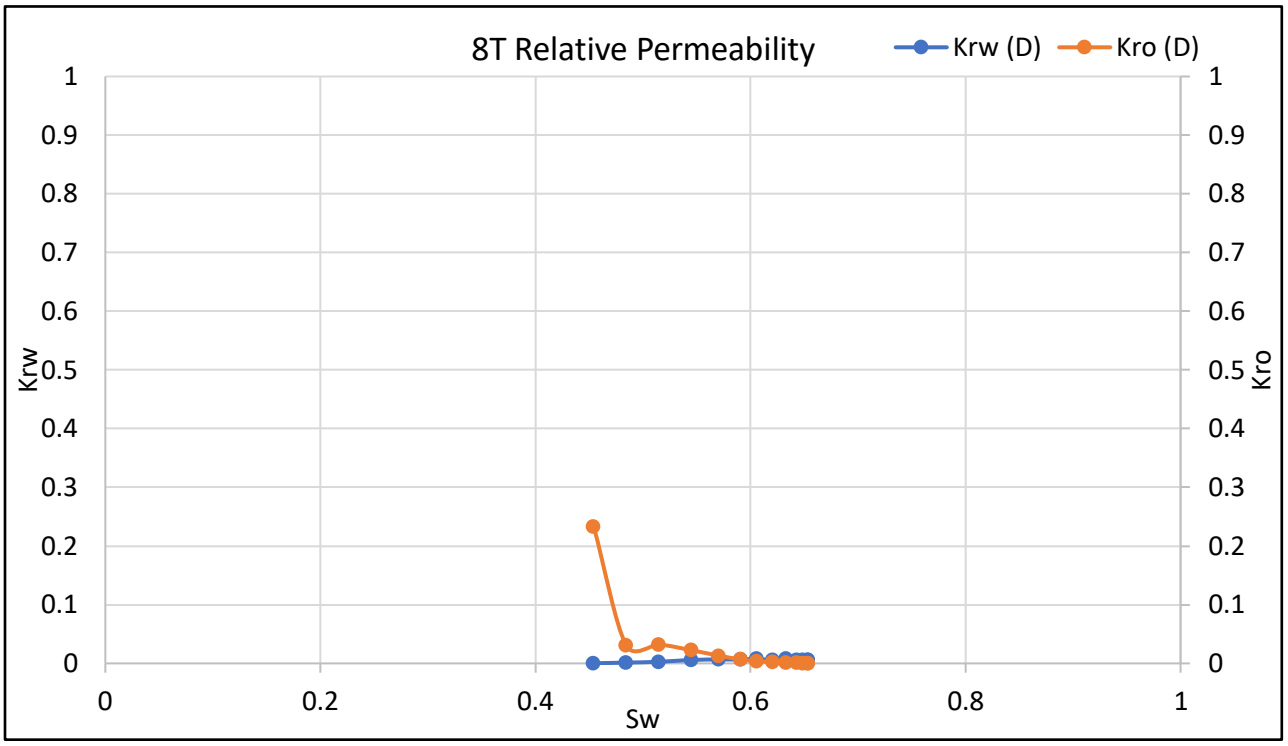

Fig 43: Initial Relative Permeability Curve of Core 8T

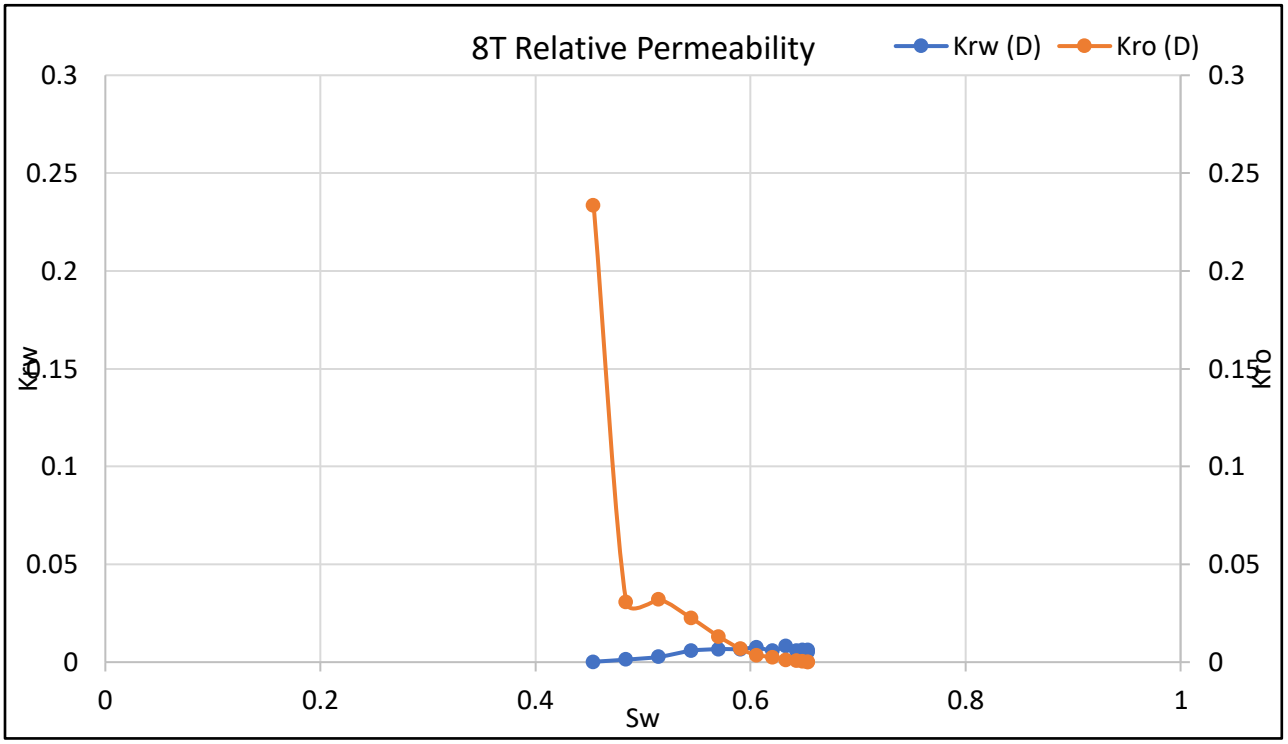

Fig 44: Initial Relative Permeability Curve of Core 8T (Scaled)

The core is slightly water wet as the intersection is at just shy of 0.6 water saturation (approximately 0.57 or 0.58). The ranges of both curves are very small with minimal with not much change in both saturations but a much higher change in saturation of oil. The largest drop in oil relative permeability occurred between the first 2 time points or right after water breakthrough. The effective oil permeability at breakthrough is 0.28 Darcy. The difference in water saturation from the beginning till the end of the relative permeability experiment is not a lot with a change of only 0.199 which explains the small scale of change on the x-axis. As the water injection did not produce around half of the oil inside the core, this would explain the low water permeability shown by the water relative permeability curve.

5.2.5.5 Core 1U Initial Relative Permeability and Waterflooding

Sample Name	Average Length (mm)	Average Width (mm)	Dry Weight (g)	Porosity (pu)	Cross Sectional Area (Cm2)	Saturated Weight (g)	Liquid Permeability (md)
1U	7.59	2.52	71.98	28.60	4.97	82.47	55.32

Table 18: Summary of Data Needed for Initial Relative Permeability of Core 1U

Recovered Volumes	Volume (cc)
Total initial recovered water	9.7
Dead Water Volume	2.6
Corrected initial water recovered	7.1
Pore Volume	9.37
Bulk Volume	36.31
Sw_i (%)	24.19
So_r (%)	46.08
Recovery Factor (%)	53.92

Table 19: Summary Data of Initial Relative Permeability for Core 1U

The oil saturation is very acceptable as the initial water saturation is just under 25 percent as these experiments are done in a lab with synthetic cores. However, the water flooding in this specific case was not as successful as the oil saturation as the recovery of the oil is only just over 50 percent but still close to 50 percent. Therefore, just over half of the oil saturated was able to be produced from the water flooding application for this core.

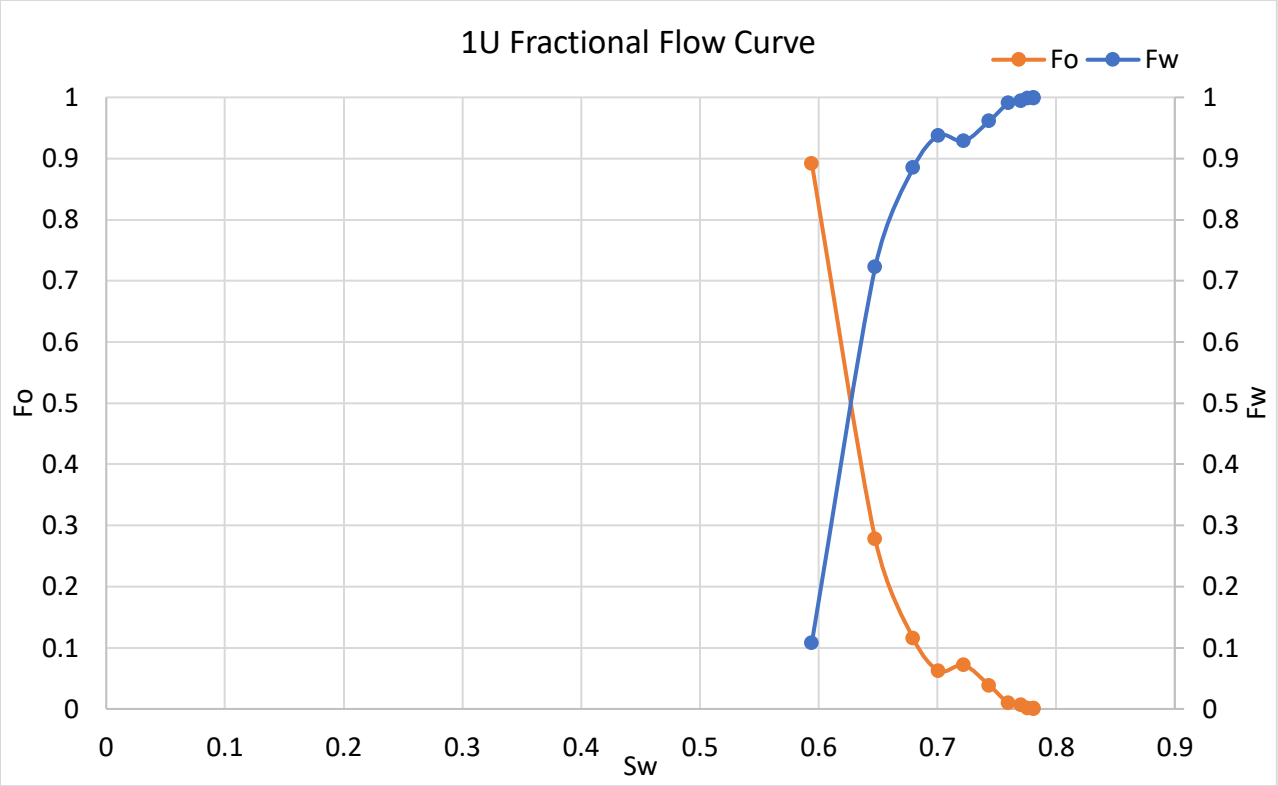

Fig 45: Initial Fractional Flow Curve for Core 1U

The fractional flow curves show the same idea as the table before that when it comes to the saturation of oil and water respectively. The oil saturation occurred very well as the fractional flow starts from 0.9 all the way to zero which means that the oil has entered and produced the majority of the water which can be confirmed by the low initial water saturation of 24 percent. The fractional water began at 0.1 and ended at 1. The slight delay as well as the large gap between the first 2 points once again approves the irreducible oil saturation over 50 percent and thus recovery of just under 50 percent. This data can be found in table A37 in the appendix.

The breakthrough time had occurred at four minutes and thirty-one seconds only which is a relatively slower time when compared to the other cores tested. The difference between the inlet pressure from breakthrough till the end is only about 55.4 psi which is amongst the highest compared to other cores but clearly not sufficient enough to produce the majority of the oil. This is further shown also by the volume of connate oil saturation being just below 50 percent. The production of water took a fairly short amount of time of just under 3 hours to produce just above 50 percent of oil. This data can be found in table A38 in the appendix.

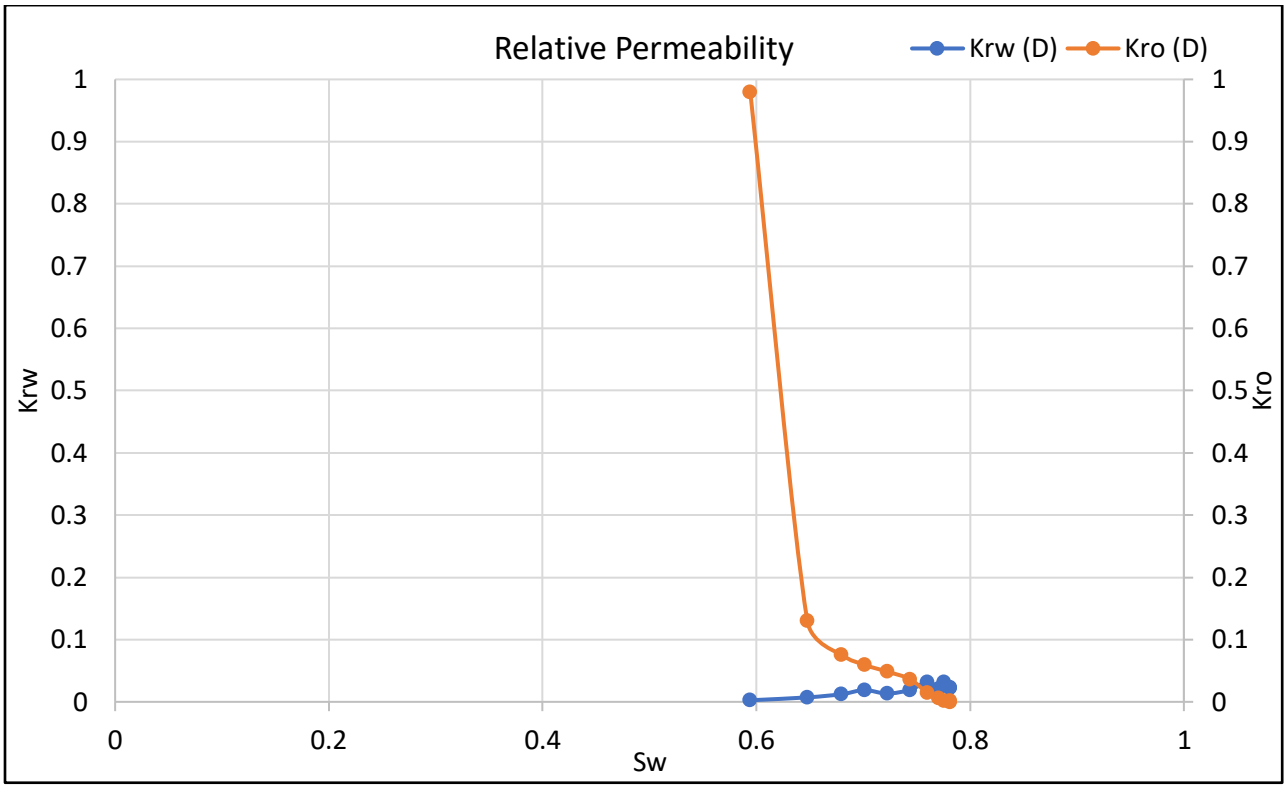

Fig 46: Initial Relative Permeability Curve for Core 1U

The core's intersection point is close to 0.8 (approximately 0.76) making it a water wet sample. The ranges of both curves are very different with the oil relative permeability curve having a full range from almost 1 to zero with minimal range of the water relative permeability curve starting from zero to 0.05. The largest drop in oil relative permeability occurred between the first 2 time points or right after water breakthrough. The effective oil permeability at breakthrough is 50 millidarcy. The difference in water saturation from the beginning till the end of the relative permeability experiment is not a lot with a change of only 0.187 which explains the small scale of change on the x-axis. As the water injection did only produce around half of the oil inside the core, this would explain the low water permeability shown by the water relative permeability curve. This data can be found in table A39 in the appendix.

5.3 Collection of Final Data After Vibration

5.3.1 Final Porosity of Selected Cores After Vibration

Porosity was measured prior and following cleaning of the cores for the second time after finishing the relative permeability and waterflooding procedures after vibration. The porosity was measured before the vibration and after the first round of relative permeability to see the damage effect that the oil saturation had on the cores. This was performed in order to isolate the effect the vibration from the effect of the damage from oil saturation in the initial phase. From these two measurements of porosity along with the original porosity measurement done in the initial phase of the experimentation phase, the difference between all three was found with the table below providing the data collected.

Sample Name	Original Porosity (pu)	Before Vibration Porosity (pu)	Percentage Change Porosity 1 (pu)	After Vibration Porosity (pu)	Percentage Change Porosity 2 (pu)	Difference of Both Percentage Changes
9S	26.45	21.92	-17.13	19.44	-11.31	5.81
4T	32.91	27.52	-16.38	23.14	-15.92	0.46
7T	33.13	30.62	-7.58	29.06	-5.09	2.48
8T	30.95	29.45	-4.85	28.91	-1.83	3.01
1U	28.60	22.74	-20.49	16.57	-27.13	-6.64

Table 20: Summary of Final Porosity of Selected Cores Before and After Vibration

From table 20, it was made clear that the saturation of oil creates damage to the cores regardless of the core itself. This is made clear by the first percentage change with all cores having damage done to them with the least damage occurring at just under 5 percent up to damage up marginally over 20 percent. This idea was tested to see if this occurs with these cores or is this a trend in general. Another core was measured for its porosity before and after oil saturation and cleaning. Before the oil saturation the test core had a porosity of 30.98 porosity units (pu); however, after the oil saturation and cleaning the porosity plummeted to 19.73 pu which is a percentage decrease of 36.31 percent. Therefore, it can be confirmed that oil saturation does damage the core porosity.

The porosity after the vibration, oil saturation and cleaning have also been measured and compared to the porosity just before vibration. In almost all of the cores the percentage decrease in porosity after vibration was less than the porosity decreases after the initial oil saturation alone. There is lower porosity decrease due to the vibration ranging from 0.5 percent to almost 5 percent with the average being around 3 percent. The only outlier to these results is of core 1U which had even more damage than the initial phase by slightly lower than 7 percent.

5.3.2 Absolute Permeability of Selected Cores After Vibration

All of the cores were measured using the liquid Permeameter and were measured using the same brine solution that was used for saturation of the cores. The inlet pressure data was collected at different flow rates of 1 to 6; however, in some cases only to 5 cubic centimeters per minute (cc/min). This was usually because the values were awfully close to each other in the case of high permeability cores and so an increase in the flow rate would not have produced any different results. Table 21 will present the liquid permeabilities of the 6 cores that were measured.

Sample Name	Initial Absolute Permeability (mD)	Absolute Permeability Before Vibration (mD)	Change in Absolute Permeability from Initial Case (%)	Absolute Permeability After Vibration (mD)	Change in Absolute Permeability Due to Vibration (%)
9S	55.08	38.76	-29.63	42.12	8.67
4T	357.24	354.60	-0.74	490.56	38.34
7T	880.44	364.32	-58.62	590.28	62.02
8T	1218.96	1218.72	-0.02	1566.12	28.51
1U	55.32	19.44	-64.86	25.92	33.33

Table 21: Summary of Final Absolute Permeabilities of Selected Cores

The absolute permeability was measured before and after vibration was applied on each one of the selected cores. There are minor differences between the absolute permeability before and after the first cleaning phase which would mean that there may be some damage that had occurred during the initial oil saturation phase. There was increase in all of the selected cores with the only difference being the percentage increase for each core. The majority of the cores had an increase of around 30 percent such as core 1U, 8T and 4T making the average around 34 mD. However, there are two extremities with cores 9S and 7T having increases of approximately 9 percent and 60 percent respectively.

With most of the cores, the increase of the absolute permeability has increased after the vibration than before but not necessarily than the original case. The damage that had occurred due to the oil saturation decreased the absolute permeability. This is because the damage that had occurred is much higher than the vibration could restore. Some of the damage has been restored but the restoration was unable to improve on the initial case of the core itself. However, it can be seen in two cases that both cores 4T and 8T that the absolute permeability after the vibration is higher than the original absolute permeability before the damage due to the initial oil saturation done during the initial measurement of absolute permeability.

Another core was also tested with a very low initial absolute permeability (core 2X) with value of 5.52 mD. This core was not taken into consideration for the remaining of the research this very low absolute permeability would not function well in the relative permeability and waterflooding measurements section. None the less, vibration was also applied to this core to test the very low absolute permeability cores and was found that the core's absolute permeability increased to 6.36 mD which is a percentage increase of 15.22 percent. This may be below the average of the other 5 selected cores for this research; however, it is still a considerable enhancement of the absolute permeability.

5.3.2.1 Core 9S Final Absolute Permeability After Vibration

Core 9S is the first core to be measured before vibration. To begin with, the measurement of the inlet pressure with every increase in brine flow rate was taken before vibration and after initial damage from oil saturation. The table A40 in the appendix will present the data collected.

From this a graph of ΔP/L and Q/A are drawn to find the slope of the trendline is to be found which will then be multiplied by the viscosity of water to find the permeability.

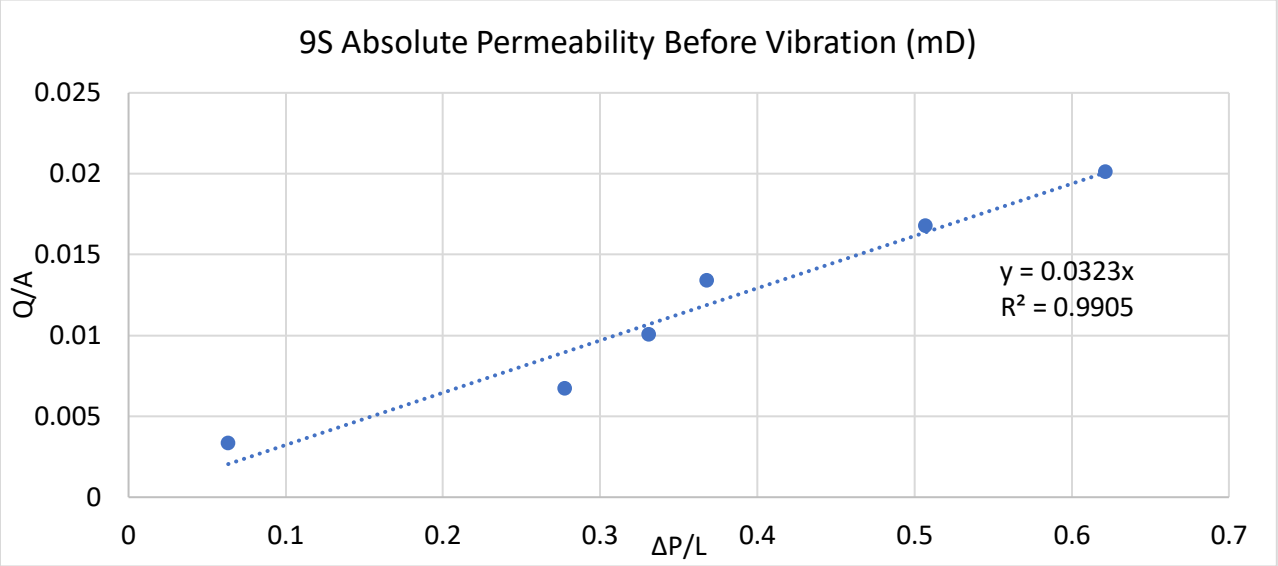

Fig 47: Absolute Permeability Curve of Core 9S Before Vibration

There is minimum scattering between the points and each other. This is made clear by the trendline where the points are very close to the trendline without any clear deviation from the trendline. This point is reinforced by the high trendline reliability value of 0.99.

Core 9S is the first core to be measured after vibration. To begin with, the measurement of the inlet pressure with every increase in brine flow rate was taken after vibration. The table A41 in the appendix will present the data collected. From this a graph of ΔP/L and Q/A are drawn to find the slope of the trendline is to be found which will then be multiplied by the viscosity of water to find the permeability.

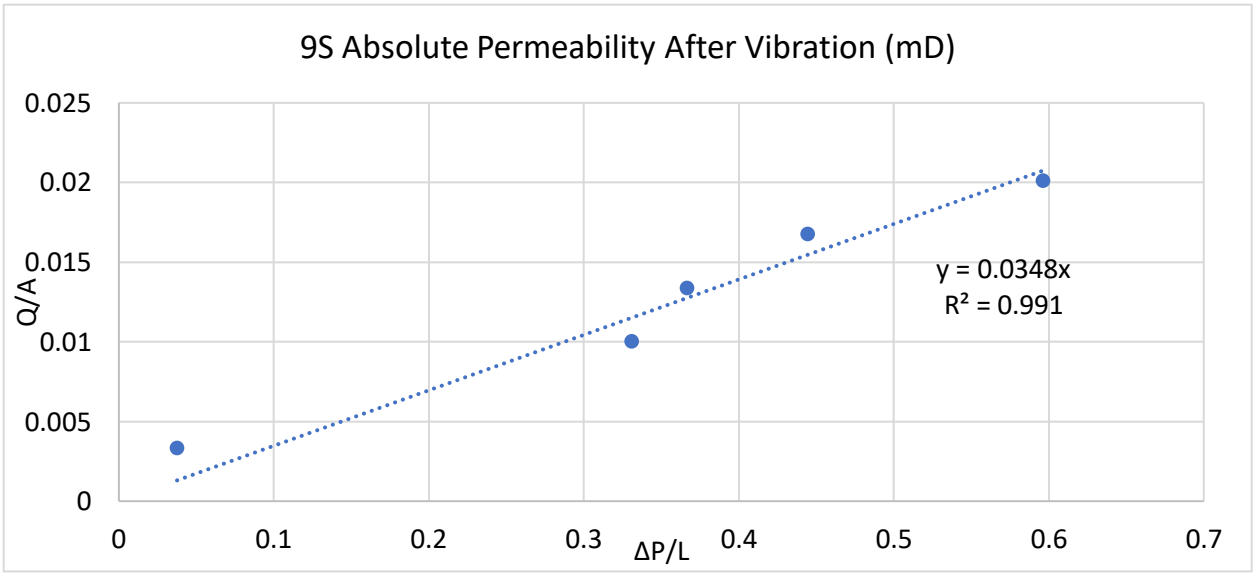

Fig 48: Absolute Permeability Curve of Core 9S After Vibration

There is minimum scattering between the points and each other. This is made clear by the trendline where the points are very close to the trendline without any clear deviation from the trendline. This point is reinforced by the high trendline reliability value of 0.97.

5.3.2.2 Core 4T Final Absolute Permeability After Vibration

Core 4T is the second core to be measured amongst the selected cores. To begin with, the measurement of the inlet pressure with every increase in brine flow rate was taken before vibration. The table A42 in the a will present the data collected. From this a graph of ΔP/L and Q/A are drawn to find the slope of the trendline is to be found which will then be multiplied by the viscosity of water to find the permeability.

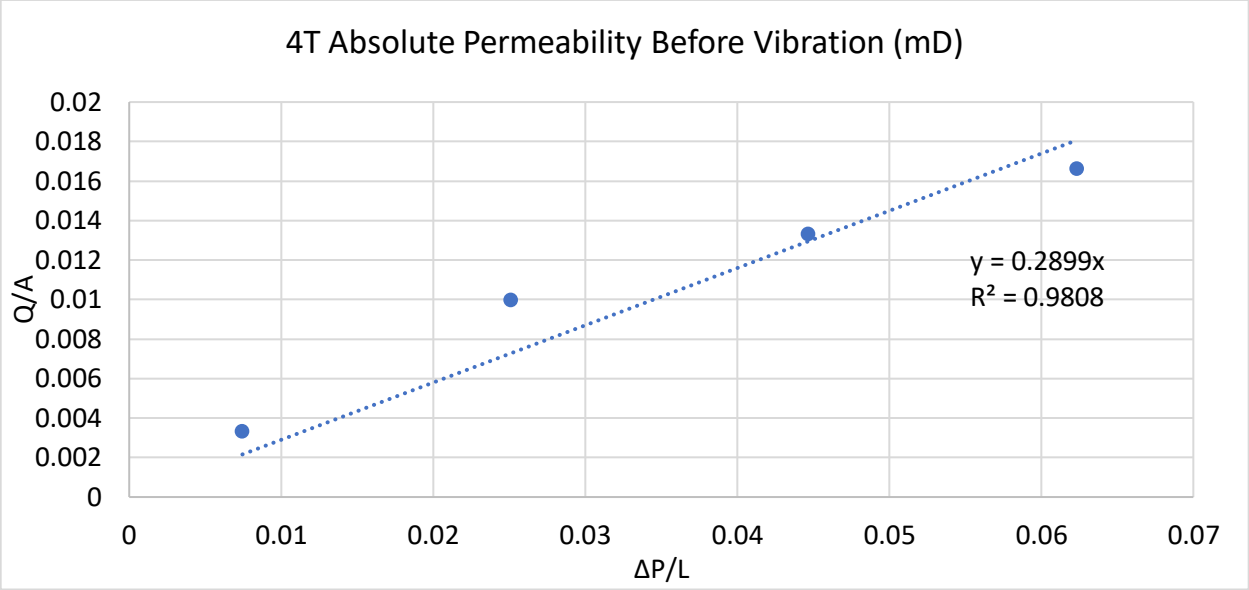

Fig 49: Absolute Permeability Curve of Core 4T Before Vibration

There are some deflections in the first two points; however, with higher flow rates the deflections or scattering is reduced which is clear by both the closeness of the points to the trendline as well as the overall trendline reliability value of 0.966.

Core 4T is the second core to be measured after vibration. To begin with, the measurement of the inlet pressure with every increase in brine flow rate was taken after the vibration process was completed. The table A44 in the appendix will present the data collected. From this a graph of ΔP/L and Q/A are drawn to find the slope of the trendline is to be found which will then be multiplied by the viscosity of water to find the permeability.

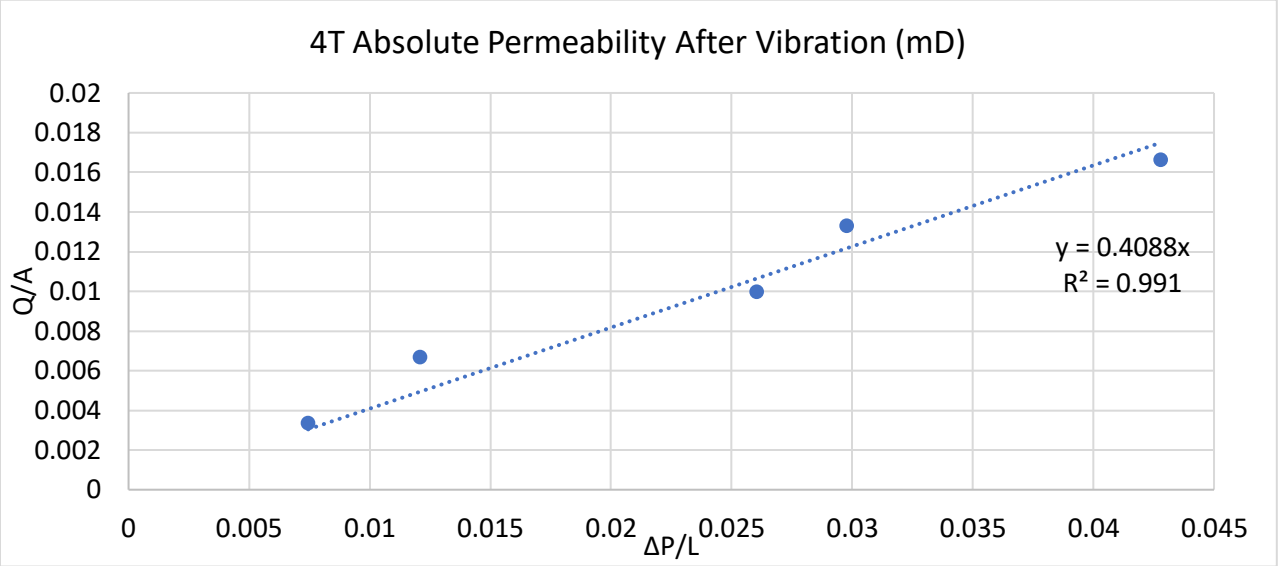

Fig 50: Absolute Permeability Curve of Core 4T After Vibration

There is minimum scattering between the points and each other. This is made clear by the trendline where the points are almost perfectly situated from one another and to the trendline. This point is reinforced by the high trendline reliability value of 0.99.

5.3.2.3 Core 7T Final Absolute Permeability After Vibration

Core 7T is the third core to be measured before and after vibration. To begin with, the measurement of the inlet pressure with every increase in brine flow rate was taken before vibration occurred. The table A43 in the appendix will present the data collected. From this a graph of ΔP/L and Q/A are drawn to find the slope of the trendline is to be found which will then be multiplied by the viscosity of water to find the permeability.

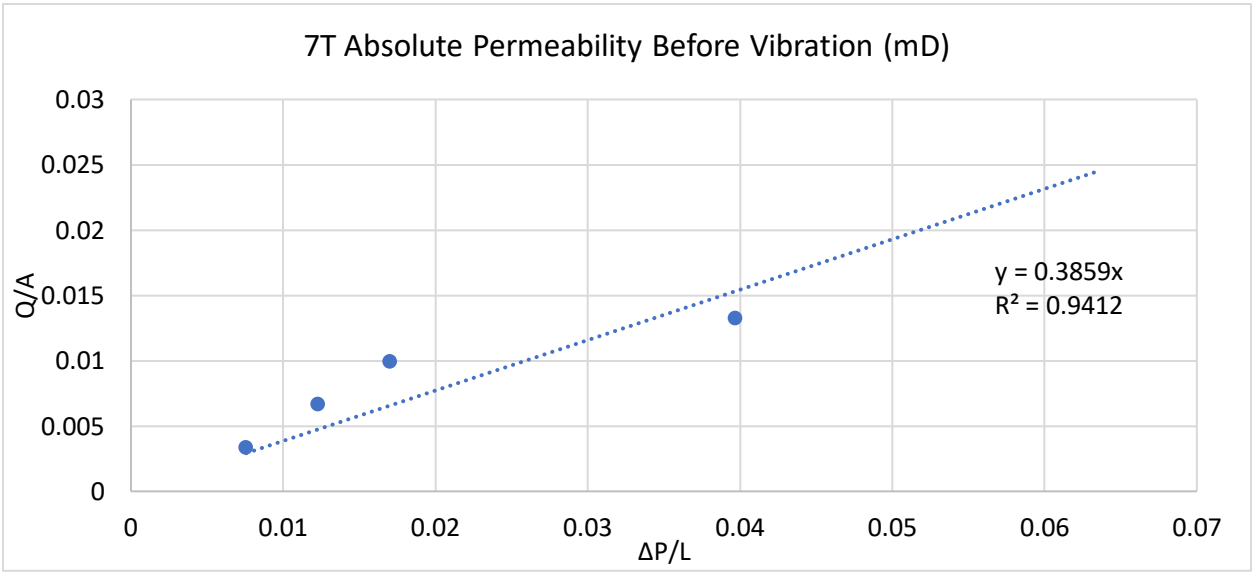

Fig 51: Absolute Permeability Curve of Core 7T Before Vibration

Some scattering is found between the first three points specifically when compared to the last 2. This is made clear by the trendline where the last two points are very close to the trendline without any clear deviation from the trendline while there is some clear deviation of the first three points progressively. However, the trendline reliability value is 0.93.

Core 7T is the third core to be measured after vibration. To begin with, the measurement of the inlet pressure with every increase in brine flow rate was taken. The table A44 in the appendix will present the data collected. From this a graph of ΔP/L and Q/A are drawn to find the slope of the trendline is to be found which will then be multiplied by the viscosity of water to find the permeability.

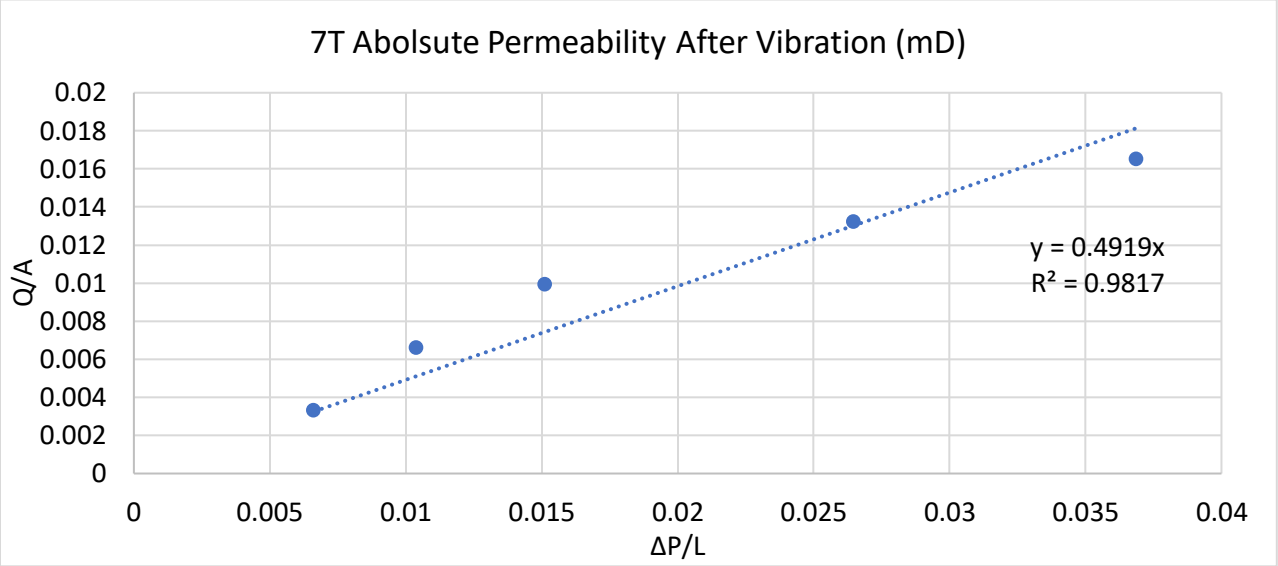

Fig 52: Absolute Permeability Curve of Core 7T After Vibration

There is minimum scattering between the points and each other. This is made clear by the trendline where the points are very close to the trendline without any clear deviation from the trendline. This point is reinforced by the high trendline reliability value of 0.98.

5.3.2.4 Core 8T Final Absolute Permeability After Vibration

Core 8T is the penultimate core to be measured before the vibration. To begin with, the measurement of the inlet pressure with every increase in brine flow rate was taken. The table A45 in the appendix will present the data collected. From this a graph of ΔP/L and Q/A are drawn to find the slope of the trendline is to be found which will then be multiplied by the viscosity of water to find the permeability.

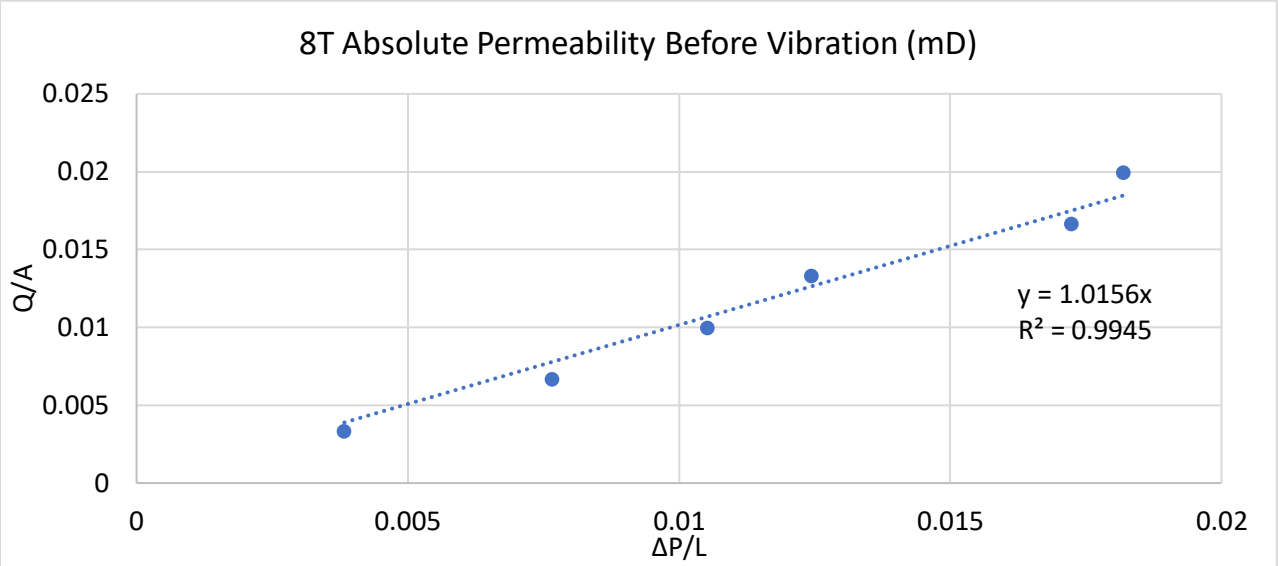

Fig 53: Absolute Permeability Curve of Core 8T Before Vibration

There is very minimum scattering between the points and each other. This is made clear by the trendline where the points are very close to the trendline without no visible divergence from the trendline which is strengthened by the trendline reliability value of 0.99.

Core 8T is the penultimate core to be measured after vibration. To begin with, the measurement of the inlet pressure with every increase in brine flow rate was taken. The table A46 in the appendix will present the data collected. From this a graph of ΔP/L and Q/A are drawn to find the slope of the trendline is to be found which will then be multiplied by the viscosity of water to find the permeability.

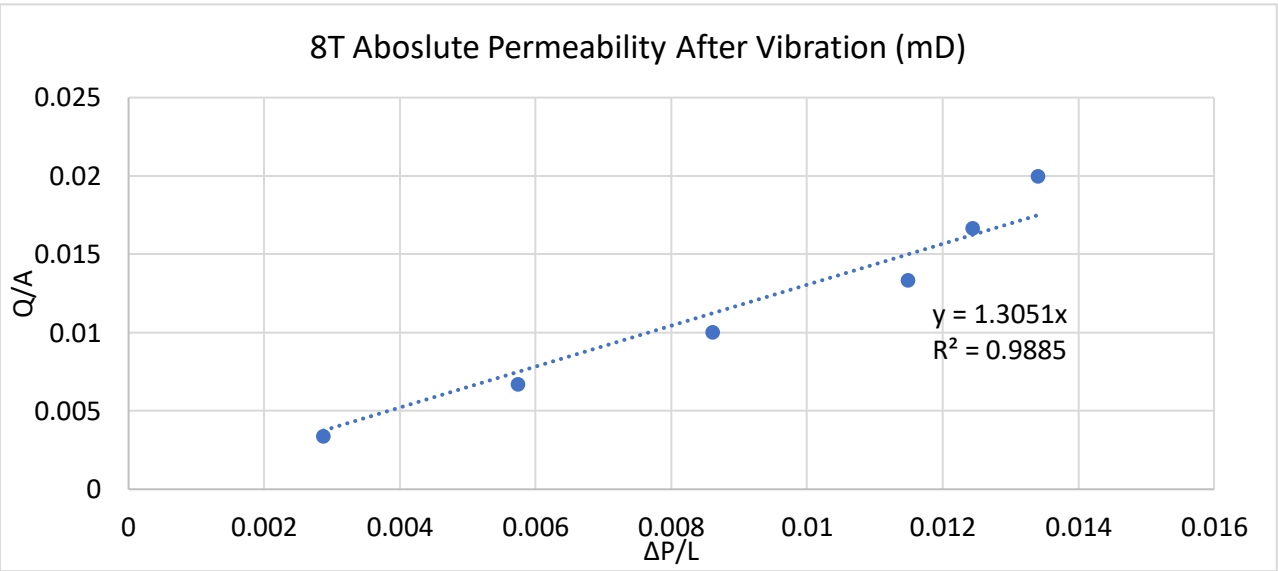

Fig 54: Absolute Permeability Curve of Core 8T After Vibration

There is minimum scattering between the points and each other. This is made clear by the trendline where the points are very close to the trendline without any clear deviation from the trendline. This point is reinforced by the high trendline reliability value of 0.988.

5.3.2.5 Core 1U Final Absolute Permeability After Vibration

Core 1U is the final core to be measured prior to the vibration process. To begin with, the measurement of the inlet pressure with every increase in brine flow rate was taken before vibration. The table A47 in the appendix will present the data collected. From this a graph of ΔP/L and Q/A are drawn to find the slope of the trendline is to be found which will then be multiplied by the viscosity of water to find the permeability.

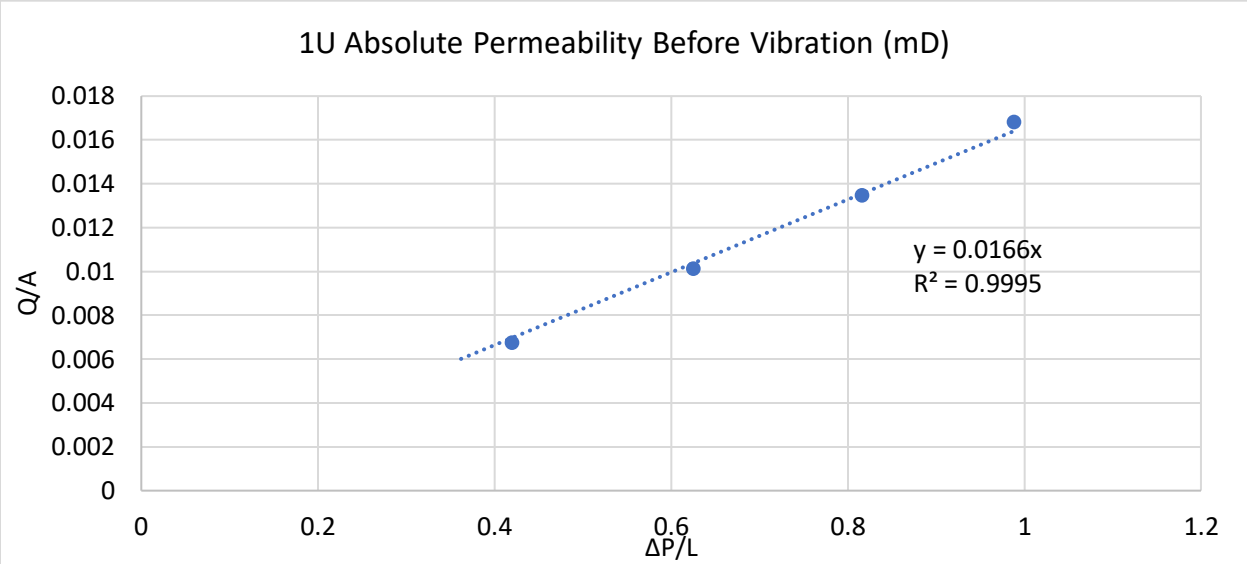

Fig 55: Absolute Permeability Curve of Core 1U Before Vibration

There is scattering only in the first point with minimal scattering later on between the last 4 points. For the last 4 points, they are almost completely matching with the trendline drawn which has allowed for the trendline reliability factor to be 0.988.

Core 1U is the final core to be measured after vibration. To begin with, the measurement of the inlet pressure with every increase in brine flow rate was taken. The table A48 in the appendix will present the data collected. From this a graph of ΔP/L and Q/A are drawn to find the slope of the trendline is to be found which will then be multiplied by the viscosity of water to find the permeability.

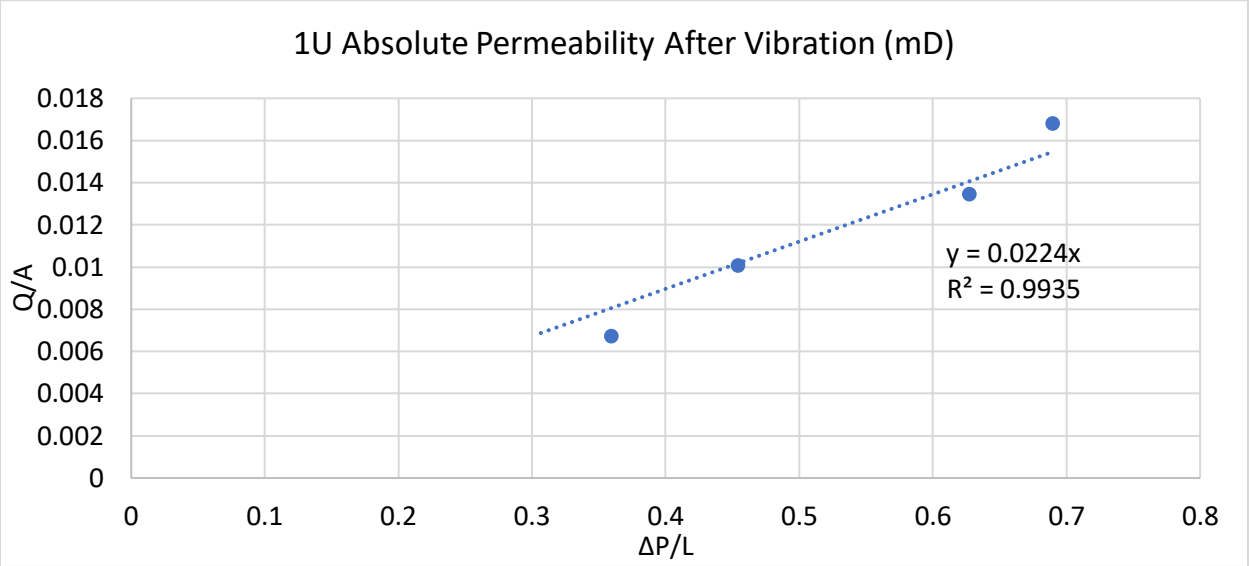

Fig 56: Absolute Permeability Curve of Core 1U After Vibration

There is some scattering between the points and each other. This is made clear by the trendline where the points are very close; however, the deviation from the trendline is minimal which is emphasized by the high trendline reliability value of 0.97.

5.3.3 Final Relative Permeabilities and Waterflooding of Selected Cores After Vibration

The relative permeability and waterflooding for this section were performed after completing all of the other needed measurements for this research. After the vibration and measuring of the absolute permeability, each of the selected cores were saturated with oil and then waterflooding was done to encompass the drainage and imbibition of these cores in order to test the relative permeability capabilities of each respective core. In addition, the volume of produced oil after the waterflooding was completed was collected in the same manner as the initial phase of this same research.

When evaluating the relative permeability and waterflooding capabilities of each core before and after vibration, the initial and final water and oil residual saturations were considered as well as the recoveries in both phases of the research. Furthermore, the shape and intersection points of each core was also put into consideration to see the relative effect of the vibration on the enhancement of the imbibition and drainage potentials for each core respectively.

Sample Name	Initial S_{wi} (%)	Final S_{wi} After Vibration (%)	Diff. S_{wi}	Initial S_{or} (%)	Final S_{or} After Vibration (%)	Diff. S_{or}	Initial Oil Recovery (%)	Final Oil Recovery After Vibration (%)	Diff. Recovery
9S	55.43	33.19	-22.24	55.02	51.22	-3.8	44.8	51.22	6.42
4T	18.18	12.16	-6.02	40.56	33.94	-6.62	59.44	66.06	6.62

7T	25.47	34.53	9.06	49.14	46.41	-2.73	50.86	53.58	2.72
8T	22.16	37.03	14.87	56.84	42.19	-14.65	43.16	57.81	14.65
1U	24.19	26.37	2.18	46.08	26.56	-19.52	53.92	73.44	19.52

Table 22: Comparison of Relative Permeability Data of Selected Cores Before and After Vibration

From the table above, several finding can be discovered. The wettability of the cores has become more water wet which can be made clear from the difference in remaining water and oil saturations. In all of the cores, the remaining oil saturations have decreased with an increase in the remaining water saturations of three of the cores. The relative permeability to oil has improved due to the wettability change to become more water wet which explains the increase in recovery. Moreover, the performance of the waterflooding has improved. This is evident from the increase in the recovery when comparing before and after the vibration regardless of the wettability alteration.

5.3.3.1 Core 9S Relative Permeability and Waterflooding After Vibration

Sample Name	Average Length (mm)	Average Width (mm)	Dry Weight (g)	Porosity (pu)	Cross Sectional Area (Cm2)	Saturated Weight (g)	Liquid Permeability (md)
9S	76.16	2.52	74.70	26.45	4.99	83.25	42.12

Table 23: Summary of Data Needed for Final Relative Permeability of Core 9S After Vibration

Recovered Volumes	Volume (cc)
Total initial recovered water	7.7
Dead Water Volume	2.6
Corrected initial water recovered	5.1
Pore Volume	7.63
Bulk Volume	36.31
S_{wi} (%)	33.19
S_{or} (%)	48.78
Recovery Factor (%)	51.22

Table 24: Summary Data of Final Relative Permeability for Core 9S After Vibration

The saturation of oil is sufficient enough with a residual water saturation of 33 percent but still more time was provided for the oil saturation to increase. The outcome was still negative as no more oil was able to saturate the core. Regarding the oil production, more than half of the

injected oil was able to be produced after the application of the vibration making the recovery factor reached around 51 percent.

Regarding the issue of the pressure not being stable which was faced when performing the waterflooding and relative permeability test in the initial phase, this issue was not faced after the vibration. There was some fluctuation as normally seen from the apparatus used; however, it was definitely not to the extreme extent that was seen in the initial phase table A47 in the appendix.

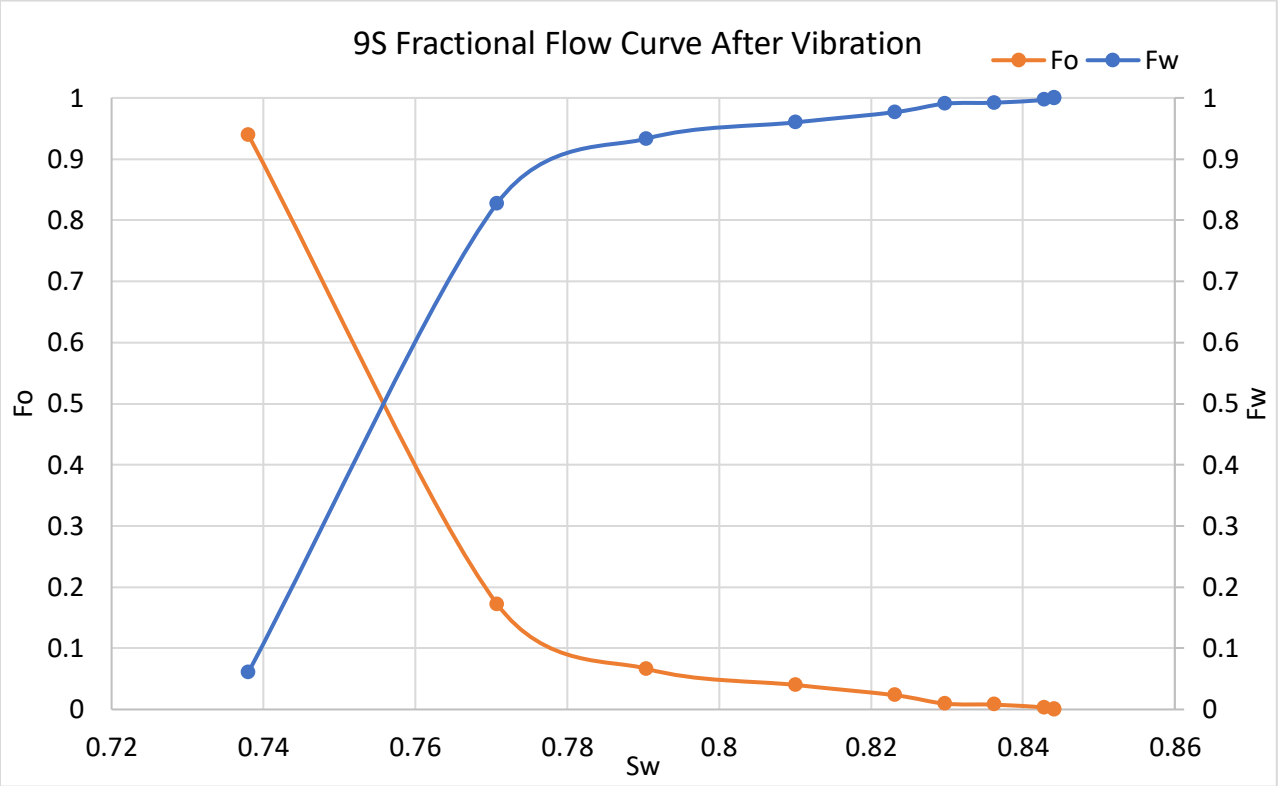

The water breakthrough occurred at four minutes and forty-five seconds (almost five minutes) with just under 4.5 centimeter cubed of oil being produced. The entirety of the oil production was finished in just under one and half hours with a mere 9 psi difference in the pressure between the beginning and the end of waterflooding. The production of oil was consistent for several time periods as can be seen from the volume of oil produced per time period. This data can be seen in table A48 in the appendix.

From the relative permeability data in table above, the relative permeability curve can be drawn. Any data that is outside the typical range has been excluded due to it not being accurate or realistic when drawing the curve itself. This data can be seen in table A49 in the appendix.

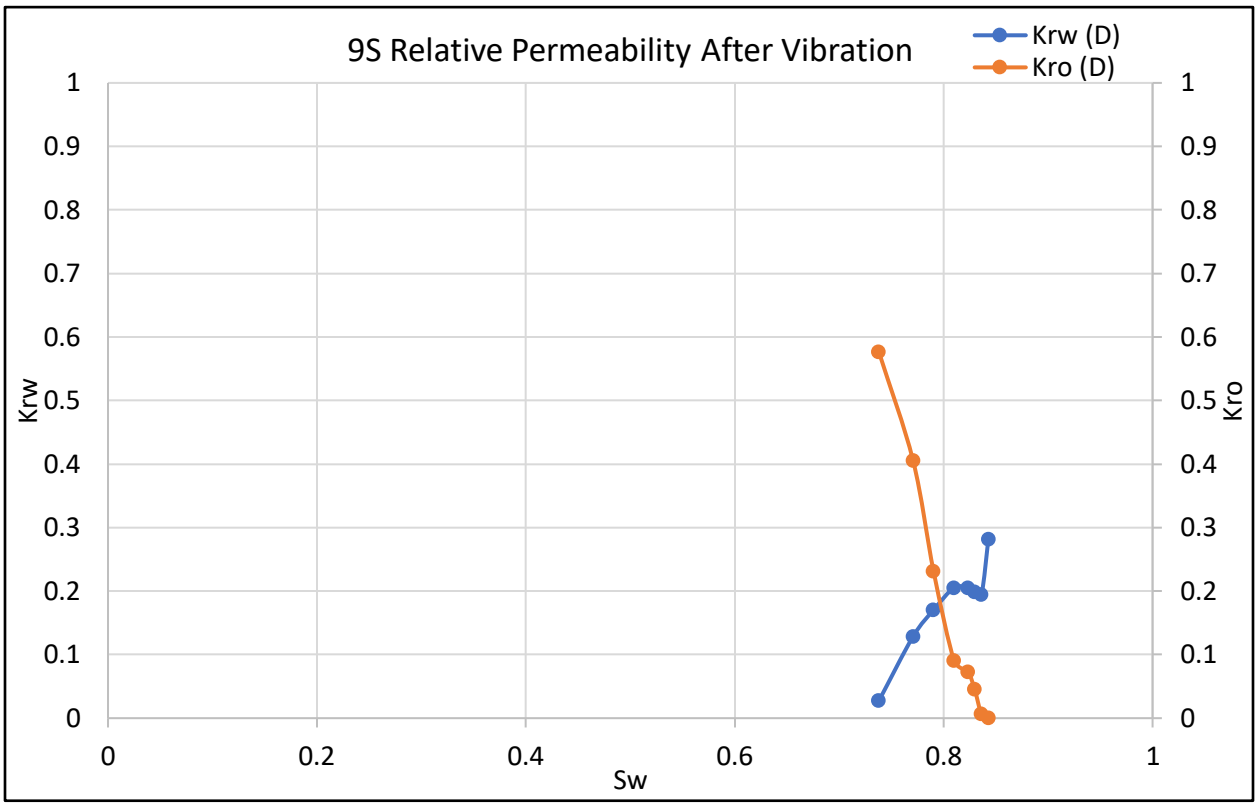

Fig 58: Final Relative Permeability Curve of Core 9S After Vibration

The relative permeability curve is once more unfortunately not an ideal one in this case. Regarding the relative permeability to oil, the first two points were completely out of range with the data collected from the apparatus. In addition, the curve itself is very steep than the typical curve. For the water relative permeability curve, the curve is once more very steep with the curve then decreasing and increasing once more. This would come back to the nature of the core itself as it was not a natural but manufactured core and so how the imbibition and drainage of water and oil operate is affected. However, the intersection of the two curves had occurred at a water saturation of 0.8 ensuring it is water wet.

5.3.3.2 Core 4T Relative Permeability and Waterflooding After Vibration

Sample Name	Average Length (cm)	Average Width (cm)	Dry Weight (g)	Porosity (pu)	Cross Sectional Area (Cm^2)	Saturated Weight (g)	Liquid Permeability (md)
4T	7.10	2.53	64.61	32.91	5.04	73.918	490.56

Table 25: Summary of Data Needed for Final Relative Permeability of Core 4T After Vibration

Recovered Volumes	Volume (cc)
Total initial recovered water	9.9

Dead Water Volume	2.6
Corrected initial water recovered	7.3
Pore Volume	8.31
Bulk Volume	36.31
Sw_i (%)	12.16
So_r (%)	33.94
Recovery Factor (%)	66.06

Table 26: Summary Data of Final Relative Permeability for Core 4T After Vibration

The oil saturation prior to waterflooding after vibration was conducted was exceedingly well as irreducible water saturation was 12 percent which is one of the lowest percentages. Due to the vibration application, the waterflooding was able to produce two-thirds of the oil which is an excellent recovery factor.

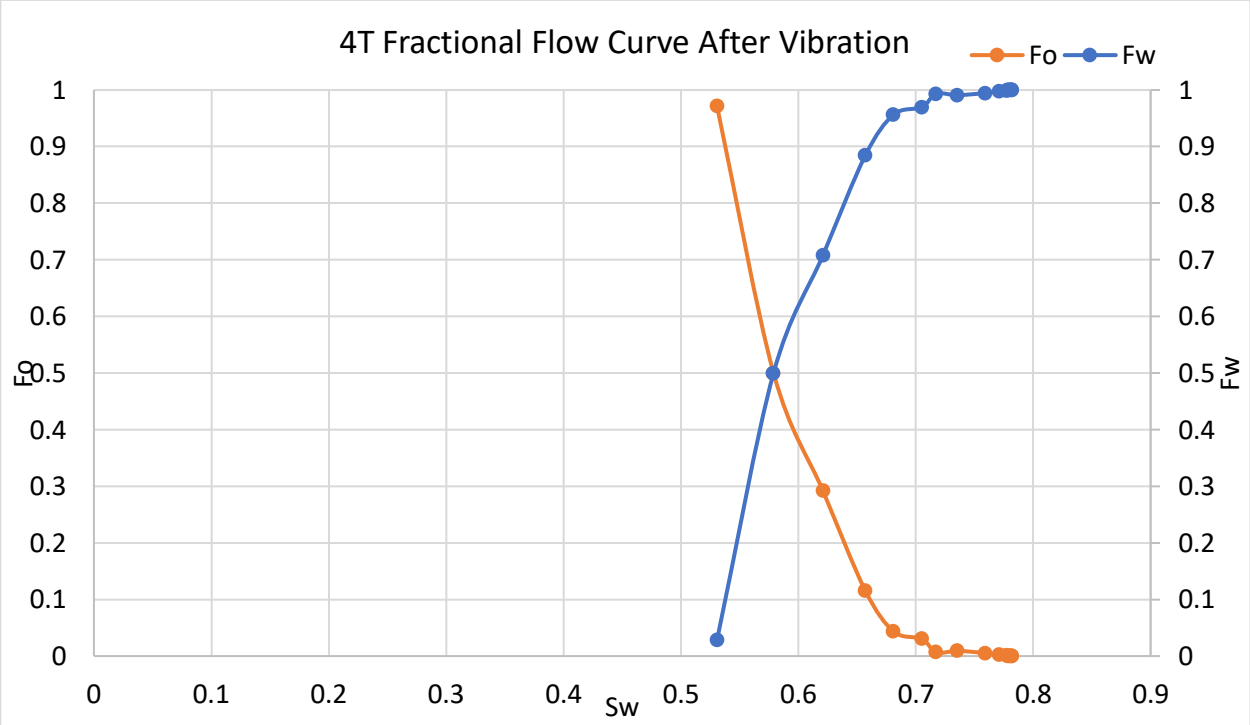

Fig 59: Fractional Flow Curve for Core 4T After Vibration

The fractional flow curve shows the imbibition and drainage process of core 4T. The fractional water curve reaches all the way to 1 or 100 percent while also the fractional oil curve starts at a relatively high value of 0.97 or 97 percent all the way to zero. This data can be found in table A50 in the appendix.

The water breakthrough occurred at four minutes and fourteen seconds with just 4.7 centimeter cubed of oil being produced until water broke through. The production of oil occurred

over an extensive period of time of just over seven hours with a significant pressure drop from 28.9 psi to 0.2 psi (a difference of 28.7 psi). The production of oil was almost consistent until nearly two hours with the remaining five hours producing just fractions of the oil. This data can be found in table A51 in the appendix.

From the relative permeability data in table A52 in the appendix, the relative permeability curve can be drawn.

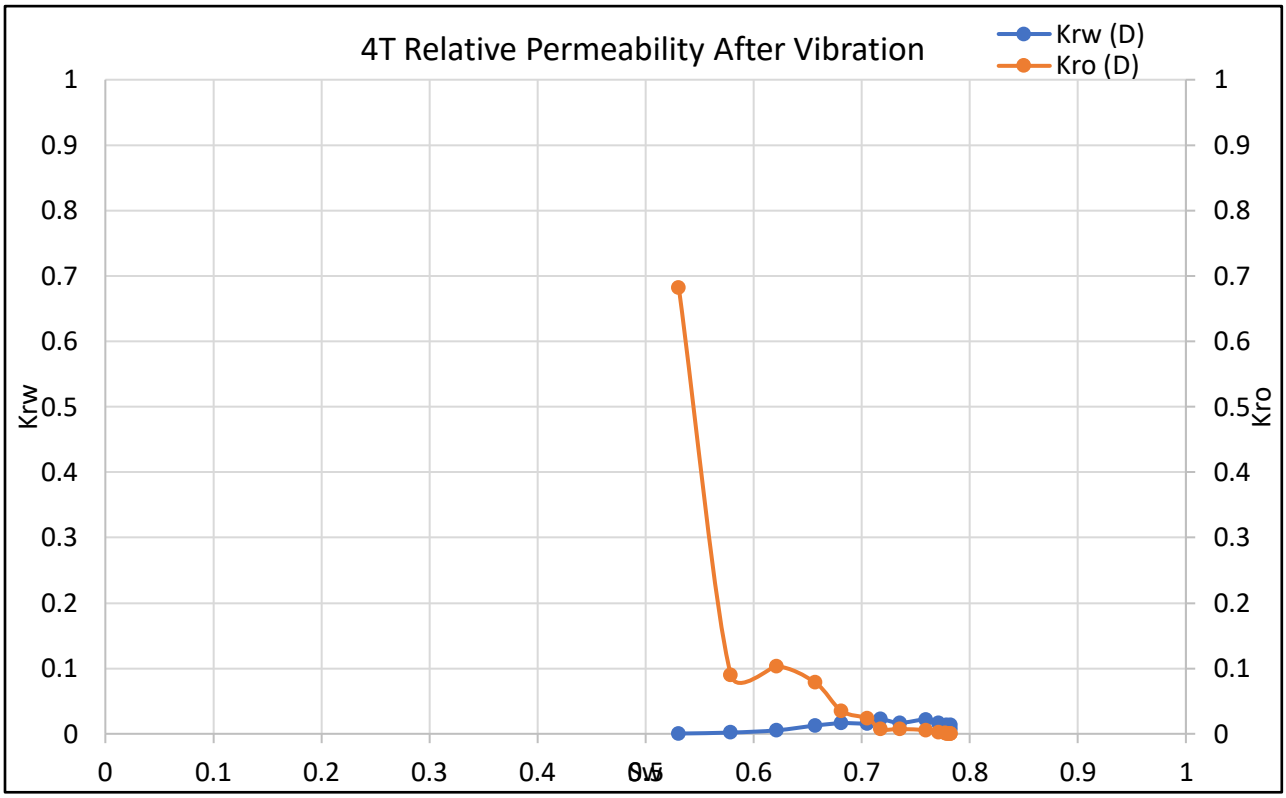

Fig 60: Final Relative Permeability Curve of Core 4T After Vibration

The relative permeability curve clearly shows that the core is water wet as the intersection point is at a water saturation is 0.72 which is water wet. There is a massive drop between the breakthrough and the second time point when it comes to the relative permeability of oil. The effective oil permeability at breakthrough is 0.33 Darcy. In addition, the relative permeability curve has taken an increasing slope when compared to the case before vibration making the intersection point much clearer.

5.3.3.3 Core 7T Relative Permeability and Waterflooding After Vibration

Sample Name	Average Length (cm)	Average Width (cm)	Dry Weight (g)	Porosity (pu)	Cross Sectional Area (Cm^2)	Saturated Weight (g)	Liquid Permeability (md)
7T	7.19	2.54	66.74	33.13	5.06	77.86	590.28

Table 27: Summary of Data Needed for Final Relative Permeability of Core 7T After Vibration

Recovered Volumes	Volume (cc)
Total initial recovered water	9.1
Dead Water Volume	2.6
Corrected initial water recovered	6.5
Pore Volume	9.93
Bulk Volume	36.31
S_{wi} (%)	34.53
S_{or} (%)	46.42
Recovery Factor (%)	53.58

Table 28: Summary Data of Final Relative Permeability for Core 7T After Vibration

The oil saturation of the core was not a successful as was needed; however, it is still very acceptable for this application of vibration and waterflooding. The core was saturated with oil at around 65 percent making the irreducible water saturation around 35 percent. With the vibration application and waterflooding, the recovery from core 7T was more than half of the oil volume (around 54 percent).

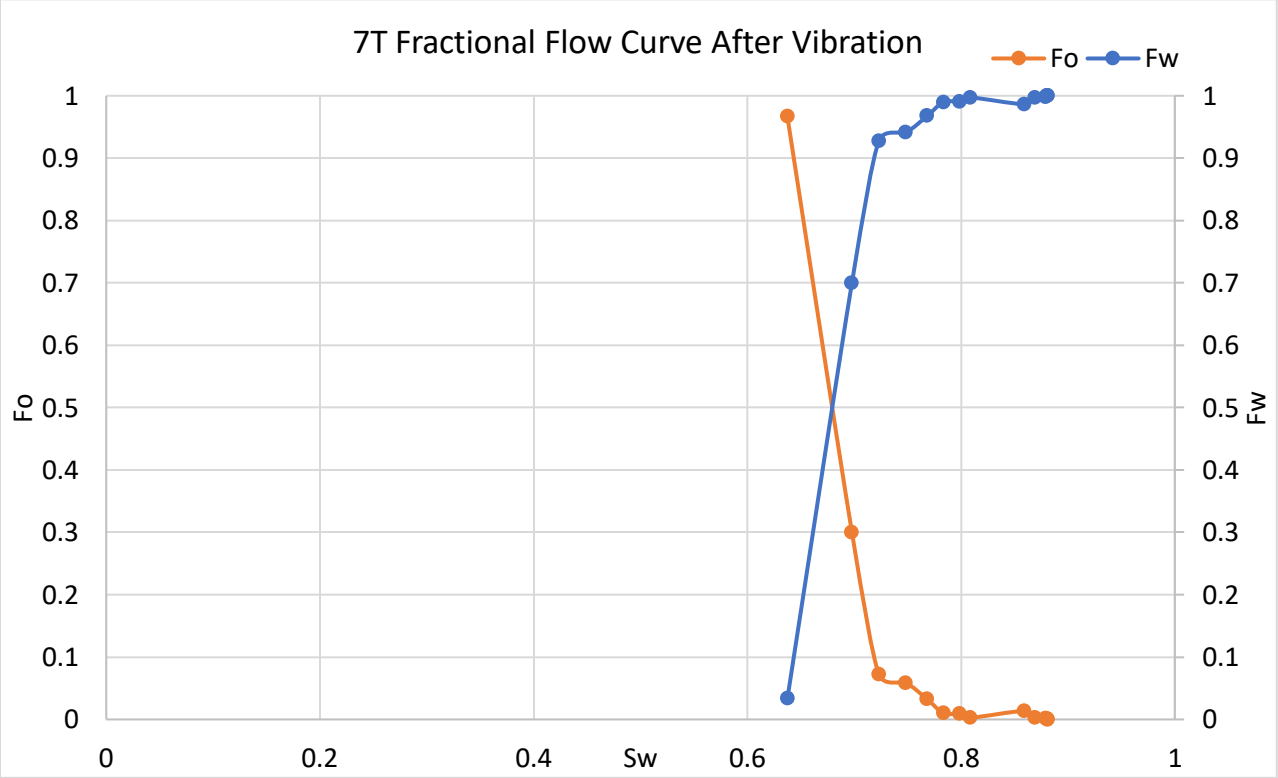

Fig 61: Fractional Flow Curve for Core 7T After Vibration

The fractional flow curve shows the imbibition and drainage process of core 7T. The fractional water curve reaches all the way to 1 or 100 percent while also the fractional oil curve starts at a relatively high value of 0.967 or just under 97 percent all the way to zero. There are steep changes especially in the first two points of either the imbibition or drainage of this core as can be seen by a steep line going down or up. This can be reiterated by the first two values of the water and oil fractional flow where the difference is large in both cases. This data can be found in table A53 in the appendix.

The water breakthrough occurred at four minutes and fifty-two seconds with 4.2 centimeter cubed of oil being produced until water broke through. The production of oil occurred over an extensive period of time of just over six and a half hours with a pressure drop of around 14 psi. The production of oil was almost consistent until nearly four hours with the remaining time producing just fractions of the oil. This data can be found in table A54 in the appendix.

From the relative permeability data in table A55 in the appendix, the relative permeability curve can be drawn. Any data that is outside the typical range has been excluded due to it not being accurate or realistic when drawing the curve itself.

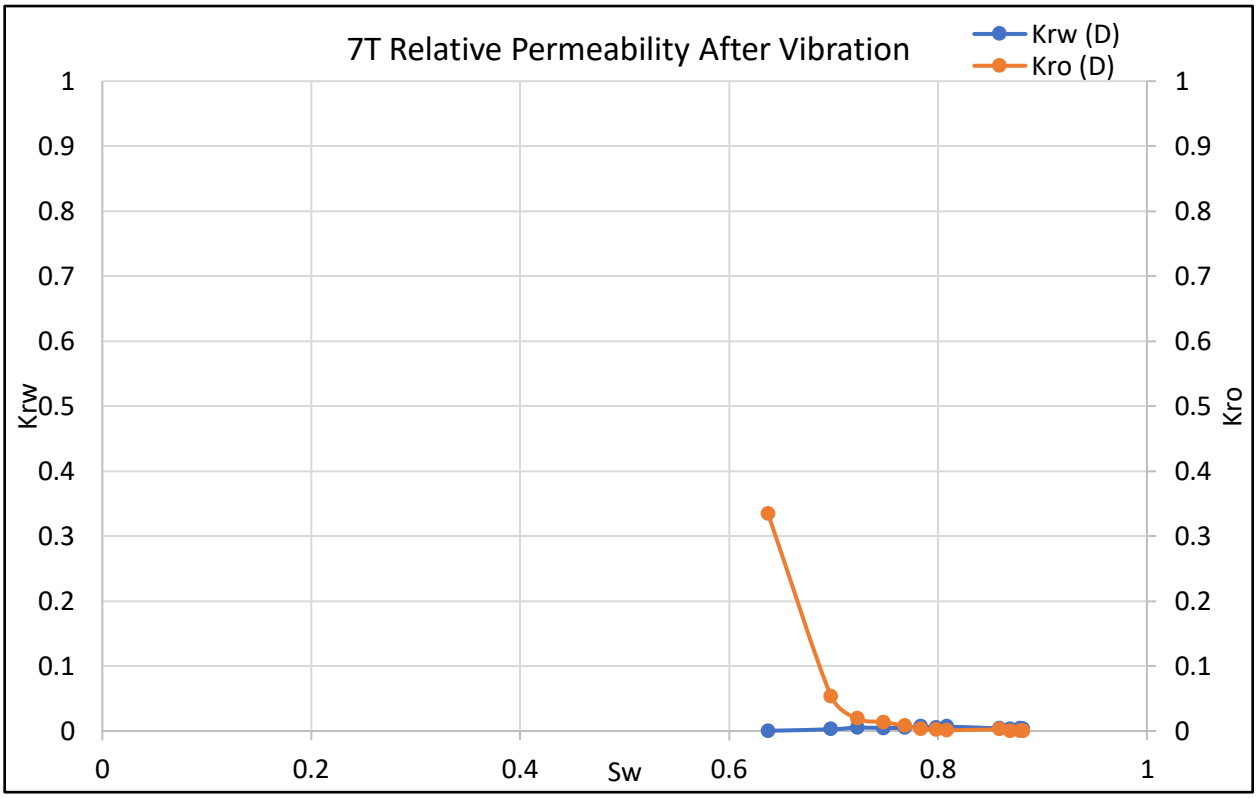

Fig 62: Final Relative Permeability Curve of Core 7T After Vibration

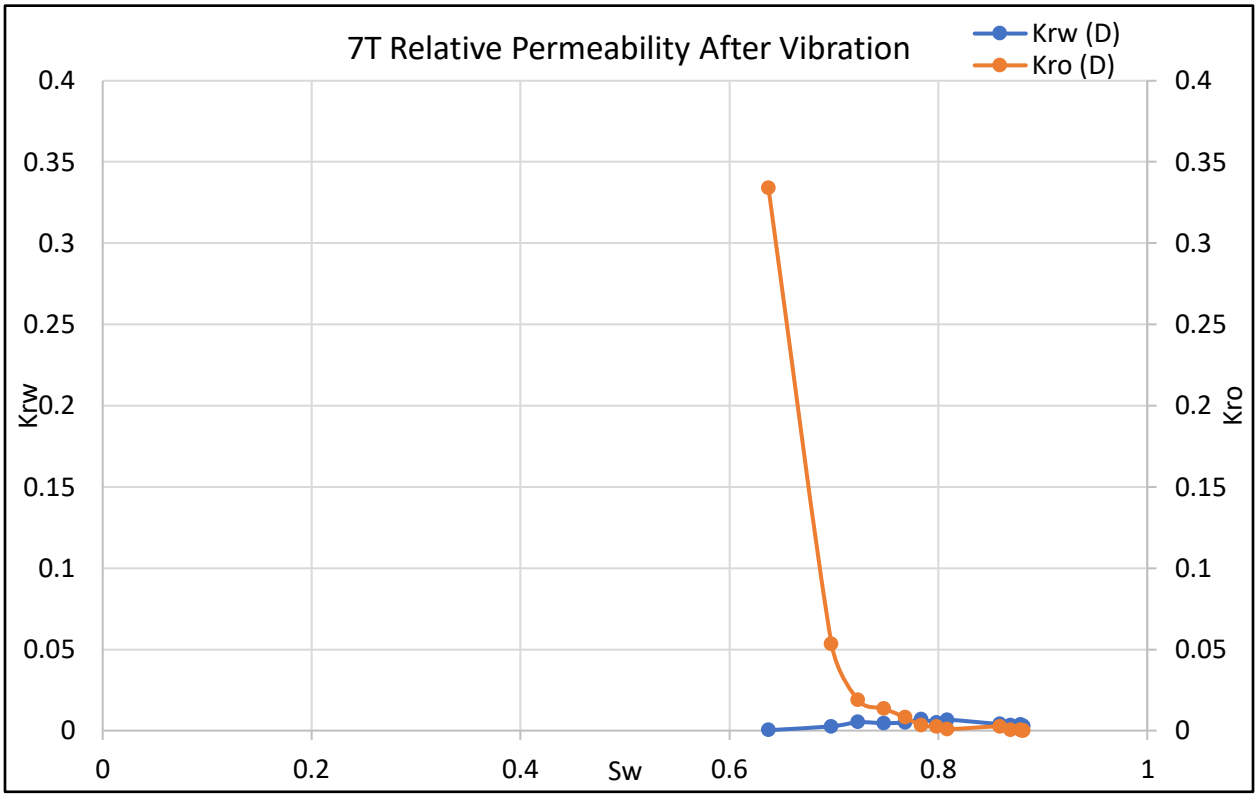

Fig 63: Final Relative Permeability Curve of Core 7T After Vibration (Scaled)

The relative permeability curve clearly shows that the core is water wet as the intersection point is at a water saturation is 0.78 which is water wet. There is a massive drop between the breakthrough and the second time point when it comes to the relative permeability of oil. The effective oil permeability at breakthrough is 0.19 Darcy. In addition, the relative permeability curve for water does not increase much unfortunately unlike the relative permeability curve for oil.

5.3.3.4 Core 8T Relative Permeability and Waterflooding After Vibration

Sample Name	Average Length (cm)	Average Width (cm)	Dry Weight (g)	Porosity (pu)	Cross Sectional Area (Cm^2)	Saturated Weight (g)	Liquid Permeability (md)
8T	7.31	2.53	68.15	30.95	5.03	79.00	1566.12

Table 29: Summary of Data Needed for Final Relative Permeability of Core 8T After Vibration

Recovered Volumes	Volume (cc)
Total initial recovered water	8.7

Dead Water Volume	2.6
Corrected initial water recovered	6.1
Pore Volume	9.69
Bulk Volume	36.31
Sw_i (%)	37.03
So_r (%)	42.19
Recovery Factor (%)	57.81

Table 30: Summary Data of Final Relative Permeability for Core 8T After Vibration

The oil saturation of the core was not a successful as was needed; however, it is still very acceptable for this application of vibration and waterflooding. The core was saturated with oil at around 63 percent making the irreducible water saturation around 37 percent. With the vibration application and waterflooding, the recovery from core 7T was more than half of the oil volume (around 58 percent).

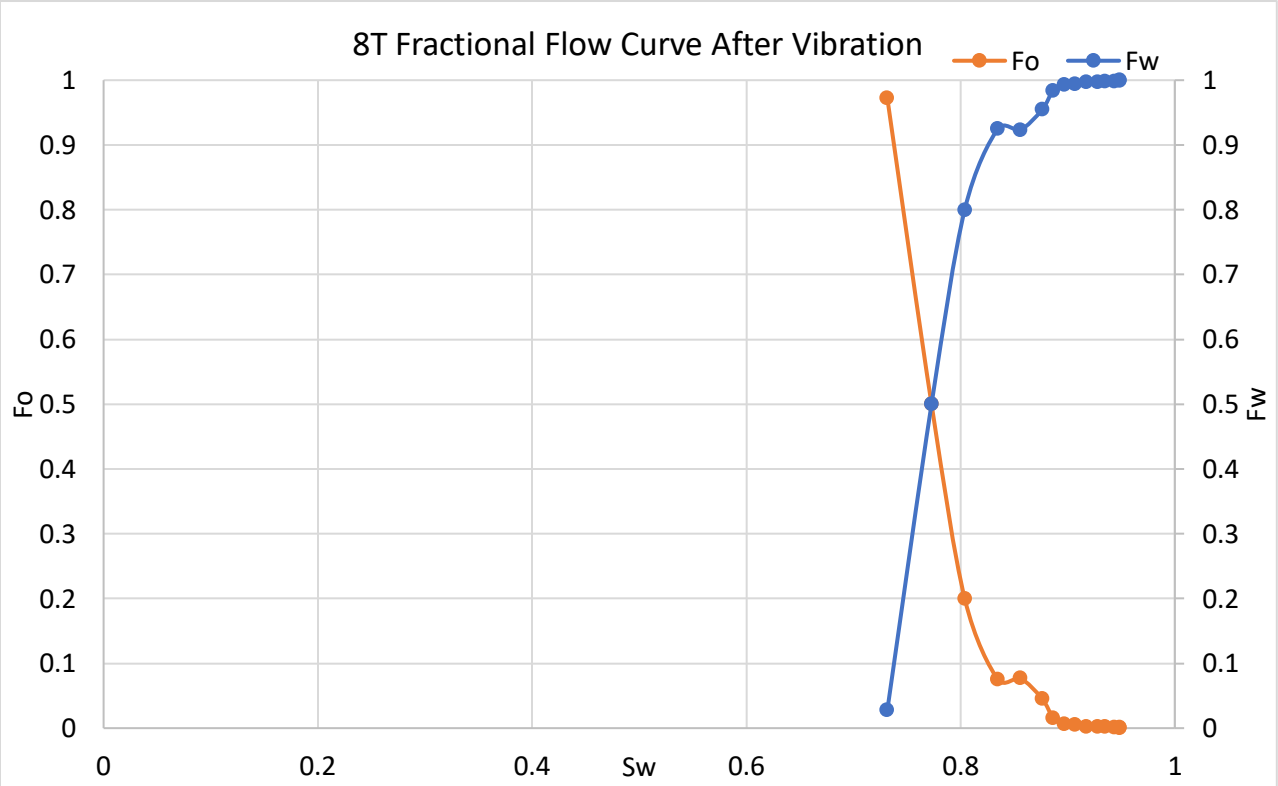

Fig 64: Fractional Flow Curve for Core 8T After Vibration

The fractional flow curve shows the imbibition and drainage process of core 8T. The fractional water curve reaches all the way to 1 or 100 percent while also the fractional oil curve starts at a relatively high value of 0.97 or 97 percent all the way to zero. There are steep changes especially in the first two points of either the imbibition or drainage of this core as can be seen by

a steep line going down or up. This can be reiterated by the first two values of the water and oil fractional flow where the difference is large in both cases. In addition, there are some clear differences between points 2, 3, 4 and 5 compared to the remaining points which are almost stuck together for both water and oil curves. This data can be found in table A56 in the appendix.

The water breakthrough occurred at three minutes and forty seconds with 4.8 centimeter cubed of oil being produced until water broke through. The production of oil occurred over an extensive period of time of just over five and a half hours with a pressure drop of exactly 11 psi from 40.4 psi to 29.4 psi. The production of oil was almost consistent until two hours and forty minutes with the remaining time producing just fractions of the oil. This data can be found in table A57 in the appendix.

From the relative permeability data in table A58 in the appendix, the relative permeability curve can be drawn. Any data that is outside the typical range has been excluded due to it not being accurate or realistic when drawing the curve itself.

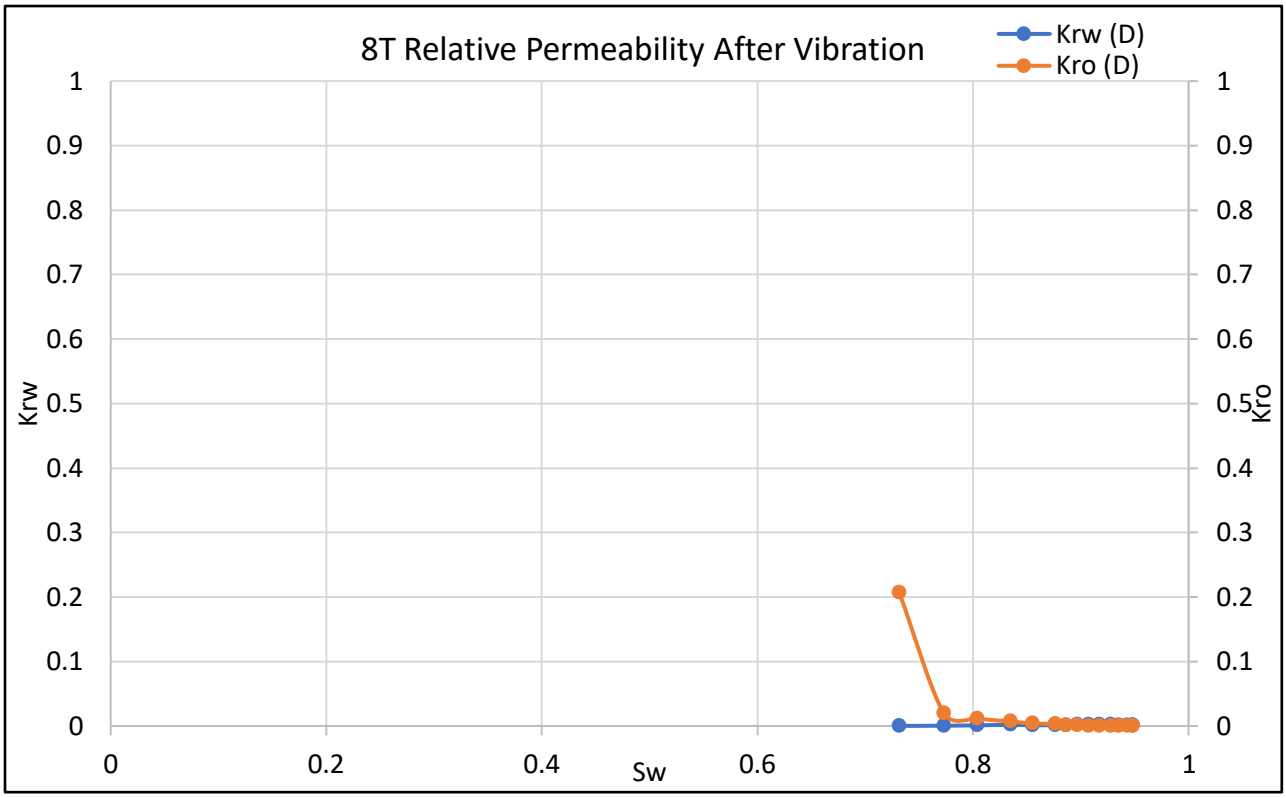

Fig 65: Final Relative Permeability Curve of Core 8T After Vibration

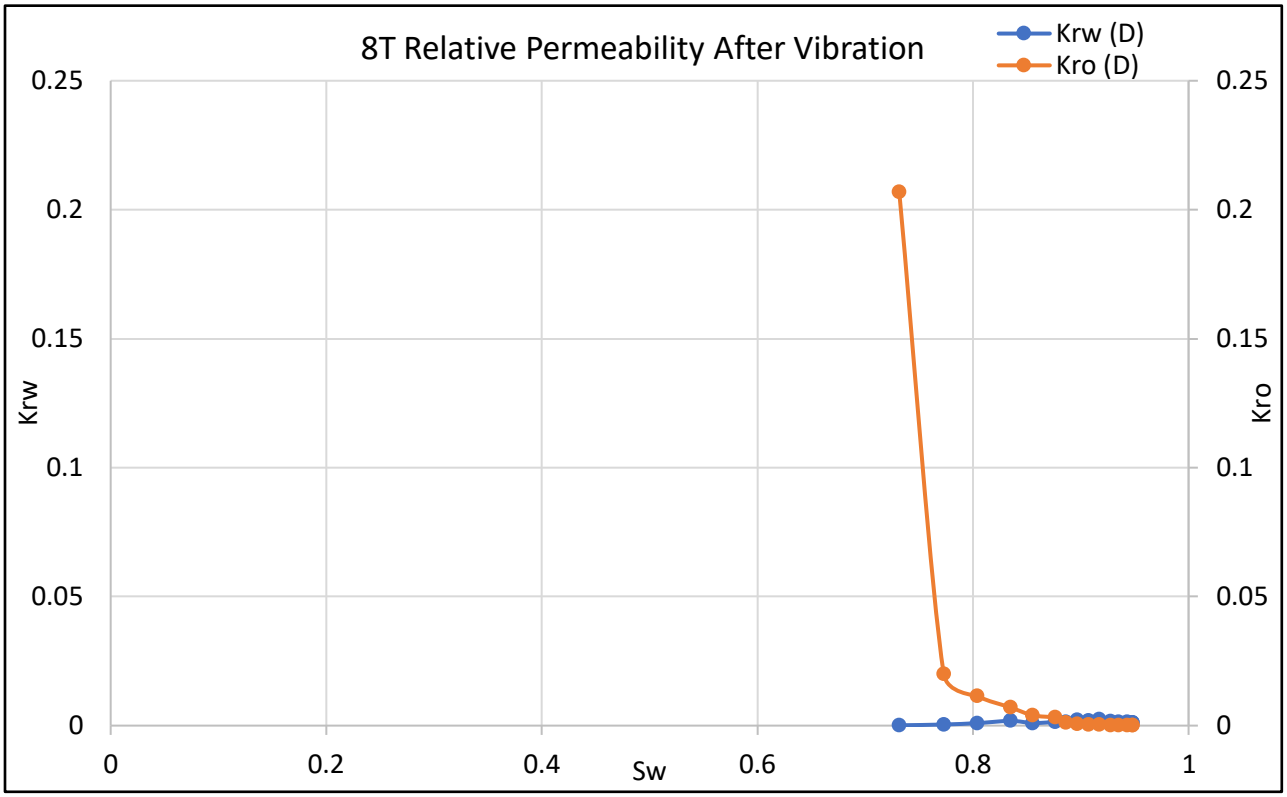

Fig 66: Final Relative Permeability Curve of Core 8T After Vibration (Scaled)

The relative permeability curve clearly shows that the core is water wet as the intersection point is at a water saturation is 0.86 which is water wet. There is a large drop between the breakthrough and the second time point when it comes to the relative permeability of oil. The effective oil permeability at breakthrough is 0.32 Darcy. In addition, the relative permeability curve for water does not increase much unfortunately unlike the relative permeability curve for oil. Furthermore, the difference between the second point and the rest of the points in the relative permeability oil curve is also very minimal especially after the fifth point.

5.3.3.5 Core 1U Relative Permeability and Waterflooding After Vibration

Sample Name	Average Length (cm)	Average Width (cm)	Dry Weight (g)	Porosity (pu)	Cross Sectional Area (Cm^2)	Saturated Weight (g)	Liquid Permeability (md)
1U	7.58	2.51	75.52	16.57	4.94	81.30	25.92

Table 31: Summary of Data Needed for Final Relative Permeability of Core 1U After Vibration

Recovered Volumes	Volume (cc)
Total initial recovered water	6.4
Dead Water Volume	2.6
Corrected initial water recovered	3.8
Pore Volume	5.16
Bulk Volume	36.31
S_{wi} (%)	26.37
S_{or} (%)	26.56
Recovery Factor (%)	73.44

Table 32: Summary Data of Final Relative Permeability for Core 1U After Vibration

The oil saturation of the core was quite a successful as only a quarter of the water remained as irreducible water which is very acceptable when compared to the other cores. The recovery of the oil using waterflooding produced a large amount. The outstanding recovery of oil from the waterflooding produced a staggering 73 percent which is the majority of the oil in place.

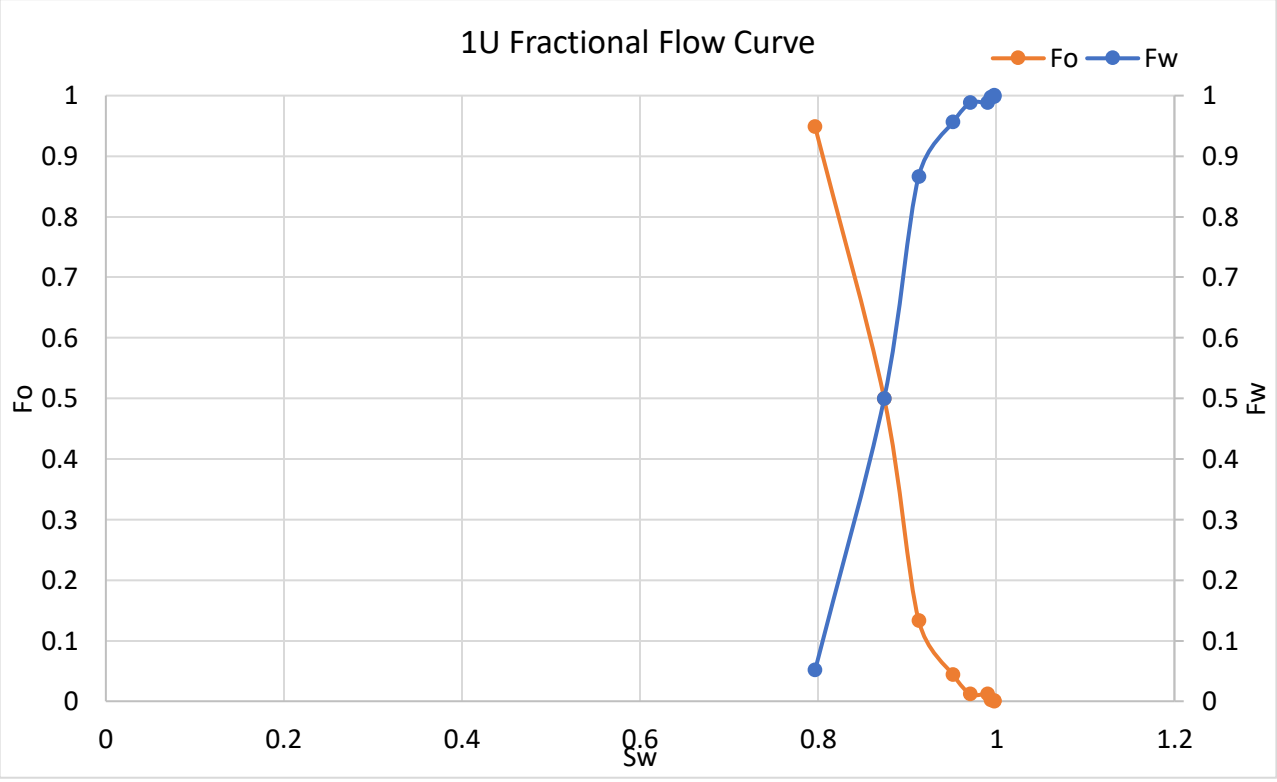

Fig 67: Fractional Flow Curve for Core 1U After Vibration

The fractional flow curve shows the imbibition and drainage process of core 1U. The fractional water curve reaches all the way to 1 or 100 percent while also the fractional oil curve starts at a relatively high value of 0.948 or 95 percent all the way to zero. There are steep changes especially in the first two points of either the imbibition or drainage of this core as can be seen by a steep line going down or up. This can be reiterated by the first two values of the water and oil fractional flow where the difference is large in both cases. In addition, there are some clear differences between points 2, 3 and 4 compared to the remaining points which are almost stuck together for both water and oil curves. This data can be found in table A59 in the appendix.

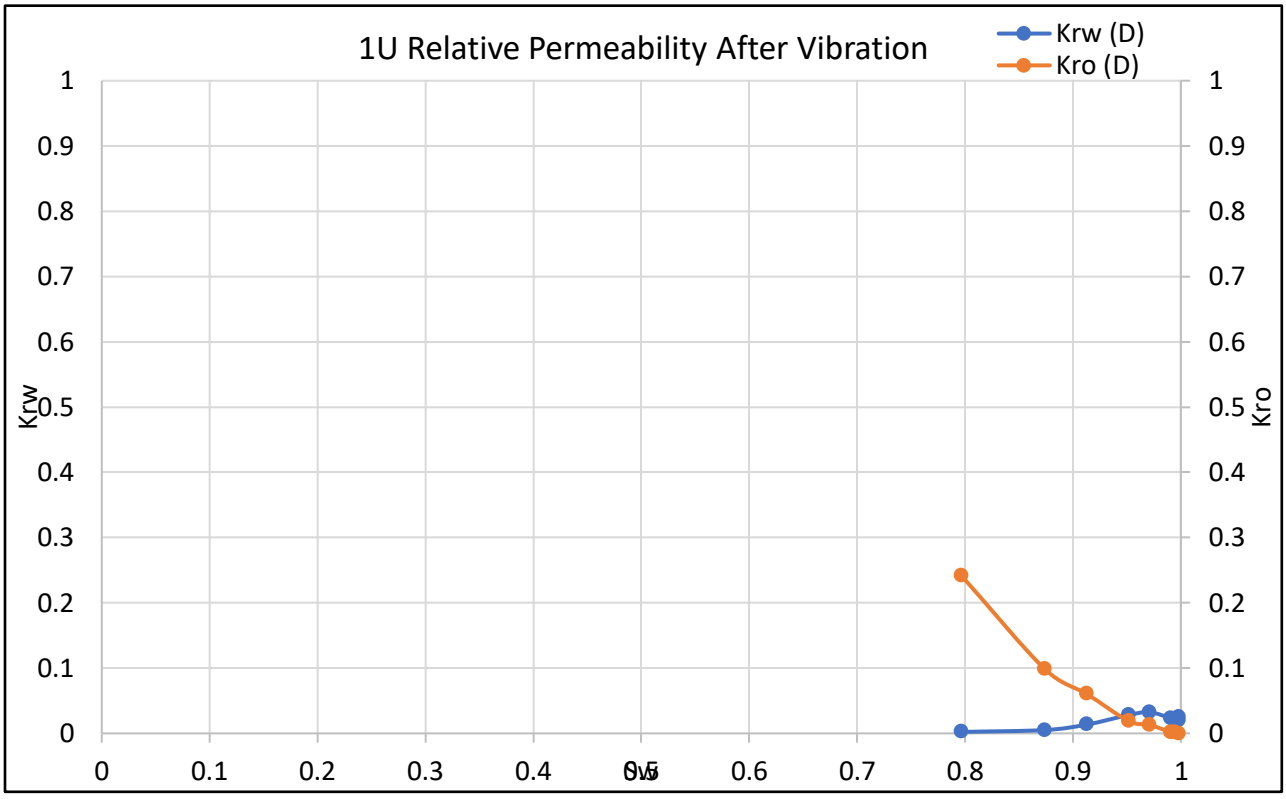

Fig 68: Final Relative Permeability Curve of Core 1U After Vibration

The water breakthrough occurred at four minutes and eighteen seconds with right over 4 centimeters cubed of oil being produced until water broke through. The production of oil occurred over an extensive period of time of just over one hour (exactly one hour and nine minutes) with a pressure drop of exactly 51.4 psi from 241.2 psi to 189.8 psi. The production of oil was almost consistent for the first half hour then decreased massively for the remainder of the time. This data can be found in table A60 in the appendix.

The relative permeability curve, drawn from the data in table 61 in the appendix, clearly shows that the core is water wet as the intersection point is at a water saturation is 0.95 which is extremely water wet. The effective oil permeability at breakthrough is 0.049 Darcy. The difference between the different points in both the relative oil and water permeability curves are very similar

which is completely different than all of the other cores. In addition, the relative permeability curve for water does increases and then slightly decreases for the last 2 points.

Chapter 6

Discussion

6.1 Summary of Hypothesis and Major Findings

The problem that was researched in this thesis was to see the relative effect of the combination of physical vibration application with waterflooding and to compare the relative effect that they have on the porosity, absolute permeability, relative permeability and oil recovery.

This hypothesis was backed up with the literature review in chapter 2 as it was shown that the optimization of the physical vibration should improve the porosity and absolute permeability. This was further proven by the paper performed about the effect of the optimization of frequency, amplitude and time would have on porosity and absolute permeability. Furthermore, the literature review has mentioned several times that changes in wettability would occur making the core more water wet which would in turn indirectly improve not only the relative permeability and its relevant curves but also the overall oil recovery.

From all of these facts and other previous research shown in the literature review in chapter 2, it led me to believe that if both vibration of the core along with waterflooding should improve all of the previously mentioned core rock and fluid parameters when compared to simply the waterflooding application on its own.

6.2 Interpretation of Results

6.2.1 Interpretation of Porosity Results

From the results chapter (chapter 5) it can be clearly seen that all of parameters mentioned in the hypothesis have improved starting off with porosity. This is true about the porosity which has shown to improve even though there is still an overall reduction in the porosity. However, this reduction has been shown to have been due to the damage and fines migration of the grains due when saturating the cores with oil in preparation for relative permeability measurements and waterflooding.

The formation damage that occurred could have been due to the nature of the oil being paraffinic along with the nature of the cores. As the cores are not naturally consolidated cores, the pressure applied to the cores when applying the oil saturation has clearly caused damage. Moreover, the type of oil being paraffinic has also caused formation damage to the cores. The damage can be seen in all for all cores especially when comparing the porosity values originally prior to any testing whatsoever and to the porosity values right after the initial phase of measurements and cleaning. As it can be seen that the average reduction in porosity between the original and after initial phase is 13.29 percent for all 5 cores. In addition, the trial core that was tested specifically for this same concept showed the same results. The core lost more than one third of its porosity value just from the oil saturation alone. Therefore, the porosity decrease was still inevitable to occur after the vibration due to the second round of oil saturations; however, what

was found was that the amount of damage was less. This would entail that the vibration did improve the porosity slightly as similar damage would have been expected in the second oil saturation phase.

The results show an average porosity decline of 12.26 percent which is more than a one percent difference than the first porosity difference. To continue on further, the differences between the first and second porosity changes, as shown in figure 25 in chapter 5, shows that four out of five cores had lower porosity decreases than in the initial phase with a difference of up to 5.8 percent for core 9S. The average porosity restoration of the 4 cores excluding core 1U as it was a clear outlier to the results found was 3 percent which is very similar to the results found in the paper published by our group where the core porosity increased by 2.44 percent.

6.2.2 Interpretation of Absolute Permeability Results

In much the same way that porosity values have improved with the selected cores the same case has occurred with the values of absolute permeability for the same selected cores. In addition, in much the same way that there was damage in the porosity of the cores due to the oil saturation the same has also occurred in much the same fashion for the values of absolute permeability.

The core damage clearly seen from the values of absolute permeability when comparing the original values to those that were measured just prior to vibration. On the one hand, there is an average reduction in absolute permeability of just over 30 percent in the 4 cores excluding 1U as it has a much higher decrease in absolute permeability of over 60 percent making it another outlier to the other core samples. On the other hand, when vibration was applied to the cores the average increase in absolute permeability of the cores was also an increase of over 30 percent (34.39 percent).

What seemed interesting was how much the values of the absolute permeability raised by on a core-by-core basis. When examining the values increases, the mode value was approximately 30 percent with improvements of 38, 28.5, and 33 percent for cores 4T, 8T, and 1U respectively. There were some major extremities such as core 9S with only a mere 8.6 percent and a colossal 62 percent for core 7T. These results would suggest that on average the improvement in absolute permeability is around 33 percent when taking into consideration the values of the 3 close cores (4T, 8T, and 1U) with the possibility that the improvement of absolute permeability may be much higher or lower depending on the core itself. Core 2X is another example of absolute permeability increase due to vibration. The core's absolute permeability increased by 15 percent which is less than half of the average increase of the other cores but still within the range of values including the extremities. When comparing these values with the value obtained from our paper on the same topic, it was found that the highest increase in absolute permeability was 12.5 percent which is only 38 percent of the average value of the 3 cores.

To put the values obtained in further perspective, if the average values of all 5 cores was taken into consideration the value will be 34.17 percent meaning that the value from our previous paper is still a sheer 36.6 percent from the average. This would suggest that the vibration could massively improve the absolute permeability of the cores with an average between 33 to 34 percent with some clear deviations however to these values.

6.2.3 Interpretation of Relative Permeability and Waterflooding Results

Not only have the porosity and absolute permeability both improved but so has the relative permeability as well as the total oil recovery percentage of the selected cores. The fractional flow curves as well as the relative permeability curves and its relation to wettability will be discussed first. It was found that there is an overall trend for the change in wettability of the selected cores.

The cores that were tested upon were surface cores in nature made up of a range of unknown material. This made the results of the relative permeability not as accurate as was hoped for. There was some damage that had occurred when performing the initial waterflooding which slightly reduces the accuracy of the results of the relative permeability. However, two of the five cores had very little to almost no damage as can be seen from table 21 with cores 4T and 8T showing no real damage. Therefore, their results are the best to be utilized to show the actual effect of the optimized Vibroseismic. It can be seen from the results that both cases showed an improvement in the overall recovery which would reiterate the fact that the optimized vibration has improved recovery.

For core 9S, the end points of the water saturation were found to be 0.89 and 1 in the initial measurements with the intersection point occurring at 0.91 water saturation and an even 0.5 on each of the fractional flow for water and oil. For the same core, the water saturation range at which the relative imbibition and drainage occurs have decreased from 0.89 to 1 initially to 0.738 to 0.84 with the same even 0.5 on each of the fractional flow for water and oil. This same concept continued when dealing with the relative permeability curves also. The saturation intersection point in the initial case was 0.988 while in the final situation after vibration the intersection point moved left to become 0.8. This would imply that the core's wettability has shifted to become more oil wet rather than more water wet. The same trend; however, was not found to be the same for the other cores.

For cores 7T, 8T and 1U the final end points of the water saturation in the fractional flow curves were found to be higher than in the initial case. For example, core 7T had initial water saturation end points 0.536 and 0.768 while the end points for the final case after vibration were 0.637 and 0.88 with the same intersection point of 0.5 for both oil and water fractional flow. To take the sample example, core 7T had an initial intersection point of 0.69 while after the vibration the intersection point altered towards the right to the value of 0.78 saturation respectively.

Core 4T had some changes in the end points of its fractional flow curves starting off at end points of water saturation of 0.53 and 0.776 and ending with end points of 0.53 and 0.781 with no change to the intersection point of the imbibition and drainage curves.

Both the fractional flow curves and the relative permeability curves present the same information regarding the wettability changes of each of the selected cores. Furthermore, the same increase in oil recovery was found to have occurred in all cores with an increase in the wettability of the same cores to become more water wet. Therefore, the alteration of wettability is the main reason for the improvement of the recovery.

Sample Name	Delta Between Inlet Pressures from Start to End Before Vibration (psi)	Delta Between Inlet Pressures from Start to End Before Vibration (psi)	Difference Between Both Deltas (psi)
9S	28.9	8.5	20.4
4T	25.9	28.7	-2.8
7T	40.9	13.9	27
8T	36.9	11	25.9
1U	160.5	51.4	109.1

Table 33: Summary of Difference in Delta Inlet Pressures Before and After Vibration

Table 33 shows that the waterflooding has become easier after the vibration has been applied. The decrease in the delta pressure across the cores when waterflooding would suggest that the easiness for the water to push the oil has definitely improved. This improvement would then suggest that the sweep efficiency of the waterflooding has enhanced allowing for more oil recovery. This would also explain the reason behind the increased oil recovery of the cores alongside the porosity, absolute permeability and relative permeability to oil.

What these results imply is that there is definitely an enhancement in the flow paths inside the core as less pressure is required to flow the oil out. Furthermore, one of the reasons mentioned in the literature was an increase in the pore pressure inside the pores which could also explain the increase in oil recovery and the need for less pressure.

Sample Name	Volume of Oil Recovered till Breakthrough Before Vibration (cc)	Volume of Oil Recovered till Breakthrough After Vibration (cc)	Difference Between Both Oil Recovered Volumes (cc)
9S	4.2	4.4	0.2
4T	4.2	4.7	0.5
7T	4.1	4.2	0.1
8T	3.6	4.8	1.2
1U	4.6	4.05	-0.55

Table 34: Summary of Oil Volume Recovered till Breakthrough Before and After Vibration

Except for core 1U, all of the other cores had a higher oil recovery after the vibration when compared to the vibration when specifically considering oil recovery until breakthrough. Both tables 1 and 2 shows that an increase in flow paths for the oil to move through has unquestionably occurred as the results have already proven a higher oil recovery from the vibration as well as less

pressure to recover said oil (table 33) and higher recovery from the beginning as it is the highest recovery step (table 34). Table 34 also shows that the period of single-phase flow of oil has been increased due to the delay in water breakthrough. This would reduce the residual oil saturation of the cores.

Another factor that was noticed when looking at the relative permeabilities was the time needed to reach to the residual oil saturation (Sor) when comparing to before and after the vibration. Except for core 4T, all of the total times after the vibration is faster to reach the residual oil saturation when contrasted to before the vibration. For cores 9S, 7T, 8T and 1U the time difference needed to reach residual oil saturation ranged from one hour and forty-five minutes for core 1U to forty-three to forty-five minutes for the rest of the cores. This once more continues to confirm the fact that improvements were done for the oil to flow out of the cores since it took less time for the cores to reach residual oil saturation. Furthermore, it also solidifies the fact that there was an alteration in wettability which closely matches the relative permeability curves. Since it has taken less time than that would mean the rock is more water wet due to the fact that more water is sticking to the rock grains allowing for more oil to flow out of the pores. This would explain why the oil recovery has increased.

6.3 Implications of Results Found

The results have clearly shown that the vibration phase in this research has proven to be successful. This has been established through the improvement of the porosity, absolute permeability and the relative permeability.

The clear improvement that has been made is the enhancement of the absolute permeability. It has been proven unequivocally that there has been a major increase in the values of the absolute permeability when it comes to all 5 of the selected cores of this research. Moreover, these results also solidify the concept that physical vibration does improve the absolute permeability of all cores regardless of their initial absolute permeability. All 5 cores and also the very tight core (core 2X) that was tested separately all showed to have higher values of absolute permeability after vibration. This has thus allowed for the enhancement of absolute permeability to be one of the main clear observations and reasons of why there was an ultimate increase in oil recovery. Furthermore, when comparing the results from this research to the previous research performed, the results presented in this research are much higher in terms of absolute permeability enhancement.

Regarding the porosity, even though there is damage to the cores; however, the vibration has still shown to be a success. It was revealed that the damage was due to the oil saturation step during the relative permeability phase of the research; therefore, the damage would occur regardless of the any work done on the core. When comparing the damage that had occurred to a core that was not directly related to this research to see the effect of the oil saturation on its own, the core damage was proven to be true with the drop in porosity found before and after the oil saturation had occurred to it. The physical vibration applied allowed for the damage percentage the drop. The damage percentage should have been higher than what the physical vibration can achieve; however, there was still some improvement to the porosity. Therefore, it has been established that the physical vibration can slightly improve the effective porosity of the core. These

results once more correlate very well with the data collected from the previous research. The percentages of increase are exceedingly similar and also in much the same way the porosity increase is not as large as the absolute permeability increase.

For the relative permeability and their respective curves, the wettability factor is a main factor in the same way as the literature has described. Also, the increase in pore pressure has definitely appeared to be a factor in the similarly as presented in the literature. The oil recovery has increased in all of the cores even though one of the cores become more oil-wet. The recovery from the oil wet core was not as great as other but still quite a high value considering that these cores are small cores. However, regarding the pore pressure it has been clearly seen that for all of the cores that had changes in their wettability, become more oil or water wet, the total delta pressure between residual water saturation to residual oil saturation which represents the waterflooding have decreased quite significantly. Moreover, the volume recorded of oil recovery until water breakthrough before and after vibration clearly favors after the vibration testing. Furthermore, the time needed for the cores to reach residual oil saturation and for the waterflooding to become complete is much shorter after the vibration has been applied. Most importantly, the oil recovered from all 5 of the cores selected to complete this research has shown increase after the vibration has been applied. Relative permeability has shown several times to have been somewhat enhanced with 3 out of the 5 cores becoming more water wet; the pore pressure increasing in 4 out 5 of the cores; the total delta becoming lower in 4 out of 5 of the cores; the total waterflooding time becoming lower in 4 out of 5 of the cores; and the oil recovery increasing in all of the cores. Therefore, it can be said that physical vibration has improved the relative permeability of the cores as the majority of the cores have improved in every single factor discussed.

Chapter 7:

Conclusion, Limitations and Recommendations

7.1 Summary of Research

The data that was collected in this research was able to provide the needed answer to the hypothesis presented before. The topic of this research was to see the effect on the core as well as oil recovery when waterflooding only is applied to a core and when waterflooding as well as physical vibration is employed. I hypothesized that the coupling of the physical vibration with waterflooding applications should improve the porosity, absolute permeability, relative permeability and ultimate oil recovery. This hypothesis was based on the previous research paper discussing the optimization of physical parameters along with the literature that was published on the topic of this research.

7.2 Conclusions

1. Enhancement in rock properties (porosity and absolute permeability), rock-fluid properties (relative permeability) and oil recovery due to optimized vibration application
2. Larger percentage increase in absolute permeability when compared to the percentage increase in porosity from vibration
3. Wettability changed to become more water wet according to the residual oil saturations decrease and increase in the residual water saturations of the cores
4. Improvement in relative permeability to oil can be mainly seen in the decrease in remaining oil saturation
5. Reduction in formation damage was present as can be seen in the values of porosity and absolute permeability when comparing before and after vibration
6. Enhancements in sweep efficiency of waterflooding with lower pumping pressures required due to better injection paths

7.3 Limitations

One of the main limitations are the materials used to perform this research in terms of the cores used and the oil used. The cores are not reservoir cores that originate from downhole reservoirs and so have not been compacted. This idea was made clear as our paper shows different optimal vibrations for synthetic and reservoir cores. These types of cores were used as the process of acquiring downhole reservoir cores is very difficult which unfortunately led me to use these synthetic surface cores instead.

The use of a sample of real crude oil from any reservoir for the purpose of oil saturation and water permeability would also have allowed for more realistic results as it would have been closer to the real world. The use of the synthetic paraffinic oil has caused formation damage that

real crude oil may not. As the properties of the oil would most definitely yield different results specifically when discussing the rock-fluid properties which once again is related to the relative permeability results of this research. Moreover, it would have been better to couple the utilization of both the actual cores and crude oil for the most representative outcomes.

Another limitation is the cleaning section of the cores in the Soxhlet apparatus. The cleaning of the cores using the Soxhlet apparatus using Toluene and Xylene may or may not affect the wettability and therefore the relative permeability. A change in the methodology can improve this area of the research to enhance the results.

7.4 Recommendations

It is recommended to reapply the research once more on real reservoir cores from producing zones at reservoir conditions. This would greatly improve the results obtained and obtain results that will be closer to real life. Furthermore, it would be recommended to reapply using crude oil from a producing zone coupled with the real reservoir core. This would produce exact results for a case study for a field to see the increase in recovery.

Regarding the methodology, it would be good to alter the steps and use two different cores with similar properties instead of cleaning the cores. This would eliminate the doubt that of the effect of the cleaning stage on the core's wettability.

There is a need to revisit core 1U due to the very conflicting results especially with the decrease in the rock properties with an increase in the final recovery. This could be done through the closer examination of the core itself under the microscope. This step is to be done to better understand the effect that the vibration has on the core grains and flow paths.

References

Abdulfatah, H. K. Application of Ultrasonic Waves in Enhancing Oil Recovery in Secondary Recovery Phase. 2018. Paper presented at the SPE Annual Technical Conference and Exhibition, Dallas, Texas, USA, 24-26 September. SPE-194031-STU. https://doi.org/10.2118/194031-STU

Alhomadhi, E., Amro, M., and Almobarky, M. 2013. Experimental Application of Ultrasound Waves to Improved Oil Recovery During Waterflooding. *Journal of King Saud University*, **26** (2013): 103-110. https://dx.doi.org/10.1016/j.jksues.2013.04.002.

Archer, J. and Wall, C. (1986). 1994. Relative Permeability and Multiphase Flow in Porous Media. In *Petroleum Engineering Principles and Practice*, Chap. 7, 102–115. London, UK: Graham and Trotman.

Ariadji, T. 2005. Effect of Vibration on Rock and Fluid Properties: On Seeking the Vibroseismic Technology Mechanisms. Paper presented at the SPE Asia Pacific Oil and Gas Conference and Exhibition, Jakarta, Indonesia, 5 – 7 April. SPE 93112. https://doi:https://doi.org/10.2118/93112-MS

Beresnev, I., Johnson, P. 1992. Elastic-Wave Stimulation of Oil Production: A Review of Methods and Results. *Journal of Geophysics*, **59** (6): 1000-1017.

Boeut, S., Oshima, T., Fujii, Y., et. al. 2019. Variation in the Permeability of Intact and Fractured Rocks due to Transient Disturbances in Axial Stress or Pore Pressure. *Advances in Civil Engineering*, **2019**, 1-16. https://doi.org/10.1155/2019/1312746.

Biot. M. 1956. Theory of Propagation of Elastic Waves in a Fluid-Saturated Porous Solid. II. Higher Frequency Range. *The Journal of The Acoustical Society of America*, **28**, (2): 179-199.

Bizzarri, A. 2012. Effects Of Permeability and Porosity Evolution On Simulated Earthquakes. *Journal of Structural Geology*, **38** (2012) 243-253. https://dx.doi.org/10.1016/j.jsg.2011.07.009.

Duan, Q. and Yang, X. 2014. Experimental Studies on Gas And Water Permeability of Fault Rocks From The Rupture of The 2008 Wenchuan Earthquake, China. *Science China Earth Sciences*, **57** (11): 2825-2834. http://dx.doi.org/10.1007/s11430-014-4948-7.

Cidoncha, J.G. 2007. Application of Acoustic Waves for Reservoir Stimulation. Paper presented at the International Oil Conference and Exhibition in Mexico, Veracruz, Mexico, 27–30 June. https://doi: https://doi.org/10.2118/108643-MS.

Hall, R., Ross, D., Stevens, G., et al. 2006. Identification and Analysis of Fields for Waterflood-Enhanced Recovery Efforts. Presented at SPE Eastern Regional Meeting, Canton, Ohio, 11–13 October, SPE 104596.

Hassan, H., Nooruldeen, A. 2018. Experimental Study of Vibration Effect on Porous Media. *Journal of University of Babylon for Engineering Sciences*, **26**, (10): 229-238.

Huppler, J. 1970. Numerical Investigation of the Effects of Core Heterogeneities on Waterflood Relative Permeabilities. Presented at SPE 45th Annual Fall Meeting, Houston, Texas, 4-7 October. SPE 2874.

Irfan. MD., Lenn. C., Ghosh. D. 2016. Seismic Stimulation and Induced Seismicity. 2009 SPE Offshore Europe Oil & Gas Conference & Exhibition held in Aberdeen, UK, 8–11 September. SPE 123304. https://doi.org/10.2118/123304-MS.

John R. Bloomberg 1997. A Study of the Above Average Waterflooding Recovery of the Richardson Berea Field, Calhoun and Roane Cos., West Virginia. Presented at Eastern Regional Meeting, Lexington, KY, 22-24 October, SPE 39215. https://doi.org/10.2118/39215-MS.

Jadhunandan, P. and Morrow, N. 1995. Effect of Wettability on Waterflood Recovery for Crude-Oil/Brine/Rock Systems. Presented at SPE Annual Technical Conference and Exhibition, Dallas, Texas, 6-9 October. SPE 22597.

Kanjirakat, A., Belaidi, A., Carvero, A. et al. 2023. Effect Of Seismic Vibration Amplitudes and Frequencies in Dislodging An Entrapped Fluid In A Pore Model. *Egyptian Journal of Petroleum* **32** (1): 1-7. http://dx.doi.org/10.1016/j.ejpe.2022.11.001.

Kitamura, K., Takahashi, M., Mizoguchi, K. et al. 2010. Effects of Pressure on Pore Characteristics and Permeability of Porous Rocks as Estimated From Seismic Wave Velocities In Cores From TCDP Hole-A. *Geophysical Journal International*, **182** (3): 1148-1160. http://dx.doi.org/10.1111/j.1365-246x.2010.04694.x

Kostrov, S. A., and William O. Wooden. 2008. Possible Mechanisms and Cases for Enhancement of Oil Recovery and Production using Seismic Stimulation. Paper presented at the SPE Symposium on Improved Oil Recovery, Tulsa, Oklahoma, USA, 20–23 April. SPE 114025-MS. https://doi.org/10.2118/114025-MS.

Kouznetsov, O., Simkin, E., Chilingar, G., et al. 1997. Improved Oil Recovery by Application of Vibro-Energy to Waterflooded Sandstones. *Journal of Petroleum Science and Engineering*, **19**, (1998): 191-200.

Kurawle, I. B., Kaul, M., Mahalle, N.A., Carvalho, V. H., Nath, N., et al. 2009. Seismic EOR—The Optimization of Aging Waterflood Reservoirs. Paper presented at the SPE Offshore Europe Oil and Gas Conference and Exhibition, Aberdeen, UK, 8-11 September. SPE 123304-MS. https://doi.org/10.2118/123304-MS.

Lockner, D. and Beeler, N. 2002. Rock Failure and Earthquakes. *International Handbook of Earthquake And Engineering Seismology*, 81A. J. Byerlee, C. Sammis, C. Scholz, R. Sibson, and W. Stuart, Chap. 32. 505-537. USA: Int'l Assoc. Seismol. & Phys. Earth's Interior, Committee on Education.

Lopuchov, G. 1999. Vibroseismic stimulation for rehabilitation of waterflooded reservoirs. *Petroleum Geoscience*, **5**, (1999): 259–263.

Manga, M., Beresnev, I., Brodsky, E. et al. 2012. Changes In Permeability Caused by Transient Stresses: Field Observations, Experiments, and Mechanisms. *Reviews of Geophysics*, **50** (2): 1-24. http://dx.doi.org/10.1029/2011rg000382.

Mohammadian, E., Shirazi, M.A, Kamal, A.I. 2011. Enhancing Oil Recovery through Application of Ultrasonic Assisted Waterflooding. Paper presented at the SPE Asia Pacific Oil and Gas Conference and Exhibition, Jakarta, Indonesia, 20-22 September. SPE 145014-MS. https://doi.org/10.2118/145014-MS.

Nikolaevskii, V.N. 1992. Rock Vibration and Finite Oil Recovery. *Theoretical and Applied Mechanics*, **7**, (5): 110-119. https://0015-4628/92/2705-0689.

Nikolaevskiy, V.N., Lopukhov, G.P., Yizhu, Liao, et al. 1996. Residual Oil Reservoir Recovery with Seismic Vibrations. *SPE Prod & Fac*, **11** (1996): 89–94. SPE 29155-PA. https://doi.org/10.2118/29155-PA.

Oraby, M., Abdalla, M., Aal, T. et al. 2022. Optimization of the vibration parameters in the Vibroseismic applications. *Journal of Petroleum Science and Engineering*, **219**: 111029. http://dx.doi.org/10.1016/j.petrol.2022.111029.

Roberts, P., Majer, E., Lo, W., Sposito, G., & Daley, T. 2002. An Integrated Approach to Seismic Stimulation of Oil Reservoirs: Laboratory, Field and Theoretical Results from Doe/Industry Collaborations. Paper presented at the 6th International Symposium on Nonlinear Acoustics, Moscow, Russia, 19-23 August. https://www.osti.gov/servlets/purl/976527.

Salem, A. and Snosy, M. 2015. The Effect of Ultrasonic Waves of EOR on the Relative Permeability Curves. Presented at SPE Kuwait Oil & Gas Show and Conference, Mishref, Kuwait, 11–14 October, SPE 175410-MS. https://doi.org/10.2118/175410-MS.

Sitompul, V., Alfian, M., Sitompul, F.O., Winata, D., et al. 2021. Breakthrough Enhanced Oil Recovery Technology with Low Cost & Fast Yield on Pilot Test of Vibroseismic EOR Technology in Tempino Field, Sumatera, Indonesia. Paper presented at the SPE/IATMI Asia Pacific Oil & Gas Conference and Exhibition, Virtual, 12-14 October. SPE 205746-MS. https://doi.org/10.2118/205746-MS.

Westermark, R.V., Brett, J.F., and D.R. Maloney. 2001. Enhanced Oil Recovery with Downhole Vibration Stimulation. Paper presented at the SPE Production and Operations Symposium, Oklahoma City, Oklahoma, 24-27 March. SPE 67303-MS. https://doi.org/10.2118/67303-MS.

Zhang, L.H., Ho, P., Yun, L., et al. 1999. Low Frequency Vibration Recovery Enhancement Process Simulation. Paper presented at the SPE Reservoir Simulation Symposium, Houston, Texas, 14-17 February. SPE 51914-MS. https://doi.org/10.2118/51914-MS.

Appendix I

Tables A1 to A3 provide the initial data of the cores including the dimensions, initial porosity and saturations

Sample Name	Length 1 (mm)	Length 2 (mm)	Length 3 (mm)	Average Length (mm)	Width 1 (mm)	Width 2 (mm)	Width 3 (mm)	Average Width (mm)
4R	7.303	7.308	7.306	7.31	2.531	2.526	2.527	2.53
5R	7.22	7.208	7.206	7.21	2.525	2.529	2.524	2.53
6R	7.2	7.209	7.208	7.21	2.53	2.527	2.526	2.53
7R	7.15	7.148	7.154	7.15	2.527	2.526	2.527	2.53
1S	7.614	7.626	7.61	7.62	2.514	2.512	2.503	2.51
2S	7.634	7.613	7.614	7.62	2.529	2.534	2.53	2.53
3S	7.575	7.572	7.57	7.57	2.525	2.527	2.527	2.53
4S	7.623	7.616	7.625	7.62	2.536	2.534	2.528	2.53
5S	7.675	7.673	7.672	7.67	2.517	2.511	2.533	2.52
6S	7.627	7.63	7.625	7.63	2.492	2.5	2.506	2.50
7S	7.624	7.629	7.626	7.63	2.526	2.526	2.524	2.53
8S	7.636	7.634	7.631	7.63	2.528	2.522	2.511	2.52
9S	7.616	7.615	7.617	7.62	2.53	2.495	2.533	2.52
1T	7.332	7.329	7.31	7.32	2.527	2.525	2.535	2.53
2T	7.294	7.29	7.291	7.29	2.528	2.516	2.532	2.53
3T	7.27	7.267	7.265	7.27	2.532	2.531	2.536	2.53
4T	7.103	7.104	7.098	7.10	2.534	2.523	2.535	2.53
5T	7.197	8.798	7.204	7.73	2.524	2.499	2.53	2.52
6T	7.268	7.264	7.269	7.27	2.525	2.538	2.531	2.53
7T	7.191	7.196	7.195	7.19	2.534	2.536	2.537	2.54
8T	7.309	7.306	7.308	7.31	2.525	2.532	2.533	2.53
9T	7.263	7.265	7.263	7.26	2.53	2.534	2.526	2.53
1U	7.588	7.586	7.587	7.59	2.528	2.502	2.516	2.52
2U	7.614	7.613	7.624	7.62	2.497	2.491	2.517	2.50
3U	7.588	7.586	7.601	7.59	2.528	2.501	2.5	2.51
4U	7.572	7.58	7.567	7.57	2.524	2.504	2.535	2.52
5U	7.648	7.649	7.647	7.65	2.509	2.53	2.532	2.52
6U	7.615	7.618	7.616	7.62	2.5	2.513	2.519	2.51
7U	7.621	7.627	7.623	7.62	2.495	2.532	2.535	2.52

8U	7.679	7.68	7.679	7.68	2.538	2.516	2.518	2.52
9U	7.648	7.632	7.627	7.64	2.502	2.522	2.513	2.51
1V	7.314	7.302	7.3	7.31	2.531	2.525	2.526	2.53
2V	7.194	7.19	7.203	7.20	2.507	2.531	2.531	2.52
3V	7.273	7.565	7.271	7.37	2.526	2.526	2.529	2.53
4V	7.182	7.185	7.182	7.18	2.534	2.53	2.529	2.53
5V	7.139	7.14	7.142	7.14	2.513	2.483	2.511	2.50
6V	7.025	7.026	7.026	7.03	2.528	2.53	2.529	2.53
7V	7.319	7.325	7.334	7.33	2.513	2.497	2.5	2.50
8V	6.822	6.818	6.819	6.82	2.531	2.485	2.532	2.52
9V	7.23	7.234	7.229	7.23	2.528	2.537	2.529	2.53
1X	7.582	7.606	7.583	7.59	2.535	2.491	2.505	2.51
2X	7.471	7.469	7.473	7.47	2.534	2.536	2.524	2.53
3X	7.308	7.307	7.315	7.31	2.531	2.529	2.532	2.53

Table A1: Cores Dimensional Data

Sample Name	Bulk Volume (cubic centimeters – cc)	Pore Volume (cubic centimeters – cc)	Porosity (porosity unit – pu)
1R	33.80	9.66	28.58
2R	33.86	9.34	27.58
3R	35.70	10.68	29.92
4R	36.67	10.49	28.61
5R	36.14	10.19	28.20
6R	36.17	9.93	27.45
7R	35.86	9.86	27.50
1S	37.69	10.31	27.35
2S	38.34	10.58	27.60
3S	37.95	10.25	27.01
4S	38.27	10.78	28.67
5S	37.41	9.89	28.17
6S	38.19	10.32	26.44
7S	38.08	10.48	27.02
8S	37.96	10.04	27.52
9S	36.79	11.77	26.45
1T	36.51	9.91	31.99
2T	36.62	11.92	27.14

3T	35.73	11.76	32.55
4T	38.51	11.81	32.91
5T	36.56	11.57	30.67
6T	36.74	11.37	31.65
7T	36.52	11.48	33.13
8T	37.69	10.78	30.95
9T	37.45	10.68	31.43
1U	37.57	11.17	28.60
2U	37.80	10.95	28.52
3U	37.71	11.04	29.73
4U	38.06	10.94	28.97
5U	38.42	11.07	29.66
6U	37.84	10.65	29.28
7U	36.64	9.94	28.74
8U	36.96	10.56	28.81
9U	36.14	9.55	28.14
1V	35.10	9.25	27.13
2V	35.29	9.44	27.27
3V	33.91	9.11	28.57
4V	36.38	9.65	26.43
5V	37.69	10.31	26.35
6V	38.34	10.58	26.75
7V	37.95	10.25	28.63
8V	38.27	10.78	26.87
9V	37.41	9.89	26.53
1X	36.58	8.41	24.81
2X	37.60	9.83	26.14
3X	36.79	8.65	23.51

Table A2: Cores Porosity Data

Sample Name	Dry Weight (g)	Saturated Weight (g)	Weight Difference (g)	Saturation of PV (%)
2R	65.92	74.97	9.05	93.69
3R	68.68	76.52	7.84	83.93
5R	70.18	78.15	7.97	74.61
6R	70.37	78.09	7.72	73.58

7R	69.82	77.62	7.80	76.54
3S	74.18	81.88	7.70	77.54
7S	74.49	82.27	7.78	78.86
9S	74.71	84.26	9.55	92.63
1T	67.55	78.58	11.03	94.71
3T	66.43	75.75	9.32	90.93
4T	64.61	73.92	9.31	86.35
7T	66.74	77.86	11.12	98.08
8T	68.15	79.23	11.08	86.82
1U	71.98	82.47	10.49	99.14
5U	72.57	83.15	10.58	98.71
4V	72.38	80.36	7.97	67.73
6V	70.47	78.23	7.76	78.31
9V	72.59	81.82	9.23	77.43
1X	77.80	86.37	8.57	72.87
2X	76.28	83.93	7.65	68.84
3X	77.04	85.17	8.13	66.12

Table A3: Cores Weight Before and After Initial Brine Saturation

Tables A4 to A24 provide the initial absolute permeability data obtained from which the absolute permeability charts were drawn from.

cc/min	cc/sec	ΔP (psig)	ΔP (atm)	ΔP (atm)/L	Q/A
1	0.0167	40.8	2.7744	0.4092438	0.003342
2	0.0334	170.6	11.6008	1.7112007	0.006684
3	0.0501	276.9	18.8292	2.7774412	0.010026
4	0.0668	371.4	25.2552	3.7253221	0.013368
5	0.0835	470.1	31.9668	4.7153309	0.016711
6	0.1002	550.8	37.4544	5.524791	0.020053

Table A4: Initial Liquid Permeability Data for Core 2R

cc/min	cc/sec	ΔP (psig)	ΔP (atm)	ΔP (atm)/L	Q/A
1	0.0167	67.5	4.59	0.6331617	0.003392
2	0.0334	170.2	11.5736	1.5965054	0.006784
3	0.0501	241.2	16.4016	2.2624977	0.010176
4	0.0668	371.5	25.262	3.4847342	0.013569

5	0.0835	471.2	32.0416	4.4199375	0.016961
6	0.1002	567.8	38.6104	5.3260622	0.020353

Table A5: Initial Liquid Permeability Data for Core 3R

cc/min	cc/sec	ΔP (psig)	ΔP (atm)	ΔP (atm)/L	Q/A
1	0.0167	76.7	5.2156	0.7232504	0.003332
2	0.0334	131.4	8.9352	1.2390496	0.006665
3	0.0501	210.8	14.3344	1.98776	0.009997
4	0.0668	311.2	21.1616	2.934492	0.01333
5	0.0835	410.8	27.9344	3.8736803	0.016662
6	0.1002	507.1	34.4828	4.7817509	0.019995

Table A6: Initial Liquid Permeability Data for Core 5R

cc/min	cc/sec	ΔP (psig)	ΔP (atm)	ΔP (atm)/L	Q/A
1	0.0167	61.3	4.1684	0.578489152	0.003328028
2	0.0334	110.8	7.5344	1.045621502	0.006656056
3	0.0501	141.7	9.6356	1.337225332	0.009984084
4	0.0668	270.9	18.4212	2.556487949	0.013312112
5	0.0835	399.5	27.166	3.770088356	0.016640141
6	0.1002	465.4	31.6472	4.391987787	0.019968169

Table A7: Initial Liquid Permeability Data for Core 6R

cc/min	cc/sec	ΔP (psig)	ΔP (atm)	ΔP (atm)/L	Q/A
1	0.0167	64.1	4.3588	0.6095655	0.003331
2	0.0334	106.1	7.2148	1.0089689	0.006661
3	0.0501	201.2	13.6816	1.9133321	0.009992
4	0.0668	318.1	21.6308	3.0250047	0.013323
5	0.0835	408.5	27.778	3.8846728	0.016653
6	0.1002	64.1	4.3588	0.6095655	0.003331

Table A8: Initial Liquid Permeability Data for Core 7R

cc/min	cc/sec	ΔP (psig)	ΔP (atm)	ΔP (atm)/L	Q/A
1	0.0167	1.3	0.0884	0.0116741	0.003332
2	0.0334	17.3	1.1764	0.155355	0.006663
3	0.0501	30.7	2.0876	0.2756878	0.009995
4	0.0668	36.8	2.5024	0.3304662	0.013326

5	0.0835	40.7	2.7676	0.3654884	0.016658
6	0.1002	46.9	3.1892	0.4211648	0.019989

Table A9: Initial Liquid Permeability Data for Core 3S

cc/min	cc/sec	ΔP (psig)	ΔP (atm)	ΔP (atm)/L	Q/A
1	0.0167	1.2	0.0816	0.0106998	0.003334
2	0.0334	7.2	0.4896	0.0641986	0.006668
3	0.0501	27.1	1.8428	0.2416364	0.010003
4	0.0668	34.2	2.3256	0.3049434	0.013337
5	0.0835	37.1	2.5228	0.3308012	0.016671
6	0.1002	40.9	2.7812	0.3646838	0.020005

Table A10: Initial Liquid Permeability Data for Core 7S

cc/min	cc/sec	ΔP (psig)	ΔP (atm)	ΔP (atm)/L	Q/A
1	0.0167	6.8	0.4624	0.0607143	0.00335
2	0.0334	7.7	0.5236	0.06875	0.0067
3	0.0501	31.4	2.1352	0.2803571	0.01005
4	0.0668	37.5	2.55	0.3348214	0.0134
5	0.0835	40.7	2.7676	0.3633929	0.01675
6	0.1002	41.4	2.8152	0.3696429	0.0201

Table A11: Initial Liquid Permeability Data for Core 9S

cc/min	cc/sec	ΔP (psig)	ΔP (atm)	ΔP (atm)/L	Q/A
1	0.0167	0.8	0.0544	0.007428	0.003325
2	0.0334	1.1	0.0748	0.0102135	0.006649
3	0.0501	2.1	0.1428	0.0194984	0.009974
4	0.0668	3.3	0.2244	0.0306404	0.013298
5	0.0835	4.1	0.2788	0.0380684	0.016623
6	0.1002	0.8	0.0544	0.007428	0.003325

Table A12: Initial Liquid Permeability Data for Core 1T

cc/min	cc/sec	ΔP (psig)	ΔP (atm)	ΔP (atm)/L	Q/A
1	0.0167	0.8	0.0544	0.0074856	0.003314
2	0.0334	1.2	0.0816	0.0112283	0.006628
3	0.0501	1.6	0.1088	0.0149711	0.009942
4	0.0668	1.7	0.1156	0.0159068	0.013256

5	0.0835	6.6	0.4488	0.0617558	0.01657
6	0.1002	7.6	0.5168	0.0711127	0.019884

Table A13: Initial Liquid Permeability Data for Core 3T

cc/min	cc/sec	ΔP (psig)	ΔP (atm)	ΔP (atm)/L	Q/A
1	0.0167	0.7	0.0476	0.0067027	0.00332
2	0.0334	1.2	0.0816	0.0114903	0.00664
3	0.0501	1.5	0.102	0.0143628	0.00996
4	0.0668	1.7	0.1156	0.0162779	0.013281
5	0.0835	6.7	0.4556	0.064154	0.016601
6	0.1002	7.5	0.51	0.0718141	0.019921

Table A14: Initial Liquid Permeability Data for Core 4T

cc/min	cc/sec	ΔP (psig)	ΔP (atm)	ΔP (atm)/L	Q/A
1	0.0167	0.7	0.0476	0.0066166	0.003307
2	0.0334	1.5	0.102	0.0141785	0.006614
3	0.0501	1.9	0.1292	0.0179594	0.009921
4	0.0668	2	0.136	0.0189046	0.013228
5	0.0835	2.1	0.1428	0.0198499	0.016535
6	0.1002	2.2	0.1496	0.0207951	0.019842

Table A15: Initial Liquid Permeability Data for Core 7T

cc/min	cc/sec	ΔP (psig)	ΔP (atm)	ΔP (atm)/L	Q/A
1	0.0167	0.6	0.0408	0.0055832	0.003322
2	0.0334	0.9	0.0612	0.0083748	0.006644
3	0.0501	1.2	0.0816	0.0111664	0.009966
4	0.0668	1.4	0.0952	0.0130274	0.013288
5	0.0835	1.7	0.1156	0.015819	0.016609
6	0.1002	1.9	0.1292	0.0176801	0.019931

Table A16: Initial Liquid Permeability Data for Core 8T

cc/min	cc/sec	ΔP (psig)	ΔP (atm)	ΔP (atm)/L	Q/A
1	0.0167	4.2	0.2856	0.0376433	0.003361
2	0.0334	7.5	0.51	0.0672202	0.006721
3	0.0501	31.4	2.1352	0.2814288	0.010082
4	0.0668	36.9	2.5092	0.3307236	0.013443

5	0.0835	40.6	2.7608	0.3638856	0.016804
6	0.1002	41.7	2.8356	0.3737446	0.020164

Table A17: Initial Liquid Permeability Data for Core 1U

cc/min	cc/sec	ΔP (psig)	ΔP (atm)	ΔP (atm)/L	Q/A
1	0.0167	0.7	0.0476	0.0062238	0.003339
2	0.0334	1.3	0.0884	0.0115586	0.006677
3	0.0501	16.6	1.1288	0.1475941	0.010016
4	0.0668	30.8	2.0944	0.2738494	0.013354
5	0.0835	36.7	2.4956	0.3263075	0.016693
6	0.1002	40.2	2.7336	0.3574268	0.020032

Table A18: Initial Liquid Permeability Data for Core 5U

cc/min	cc/sec	ΔP (psig)	ΔP (atm)	ΔP (atm)/L	Q/A
1	0.0167	30.9	2.1012	0.292524	0.003319
2	0.0334	40.9	2.7812	0.387192	0.006639
3	0.0501	67.1	4.5628	0.6352221	0.009958
4	0.0668	96.8	6.5824	0.9163859	0.013277
5	0.0835	131.2	8.9216	1.2420437	0.016596
6	0.1002	169.9	11.5532	1.6084087	0.019916

Table A19: Initial Liquid Permeability Data for Core 4V

cc/min	cc/sec	ΔP (psig)	ΔP (atm)	ΔP (atm)/L	Q/A
1	0.0167	26.6	1.8088	0.257456	0.003325
2	0.0334	37.2	2.5296	0.3600512	0.006649
3	0.0501	56.8	3.8624	0.5497557	0.009974
4	0.0668	70.4	4.7872	0.6813873	0.013298
5	0.0835	97.3	6.6164	0.9417469	0.016623
6	0.1002	136.8	9.3024	1.3240594	0.019947

Table A20: Initial Liquid Permeability Data for Core 6V

cc/min	cc/sec	ΔP (psig)	ΔP (atm)	ΔP (atm)/L	Q/A
1	0.0167	6.7	0.4556	0.0630065	0.003318
2	0.0334	31.2	2.1216	0.2934034	0.006637
3	0.0501	40.6	2.7608	0.3818006	0.009955
4	0.0668	67	4.556	0.630065	0.013274

5	0.0835	77.1	5.2428	0.7250449	0.016592
6	0.1002	109.2	7.4256	1.0269119	0.01991

Table A21: Initial Liquid Permeability Data for Core 9V

cc/min	cc/sec	ΔP (psig)	ΔP (atm)	ΔP (atm)/L	Q/A
1	0.0167	77.3	5.2564	0.6925124	0.003374
2	0.0334	140.8	9.5744	1.2613939	0.006748
3	0.0501	310.2	21.0936	2.7790084	0.010122
4	0.0668	370.6	25.2008	3.3201177	0.013497
5	0.0835	417.4	28.3832	3.7393878	0.016871
6	0.1002	570.2	38.7736	5.1082869	0.020245

Table A22: Initial Liquid Permeability Data for Core 1X

cc/min	cc/sec	ΔP (psig)	ΔP (atm)	ΔP (atm)/L	Q/A
1	0.0167	90.3	6.1404	0.821898	0.003318
2	0.0334	141.2	9.6016	1.2851827	0.006637
3	0.0501	240.7	16.3676	2.1908178	0.009955
4	0.0668	310.4	21.1072	2.8252175	0.013274
5	0.0835	410.7	27.9276	3.7381341	0.016592
6	0.1002	470.6	32.0008	4.2833356	0.01991

Table A23: Initial Liquid Permeability Data for Core 2X

cc/min	**cc/sec**	**ΔP (psig)**	**ΔP (atm)**	**ΔP (atm)/L**	**Q/A**
1	0.0167	97.2	6.6096	0.904186	0.00332
2	0.0334	241.3	16.4084	2.2446512	0.00664
3	0.0501	310.7	21.1276	2.8902326	0.00996
4	0.0668	442	30.056	4.1116279	0.013281
5	0.0835	512.9	34.8772	4.7711628	0.016601

Table A24: Initial Liquid Permeability Data for Core 3X

Tables A25 to A39 provide the initial relative permeability data of the selected cores including the input data obtained from the apparatus before calculations; the outputs of the fractional flow curves and the outputs of the relative permeability data.

Time (hr.: min: sec)	**Inlet P (psig)**	**Water Vol (cc)**	**Oil Vol (cc)**
0:04:35	141.2	0.7	4.2

0:07:07	133.7	2.3	0.3
0:10:34	132.9	3.4	0.2
0:14:00	128.6	3.3	0.1
0:16:47	118.8	3.2	0.1
0:21:59	113.4	5.4	0.1
0:28:32	113.4	6.8	0.05
0:42:51	113.2	14.8	0.05
0:58:48	112.7	16.5	0.01
1:32:25	113.3	37.5	0.01
2:11:02	112.3	37.6	0

Table A25: Initial Relative Permeability Input Data for Core 9S

F_O	F_W	Water Saturation
0.80556	0.19444	0.894450262
0.11538	0.88462	0.929633508
0.05556	0.94444	0.953089005
0.02941	0.97059	0.964816754
0.0303	0.9697	0.976544503
0.01818	0.98182	0.988272251
0.0073	0.9927	0.994136126
0.00337	0.99663	1
0.00061	0.99939	1.001172775
0.00027	0.99973	1.00234555
0	1	1.00234555

Table A26: Initial Fractional Flow for Core 9S

Kw effective (D)	Ko effective (D)	Krw (D)	Kro (D)	Vo cumulative (cc)	Water Saturation
0.00406588	0.797603207	0.07382	14.4808	2.9	0.894450262
0.009038605	0.055824801	0.1641	1.01352	3.2	0.929633508

0.009047709	0.02520125	0.16426	0.45754	3.4	0.953089005
0.006826904	0.009795852	0.12395	0.17785	3.5	0.964816754
0.005927541	0.008771159	0.10762	0.15924	3.6	0.976544503
0.007958572	0.006978688	0.14449	0.1267	3.7	0.988272251
0.007721316	0.002688344	0.14018	0.04881	3.75	0.994136126
0.011207904	0.001792937	0.20348	0.03255	3.8	1
0.00914158	0.000262343	0.16597	0.00476	3.81	1.001172775
0.013156945	0.000166133	0.23887	0.00302	3.82	1.00234555
0.009377486	0	0.17025	0	3.82	1.00234555

Table A27: Initial Relative Permeability Data for Core 9S

Time (hr.: min: sec)	Inlet P (psig)	Water Vol (cc)	Oil Vol (cc)
0:03:07	32.8	0.1	4.2
0:03:53	30.8	0.55	0.35
0:05:37	29.7	1.25	0.35
0:08:21	29.6	2.6	0.3
0:11:35	29.4	3.2	0.2
0:16:54	28.9	5.6	0.15
0:24:14	26.4	7.6	0.13
0:56:57	23.6	17.8	0.12
1:31:58	19.5	37.2	0.11
2:10:00	14.2	39.8	0.12
3:06:23	13.8	57.5	0.1
4:05:31	11.5	59.5	0.07
5:00:53	8.3	57.3	0.04
6:50:46	6.9	112.8	0

Table A28: Initial Relative Permeability Input Data for Core 4T

F_O	F_W	Water Saturation

0.96667	0.03333	0.530726257
0.38889	0.61111	0.572840567
0.21875	0.78125	0.614954878
0.10345	0.89655	0.651052858
0.05882	0.94118	0.675118178
0.02609	0.97391	0.693167168
0.01682	0.98318	0.708809626
0.0067	0.9933	0.723248818
0.00295	0.99705	0.736484744
0.00301	0.99699	0.750923936
0.00174	0.99826	0.762956596
0.00118	0.99882	0.771379459
10.0007	0.9993	0.776192523
0	1	0.776192523

Table A29: Initial Fractional Flow for Core 4T

Kw effective (D)	Ko effective (D)	Krw (D)	Kro (D)	Vo cumulative (cc)	Water Saturation
0.000259081	0.355766629	0.00073	0.99588	2.9	0.530726257
0.001193893	0.035975195	0.00334	0.1007	3.25	0.572840567
0.001922504	0.025489282	0.00538	0.07135	3.6	0.614954878
0.002695889	0.014729304	0.00755	0.04123	3.9	0.651052858
0.002402684	0.007110646	0.00673	0.0199	4.1	0.675118178
0.002914967	0.003697168	0.00816	0.01035	4.25	0.693167168
0.002926695	0.002370498	0.00819	0.00664	4.38	0.708809626
0.003130014	0.000999171	0.00876	0.0028	4.5	0.723248818
0.004536336	0.000635166	0.0127	0.00178	4.61	0.736484744
0.00406313	0.000580084	0.01137	0.00162	4.73	0.750923936
0.004151784	0.0003419	0.01162	0.00096	4.83	0.762956596
0.003547754	0.000197636	0.00993	0.00055	4.9	0.771379459

0.003175758	0.000104975	0.00889	0.00029	4.94	0.776192523
0.004876171	0	0.01365	0	4.94	0.776192523

Table A30: Initial Relative Permeability Data for Core 4T

Time (hr.: min: sec)	Inlet P (psig)	Water Vol (cc)	Oil Vol (cc)
0:03:49	41.6	0.1	4.1
0:04:37	30.7	0.5	0.4
0:05:55	29.5	1.2	0.3
0:08:24	16.3	2.5	0.25
0:12:43	14.3	4.4	0.2
0:19:14	13.6	5.4	0.2
0:34:54	4.2	15.4	0.2
0:51:18	3.6	16.55	0.15
1:09:04	2.5	17.1	0.15
1:46:33	2.1	38.4	0.15
2:25:32	1.7	38.8	0.1
3:19:47	1.3	54.35	0.1
4:17:03	1.1	56.5	0.05
5:19:07	0.8	60.7	0.05
7:13:01	0.7	112.7	0

Table A31: Initial Relative Permeability Input Data for Core 7T

F_O	F_W	Water Saturation
0.96552	0.03448	0.536690647
0.44444	0.55556	0.576978417
0.2	0.8	0.607194245
0.09091	0.90909	0.632374101
0.04348	0.95652	0.652517986
0.03571	0.96429	0.672661871

0.01282	0.98718	0.692805755
0.00898	0.99102	0.707913669
0.0087	0.9913	0.723021583
0.00389	0.99611	0.738129496
0.00257	0.99743	0.748201439
0.00184	0.99816	0.758273381
0.00088	0.99912	0.763309353
0.00082	0.99918	0.768345324
0	1	0.768345324

Table A32: Initial Fractional Flow for Core 7T

Kw effective (D)	Ko effective (D)	Krw (D)	Kro (D)	Vo cumulative (cc)	Water Saturation
0.000180103	0.23878789	0.0002	0.27121	2.8	0.536690647
0.000923209	0.034972165	0.00105	0.03972	3.2	0.576978417
0.00177581	0.021021746	0.00202	0.02388	3.5	0.607194245
0.003715468	0.017593244	0.00422	0.01998	3.75	0.632374101
0.004617383	0.009938151	0.00524	0.01129	3.95	0.652517986
0.003839435	0.006733423	0.00436	0.00765	4.15	0.672661871
0.009035413	0.005556351	0.01026	0.00631	4.35	0.692805755
0.006822508	0.002927991	0.00775	0.00333	4.5	0.707913669
0.00557075	0.002313882	0.00633	0.00263	4.65	0.723021583
0.008302005	0.00153559	0.00943	0.00174	4.8	0.738129496
0.006291293	0.000767787	0.00715	0.00087	4.9	0.748201439
0.006580135	0.000573281	0.00747	0.00065	5	0.758273381
0.005383792	0.000225602	0.00611	0.00026	5.05	0.763309353
0.004749217	0.00018524	0.00539	0.00021	5.1	0.768345324
0.006540532	0	0.00743	0	5.1	0.768345324

Table A33: Initial Relative Permeability Data for Core 7T

F_O	F_W	Water Saturation
0.95833	0.04167	0.454151625
0.33333	0.66667	0.484476534
0.2	0.8	0.514801444
0.075	0.925	0.545126354
0.04	0.96	0.570397112
0.02105	0.97895	0.590613718
0.00993	0.99007	0.605776173
0.00943	0.99057	0.620938628
0.00325	0.99675	0.633068592
0.00265	0.99735	0.643176895
0.0009	0.9991	0.648231047
0.00082	0.99918	0.653285199
0	1	0.653285199

Table A34: Initial Fractional Flow for Core 8T

Time (hr.: min: sec)	Inlet P (psig)	Water Vol (cc)	Oil Vol (cc)
0:02:55	37.1	0.1	3.6
0:03:52	24.1	0.6	0.3
0:05:31	11.3	1.2	0.3
0:09:20	7.3	3.7	0.3
0:15:21	4.3	6	0.25
0:24:36	3.7	9.3	0.2
0:39:30	1.6	14.95	0.15
0:55:13	1.2	15.75	0.15
1:32:23	1.1	36.8	0.12
2:08:46	1.1	37.7	0.1
3:04:48	0.7	55.8	0.05

4:05:30	0.4	61	0.05
5:45:22	0.2	100	0

Table A35: Initial Relative Permeability Input Data for Core 8T

Kw effective (D)	Ko effective (D)	Krw (D)	Kro (D)	Vo cumulative (cc)	Water Saturation
0.000261366	0.284649056	0.00021	0.23352	2.3	0.454151625
0.001579243	0.037389638	0.0013	0.03067	2.6	0.484476534
0.003303674	0.039108363	0.00271	0.03208	2.9	0.514801444
0.007115548	0.027318715	0.00584	0.02241	3.2	0.545126354
0.008123728	0.016027895	0.00666	0.01315	3.45	0.570397112
0.008113273	0.008261816	0.00666	0.00678	3.65	0.590613718
0.009169013	0.004356172	0.00752	0.00357	3.8	0.605776173
0.007084013	0.003194644	0.00581	0.00262	3.95	0.620938628
0.009955503	0.001537195	0.00817	0.00126	4.07	0.633068592
0.007317233	0.000919047	0.006	0.00075	4.17	0.643176895
0.007742436	0.000328508	0.00635	0.00027	4.22	0.648231047
0.006497817	0.000252197	0.00533	0.00021	4.27	0.653285199
0.007673604	0	0.0063	0	4.27	0.653285199

Table A36: Initial Relative Permeability Data for Core 8T

F_O	F_W	Water Saturation
0.89189	0.10811	0.454151625
0.27778	0.72222	0.484476534
0.11538	0.88462	0.514801444
0.0625	0.9375	0.545126354
0.07143	0.92857	0.570397112
0.03846	0.96154	0.590613718
0.00971	0.99029	0.605776173
0.00637	0.99363	0.620938628

0.00134	0.99866	0.633068592
0.00134	0.99866	0.643176895
0	1	0.648231047

Table A37: Initial Fractional Flow for Core 1U

Time (hr.: min: sec)	Inlet P (psig)	Water Vol (cc)	Oil Vol (cc)
0:04:31	250	0.4	4.6
0:06:04	210.5	1.3	0.5
0:08:19	153.6	2.3	0.3
0:11:17	91.1	3	0.2
0:13:54	90.5	2.6	0.2
0:18:34	90.2	5	0.2
0:33:19	94.2	15.3	0.15
0:48:16	102.7	15.6	0.1
1:24:24	89.9	37.2	0.05
2:00:26	89.7	37.4	0.05
2:54:50	89.5	55.8	0

Table A38: Initial Relative Permeability Input Data for Core 1U

Kw effective (D)	Ko effective (D)	Krw (D)	Kro (D)	Vo cumulative (cc)	Water Saturation
0.00013877	0.05421029	0.00251	0.97994	3.3	0.594280267
0.000394668	0.007187722	0.00713	0.12993	3.8	0.647664442
0.000681556	0.004209472	0.01232	0.07609	4.1	0.679694948
0.001042331	0.003290385	0.01884	0.05948	4.3	0.701048618
0.00073748	0.002686205	0.01333	0.04856	4.5	0.722402288
0.0010648	0.002016788	0.01925	0.03646	4.7	0.743755958
0.001749079	0.000811973	0.03162	0.01468	4.85	0.759771211
0.00114187	0.000346597	0.02064	0.00627	4.95	0.770448046
0.001747738	0.000111234	0.03159	0.00201	5	0.775786463

0.001233763	7.81021E-05	0.0223	0.00141	5.05	0.781124881
0.001270427	0	0.02297	0	5.05	0.781124881

Table A39: Initial Relative Permeability Data for Core 1U

Tables A40 to A49 provide the absolute permeability data just before vibration and after cleaning and just after vibration and prior to the relative permeability of the selected cores.

cc/min	cc/sec	ΔP (psig)	ΔP (atm)	ΔP (atm)/L	Q/A
1	0.0167	7.1	0.4828	0.0633929	0.00335
2	0.0334	31.1	2.1148	0.2776786	0.0067
3	0.0501	37.1	2.5228	0.33125	0.01005
4	0.0668	41.2	2.8016	0.3678571	0.0134
5	0.0835	56.8	3.8624	0.5071429	0.01675
6	0.1002	69.6	4.7328	0.6214286	0.0201

Table A40: Final Liquid Permeability Data for Core 9S Before Vibration

cc/min	cc/sec	ΔP (psig)	ΔP (atm)	ΔP (atm)/L	Q/A
1	0.0167	4.2	0.2856	0.0375	0.003350081
2	0.0334	6.7	0.4556	0.059821429	0.006700162
3	0.0501	37.1	2.5228	0.33125	0.010050243
4	0.0668	41.1	2.7948	0.366964286	0.013400325
5	0.0835	49.8	3.3864	0.444642857	0.016750406
6	0.1002	66.8	4.5424	0.596428571	0.020100487

Table A41: Final Liquid Permeability Data for Core 9S After Vibration

cc/min	cc/sec	ΔP (psig)	ΔP (atm)	ΔP (atm)/L	Q/A
1	0.0167	0.8	0.0544	0.0074442	0.003322
2	0.0334	1.3	0.0884	0.0120969	0.006644
3	0.0501	2.7	0.1836	0.0251243	0.009966
4	0.0668	4.8	0.3264	0.0446654	0.013288
5	0.0835	6.7	0.4556	0.0623455	0.016609

Table A42: Final Liquid Permeability Data for Core 4T Before Vibration

cc/min	cc/sec	ΔP (psig)	ΔP (atm)	ΔP (atm)/L	Q/A
1	0.0167	0.8	0.0544	0.007444237	0.003321892
2	0.0334	1.3	0.0884	0.012096885	0.006643785

3	0.0501	2.8	0.1904	0.026054828	0.009965677
4	0.0668	3.2	0.2176	0.029776947	0.013287569
5	0.0835	4.6	0.3128	0.042804361	0.016609461

Table A43: Final Liquid Permeability Data for Core 4T After Vibration

cc/min	cc/sec	ΔP (psig)	ΔP (atm)	ΔP (atm)/L	Q/A
1	0.0167	0.8	0.0544	0.0075619	0.003307
2	0.0334	1.3	0.0884	0.012288	0.006614
3	0.0501	1.8	0.1224	0.0170142	0.009921
4	0.0668	4.2	0.2856	0.0396997	0.013228
5	0.0835	6.7	0.4556	0.0633306	0.016535

Table A44: Final Liquid Permeability Data for Core 7T Before Vibration

cc/min	cc/sec	ΔP (psig)	ΔP (atm)	ΔP (atm)/L	Q/A
1	0.0167	0.7	0.0476	0.0066166	0.003307
2	0.0334	1.1	0.0748	0.0103976	0.006614
3	0.0501	1.6	0.1088	0.0151237	0.009921
4	0.0668	2.8	0.1904	0.0264665	0.013228
5	0.0835	3.9	0.2652	0.0368641	0.016535

Table A45: Final Liquid Permeability Data for Core 7T After Vibration

cc/min	cc/sec	ΔP (psig)	ΔP (atm)	ΔP (atm)/L	Q/A
1	0.0167	0.4	0.0272	0.0038301	0.00332
2	0.0334	0.8	0.0544	0.0076602	0.00664
3	0.0501	1.1	0.0748	0.0105327	0.00996
4	0.0668	1.3	0.0884	0.0124478	0.013281
5	0.0835	1.8	0.1224	0.0172354	0.016601
6	0.1002	1.9	0.1292	0.0181929	0.019921

Table A46: Final Liquid Permeability Data for Core 8T Before Vibration

cc/min	cc/sec	ΔP (psig)	ΔP (atm)	ΔP (atm)/L	Q/A
1	0.0167	0.3	0.0204	0.0028726	0.00332
2	0.0334	0.6	0.0408	0.0057451	0.00664
3	0.0501	0.9	0.0612	0.0086177	0.00996
4	0.0668	1.2	0.0816	0.0114903	0.013281
5	0.0835	1.3	0.0884	0.0124478	0.016601

6	0.1002	1.4	0.0952	0.0134053	0.019921

Table A47: Final Liquid Permeability Data for Core 8T After Vibration

cc/min	cc/sec	ΔP (psig)	ΔP (atm)	ΔP (atm)/L	Q/A
1	0.0167	40.4	2.7472	0.3620931	0.003361
2	0.0334	46.9	3.1892	0.4203506	0.006721
3	0.0501	69.8	4.7464	0.6255964	0.010082
4	0.0668	91.1	6.1948	0.8165019	0.013443
5	0.0835	110.3	7.5004	0.9885857	0.016804

Table A48: Final Liquid Permeability Data for Core 1U Before Vibration

cc/min	cc/sec	ΔP (psig)	ΔP (atm)	ΔP (atm)/L	Q/A
1	0.0167	34.2	2.3256	0.3065243	0.003361
2	0.0334	40.1	2.7268	0.3594042	0.006721
3	0.0501	50.7	3.4476	0.4544089	0.010082
4	0.0668	70	4.76	0.627389	0.013443
5	0.0835	77	5.236	0.6901279	0.016804

Table A49: Final Liquid Permeability Data for Core 1U

Tables A50 to A64 provide the final relative permeability data after vibration of the selected cores including the input data obtained from the apparatus before calculations; the outputs of the fractional flow curves and the outputs of the relative permeability data.

F_O	F_W	Water Saturation
0.93939	0.06061	0.738011696
0.17241	0.82759	0.770760234
0.06667	0.93333	0.790409357
0.04	0.96	0.81005848
0.02326	0.97674	0.823157895
0.00952	0.99048	0.829707602
0.00787	0.99213	0.83625731
0.00337	0.99663	0.842807018
0.00062	0.99938	0.844116959
0	1	0.844116959

Table A50: Fractional Flow Data for Core 9S After Vibration

Time (hr.: min: sec)	Inlet P (psig)	Water Vol (cc)	Oil Vol (cc)
0:04:45	137.1	0.2	4.4
0:06:05	136.4	1.2	0.25
0:08:22	130.4	2.1	0.15
0:11:58	129.6	3.6	0.15
0:14:02	129.4	4.2	0.1
0:17:56	128.8	5.2	0.05
0:22:55	124.4	6.3	0.05
0:37:20	123.9	14.8	0.05
0:53:02	126.5	16.1	0.01
1:28:30	128.6	37.3	0

Table A51: Final Relative Permeability Input Data for Core 9S After Vibration

Kw effective (D)	Ko effective (D)	Krw (D)	Kro (D)	Vo cumulative (cc)	Water Saturation
0.001151194	0.844914503	0.02733	20.0597	3.1	0.738011696
0.005418253	0.053450329	0.12864	1.269	3.35	0.770760234
0.007179323	0.024282189	0.17045	0.5765	3.5	0.790409357
0.008652608	0.017071363	0.20543	0.4053	3.65	0.81005848
0.008620025	0.00971833	0.20465	0.23073	3.75	0.823157895
0.008386379	0.003818331	0.19911	0.09065	3.8	0.829707602
0.008202496	0.003082534	0.19474	0.07318	3.85	0.83625731
0.011870959	0.001899007	0.28184	0.04509	3.9	0.842807018
0.008923317	0.000262442	0.21185	0.00623	3.91	0.844116959
0.012206845	0	0.28981	0	3.91	0.844116959

Table A52: Final Relative Permeability Data for Core 9S After Vibration

F_O	F_W	Water Saturation
0.97143	0.02857	0.97143
0.5	0.5	0.5
0.29167	0.70833	0.29167
0.11538	0.88462	0.11538
0.04348	0.95652	0.04348
0.0303	0.9697	0.0303
0.00667	0.99333	0.00667
0.00912	0.99088	0.00912
0.00548	0.99452	0.00548
0.00265	0.99735	0.00265
0.00131	0.99869	0.00131
0.00018	0.99982	0.00018
0.00017	0.99983	0.00017
0.00018	0.99982	0.00018
0.00018	0.99982	0.00018
0	1	0

Table A53: Fractional Flow Data for Core 9S After Vibration

Time (hr.: min: sec)	Inlet P (psig)	Water Vol (cc)	Oil Vol (cc)
0:04:14	28.9	0.1	4.7
0:04:51	19.2	0.4	0.4
0:05:48	6.9	0.85	0.35
0:07:53	3.3	2.3	0.3
0:12:08	2.7	4.4	0.2
0:18:16	2.4	6.4	0.2
0:32:53	1.2	14.9	0.1
0:48:51	0.9	16.3	0.15

1:23:09	0.8	36.3	0.2
1:58:57	0.7	37.6	0.1
2:36:16	0.5	38.2	0.05
3:30:42	0.5	55.4	0.01
4:29:35	0.4	59.3	0.01
5:24:34	0.4	56.9	0.01
6:17:58	0.3	54.6	0.01
7:11:34	0.2	112.5	0

Table A54: Final Relative Permeability Input Data for Core 9S After Vibration

Kw effective (D)	Ko effective (D)	Krw (D)	Kro (D)	Vo cumulative (cc)	Water Saturation
0.000207802	0.33455008	0.00042	0.681975865	3.4	0.530726257
0.00093312	0.044184478	0.0019	0.090069468	3.8	0.578856897
0.002602292	0.050738483	0.0053	0.103429719	4.15	0.620971208
0.006216762	0.038396358	0.01267	0.078270463	4.45	0.657069188
0.007993594	0.017204886	0.01629	0.03507193	4.65	0.681134508
0.007858567	0.011628555	0.01602	0.023704654	4.85	0.705199828
0.010930301	0.003473587	0.02228	0.007080861	4.95	0.717232488
0.008203841	0.003574813	0.01672	0.007287208	5.1	0.735281478
0.010802679	0.0028183	0.02202	0.005745067	5.3	0.759346798
0.00787266	0.000991439	0.01605	0.002021035	5.4	0.771379459
0.006168396	0.000382306	0.01257	0.000779326	5.45	0.777395789
0.006634687	5.67078E-05	0.01352	0.000115598	5.46	0.778599055
0.005587319	4.4615E-05	0.01139	9.09471E-05	5.47	0.779802321
0.004452974	3.7057E-05	0.00908	7.55402E-05	5.48	0.781005587
0.003693743	3.20336E-05	0.00753	6.53002E-05	5.49	0.782208853
0.006710226	0	0.01368	0	5.49	0.782208853

Table A55: Final Relative Permeability Data for Core 4T After Vibration

F_O	F_W	Water Saturation
0.96667	0.03333	0.637410072
0.3	0.7	0.697841727
0.07246	0.92754	0.723021583
0.05882	0.94118	0.748201439
0.03226	0.96774	0.768345324
0.01003	0.98997	0.783453237
0.00929	0.99071	0.798561151
0.00275	0.99725	0.808633094
0.01355	0.98645	0.858992806
0.0027	0.9973	0.869064748
0.00181	0.99819	0.879136691
0.00018	0.99982	0.880143885
0.00017	0.99983	0.881151079
0	1	0.881151079

Table A56: Fractional Flow Data for Core 7T After Vibration

Time (hr.: min: sec)	Inlet P (psig)	Water Vol (cc)	Oil Vol (cc)
0:04:52	40.7	0.1	4.2
0:06:22	40.4	1.4	0.6
0:09:07	30.2	3.2	0.25
0:12:54	29.9	4	0.25
0:17:30	29.7	6	0.2
0:31:52	29.6	14.8	0.15
0:47:27	29.5	16	0.15
1:21:30	29.2	36.3	0.1
2:18:45	28.9	36.4	0.5
2:57:00	28.8	36.9	0.1

3:51:27	28.8	55.2	0.1
4:45:53	28.7	56.4	0.01
5:45:24	27.3	58.8	0.01
6:38:25	26.8	65.5	0

Table A57: Final Relative Permeability Input Data for Core 7T After Vibration

Kw effective (D)	Ko effective (D)	Krw (D)	Kro (D)	Vo cumulative (cc)	Water Saturation
0.00014354	0.19710767	0.000243	0.333922326	2.9	0.637410072
0.001544468	0.031342558	0.002617	0.0530977799	3.5	0.697841727
0.003025395	0.011191917	0.005125	0.018960353	3.75	0.723021583
0.002690605	0.007962736	0.004558	0.013489761	4	0.748201439
0.002988441	0.004716891	0.005063	0.007990939	4.2	0.768345324
0.004057288	0.001947143	0.006873	0.003298676	4.35	0.783453237
0.002952406	0.001310629	0.005002	0.002220351	4.5	0.798561151
0.00392644	0.000512183	0.006652	0.000867694	4.6	0.808633094
0.002328608	0.001514598	0.003945	0.002565898	5.1	0.858992806
0.00185472	0.000238004	0.003142	0.000403205	5.2	0.869064748
0.002121813	0.000182012	0.003595	0.000308349	5.3	0.879136691
0.001759199	1.47696E-05	0.00298	2.50213E-05	5.31	0.880143885
0.001568629	1.26321E-05	0.002657	2.14002E-05	5.32	0.881151079
0.001533099	0	0.002597	0	5.32	0.881151079

Table A58: Final Relative Permeability Data for Core 7T After Vibration

F_O	F_W	Water Saturation
0.97222	0.02778	0.731612903
0.5	0.5	0.772903226
0.2	0.8	0.803870968
0.075	0.925	0.83483871
0.07692	0.92308	0.855483871

0.04545	0.95455	0.876129032
0.01587	0.98413	0.886451613
0.00667	0.99333	0.896774194
0.00568	0.99432	0.907096774
0.00268	0.99732	0.917419355
0.00266	0.99734	0.927741935
0.00181	0.99819	0.934967742
0.00142	0.99858	0.943225806
0.00086	0.99914	0.948387097
0	1	0.948387097

Table A59: Fractional Flow Data for Core 8T After Vibration

Time (hr.: min: sec)	Inlet P (psig)	Water Vol (cc)	Oil Vol (cc)
0:03:40	40.4	0.1	4.8
0:04:22	40	0.4	0.4
0:05:44	39.8	1.2	0.3
0:09:24	39.5	3.7	0.3
0:11:39	36.7	2.4	0.2
0:15:44	34.3	4.2	0.2
0:21:42	33.7	6.2	0.1
0:36:05	31.6	14.9	0.1
0:53:09	30.6	17.5	0.1
1:28:17	30.4	37.2	0.1
2:03:28	30.1	37.5	0.1
2:41:15	29.9	38.7	0.07
3:36:36	29.8	56.2	0.08
4:32:10	29.6	57.8	0.05
5:31:04	29.4	59.8	0

Table A60: Final Relative Permeability Input Data for Core 8T After Vibration

Kw effective (D)	Ko effective (D)	Krw (D)	Kro (D)	Vo cumulative (cc)	Water Saturation
0.000195453	0.323924267	0.00012	0.206832342	3.5	0.731612903
0.000661285	0.031312742	0.00042	0.019993833	3.9	0.772903226
0.001516504	0.017952132	0.00097	0.011462807	4.2	0.803870968
0.002867746	0.011010133	0.00183	0.007030198	4.5	0.83483871
0.001582662	0.0062451	0.00101	0.003987626	4.7	0.855483871
0.002151288	0.004850781	0.00137	0.003097324	4.9	0.876129032
0.002331056	0.001780301	0.00149	0.001136759	5	0.886451613
0.0035218	0.001119208	0.00225	0.000714637	5.1	0.896774194
0.002870137	0.000776599	0.00183	0.000495875	5.2	0.907096774
0.003689383	0.000469616	0.00236	0.00029986	5.3	0.917419355
0.002677131	0.000338042	0.00171	0.000215847	5.4	0.927741935
0.002124919	0.000181996	0.00136	0.000116208	5.47	0.934967742
0.002302417	0.000155192	0.00147	9.90935E-05	5.55	0.943225806
0.00189302	7.75407E-05	0.00121	4.95114E-05	5.6	0.948387097

Table A61: Final Relative Permeability Data for Core 8T After Vibration

F_O	F_W	Water Saturation
0.94828	0.05172	0.796539792
0.5	0.5	0.874048443
0.13333	0.86667	0.912802768
0.04348	0.95652	0.951557093
0.01205	0.98795	0.970934256
0.01176	0.98824	0.990311419
0.00232	0.99768	0.994186851
0.0012	0.9988	0.998062284
0	1	0.998062284

Table A62: Fractional Flow Data for Core 1U After Vibration

Time (hr.: min: sec)	Inlet P (psig)	Water Vol (cc)	Oil Vol (cc)
0:04:18	241.2	0.15	4.05
0:04:56	240.6	0.4	0.4
0:06:05	239.9	1.3	0.2
0:10:17	230.3	4.4	0.2
0:18:04	210.1	8.2	0.1
0:26:07	209.2	8.4	0.1
0:35:34	194.3	8.6	0.02
0:52:19	190.9	16.7	0.02
1:09:35	189.8	17.7	0

Table A63: Final Relative Permeability Input Data for Core 1U After Vibration

Kw effective (D)	Ko effective (D)	Krw (D)	Kro (D)	Vo cumulative (cc)	Water Saturation
5.68345E-05	0.04933851	0.00219	1.90349	2.75	0.796539792
0.000132412	0.006269903	0.00511	0.24189	3.15	0.874048443
0.000349948	0.002549307	0.0135	0.09835	3.35	0.912802768
0.000728136	0.001567192	0.02809	0.06046	3.55	0.951557093
0.000841781	0.000486091	0.03248	0.01875	3.65	0.970934256
0.000598918	0.000337614	0.02311	0.01303	3.75	0.990311419
0.000482357	5.31169E-05	0.01861	0.00205	3.77	0.994186851
0.000647311	3.67078E-05	0.02497	0.00142	3.79	0.998062284
0.000518602	0	0.02001	0	3.79	0.998062284

Table A64: Final Relative Permeability Data for Core 1U After Vibration